Thin films based on Gadolinium applied to the magnetic refrigeration

Asmaa Endichi

THESE

Pour l'obtention du titre de :

DOCTEUR de L'UNIVERSITE DE LORRAINE

Spécialité : Physique

Présenté par :

Asmaa ENDICHI

Thin films based on Gadolinium applied to the magnetic refrigeration.

Thèse soutenue publiquement le 02 Octobre 2020 à Rabat devant le jury composé de :

M. Mohamed El BOUZIANI	Pr, Université Chouaïb Doukkali, Faculté des Sciences, El Jadida	Président/Rapporteur
M. Stéphane MANGIN	Pr, Université de Lorraine, Institut Jean Lamour, Nancy	Directeur de Thèse
M. Abdallah EL KENZ	Pr, Université Mohammed V-Rabat, Faculté des sciences	Co-Directeur de Thèse
M. Mohammed SAJIEDDINE	Pr, Université Sultan Moulay Slimane, FST, Béni Mellal	Rapporteur
M. Mohamed BALLI	Pr, Université internationale de Rabat	Examinateur
M. Thomas HAUET	Pr, Université de Lorraine, Institut Jean Lamour, Nancy	Examinateur
Mme. Salma LAHBABI	Pr, Université Hassan II, ENSEM, Casablanca	Examinatrice
M. Abdelilah BENYOUSSEF	Pr, Académie Hassan II de Rabat	Invité
M. Hamid EZ-ZAHRAOUY	Pr, Université Mohammed V-Rabat, Faculté des sciences	Invité
M. Omar MOUNKACHI	Pr, Université Mohammed V-Rabat, Faculté des sciences	Invité

Institut Jean Lamour
Université de Lorraine, Nancy

Remerciement

L'ensemble des travaux de ce projet de recherche doctoral en cotutelle ont été réalisés dans le cadre d'un programme de coopération scientifique bilatéral franco-marocain le PHC-Toubkal, au sein de l'institut Jean Lamour « Equipe de nanomagnétisme et électronique de spin » à l'université de lorraine à Nancy et Laboratoire de la matière condensée et sciences interdisciplinaires « LaMCScI » de la Faculté des Sciences de l'Université Mohammed V-Rabat sous la direction des monsieurs les professeurs M. Stéphane MANGIN et M. Abdallah EL KENZ.

Que mon directeur de thèse **M. Stéphane MANGIN**, Professeur à l'université de Lorraine, Institut Jean Lamour, trouve ici toute la gratitude et la reconnaissance pour m'avoir accompagnée et encadrée tout au long de cette thèse et qui m'a fait bénéficier de ses brillantes qualités scientifiques et humaines. Qu'il soit aussi remercié pour sa gentillesse, sa disponibilité permanente et pour les nombreux encouragements et conseils qu'ils m'ont prodigués.

Je tiens à remercier **M. Abdallah EL KENZ**, Professeur à l'Université Mohammed V-Rabat, Faculté des sciences, mon co-directeur de thèse qui fut pour moi un directeur attentif, généreux et disponible malgré ses nombreuses charges. Il avait des solutions à tous les problèmes rencontrés, une vision claire sur ma recherche et n'hésitait pas à présenter ses conseils et ses orientations qui témoignent de sa compétence et de sa rigueur scientifiques.

Ma reconnaissance et mon profond respect pour mon professeur, **M. Abdelilah BENYOUSSEF**, Membre résident à l'Académie Hassan II des Sciences et Techniques, qui a été toujours une ressource scientifique de référence et une source capitale de motivation et d'encouragement. C'est à ses côtés que j'ai acquis les incontournables qualités de la recherche scientifique, notamment en termes de rigueur et de précision. Je le remercie également pour sa disponibilité permanente et pour le grand intérêt qu'il a accordé à ce travail.

Je tiens à exprimer mes sincères remerciements à **M. Mohamed El BOUZIANI**, Professeur à l'université Chouaïb Doukkali, Faculté des Sciences, El Jadida, pour avoir accepté de participer à ce jury en tant que Président de jury et rapporteur.

J'adresse tous mes remerciements également à **M. Mohamed SAJIEDDINE**, Professeur à l'université Sultan Moulay Slimane, FST, Béni Mellal de l'honneur qu'il m'a fait en acceptant d'être rapporteur de cette thèse.

J'exprime ma reconnaissance à **M. Thomas HAUET,** Professeur à l'Université de Lorraine, Institut Jean Lamour à Nancy, d'avoir accepté de participer à ce jury en tant qu'examinateur.

Je tiens à exprimer mes sincères remerciements à **M. Mohammed BALLI**, Professeur à l'Université internationale de Rabat, d'avoir accepté de participer à ce jury en tant qu'examinateur.

J'exprime ma reconnaissance à **Mme. Salma LAHBABI,** Professeur à l'Université Hassan II, ENSEM de Casablanca d'avoir acceptée de participer à ce jury en tant qu'examinatrice.

Je tiens à exprimer mes sincères remerciements à **M. Hamid EZ-ZAHRAOUY**, Professeur à l'Université Mohammed V-Rabat, Faculté des sciences, d'avoir accepté de participer à ce jury en tant qu'invité.

Je tiens aussi à remercier **M. Omar MOUNKACHI**, Professeur à l'Université Mohammed V-Rabat, Faculté des sciences, pour les conseils et le soutien qu'il m'a prodiguée tout au long de ces années de thèse, et d'avoir accepté de participer à ce jury en tant qu'invité.

Je suis très reconnaissante également à **M. Mohammed Salah EL HADRI**, Docteur de l'université de Lorraine, grâce à lui ce projet de recherche s'est achevé.

Toute ma gratitude et toute ma reconnaissance s'adressent **à Mme. Halima ZAARI**, Professeur à l'Université Mohammed V-Rabat, Faculté des sciences, qui, grâce à ses qualités humaines et scientifiques a su m'orienter tout au long de la période de réalisation de ce travail de recherche.

Un grand merci aussi spécial qu'il puisse l'être, à l'attention de **mes parents**. Merci d'être mes parents, de m'avoir donné des racines et des ailes, de m'avoir supportée et appuyée durant toutes ces années, de me faire confiance, de m'avoir inculquée de vraies valeurs et de m'avoir permis de devenir la personne que je suis aujourd'hui. Grace à vous j'ai pu m'épanouir et m'ouvrir à la vie et surtout surmonter toute sorte d'épreuves que je rencontre. Je n'oublierai pas de remercier **mes grands-parents** pour leurs Douaa, tendresse, générosité et amour.

Je dédie également ce travail à **mes frères**, **mes sœurs**, **mes beaux-frères** et **mes belles sœurs**, surtout **mon grand frère Younes** et **sa femme Samiha** qui ont été toujours à mes côtés dès mon arrivée en France, qui m'ont accueillie et accompagnée durant tout mon séjour en veillant à ce qu'il se déroule dans de bonnes conditions. Je vous remercie infiniment pour le soutien moral et financier et pour tout ce que vous avez fait pour moi… je vous remercie tous du fond du cœur.

Enfin, Je tiens à remercier chaleureusement toutes les personnes qui, de près ou de loin, ont contribué à l'accomplissement de ce cheminement.

Résumé

La recherche en matière de caractérisation de matériaux à effet magnétocalorique géant à l'état massif et à une température proche de la température ambiante est d'un grand intérêt pour l'application de la réfrigération magnétique. Il est admis que la transition de premier ordre dans ces matériaux présente une hystérésis thermique considérable, les rendant ainsi difficiles à manipuler dans les applications pour les réfrigérateurs fonctionnant de manière cyclique. Beaucoup d'efforts ont été accomplis au cours de ces dernières années pour réduire cette hystérésis, mais les performances obtenues avec ces matériaux massifs ne répondent pas aux exigences d'une réfrigération magnétique efficace. Si les matériaux magnétocaloriques à l'état massif ont été largement étudiés; l'échelle nanométrique correspondante reste cependant insuffisamment explorée. A cet effet, la nanostructuration, une approche largement bien connue et utilisée pour la mise au point et l'optimisation des relations structure-propriété des matériaux en questions, permet des nouvelles perspectives en matière d'amélioration de leurs caractéristiques magnétiques et magnétocaloriques en modifiant leur taille et leur forme.

Pour ce faire, l'étude des propriétés magnétocaloriques des matériaux sous forme de couches minces est centrale pour pouvoir réduire au maximum l'hystérésis thermique, sachant que l'effet magnétocalorique dans les couches minces magnétiques est particulièrement intéressant pour la micro-réfrigération. Dans ce sens, peu d'études ont été menées pour montrer le potentiel des matériaux sous forme de couches minces pour la réfrigération magnétique. De même, les propriétés magnétiques (aimantation de saturation, la variation de l'entropie magnétique et du rapport de refroidissement relatif…) mesurées restent limitées.

C'est dans ce cadre que le pèsent travail a été mené en étudiant le gadolinium métallique, en tant que matériau réfrigérant magnétique de référence pour la plupart des prototypes de régénérateur magnétique actif (AMR) sous forme de couche mince. Les propriétés magnétocaloriques (MCE) et électrocaloriques (ECE) des films de gadolinium fabriqués à cette fin (Si/Ta/Gd(100nm)/Pt(3nm)) sont alors mesurées dans le but d'obtenir plus d'informations sur la physique derrière ses intéressantes propriétés électroniques et magnétique en démontrant notamment l'effet magnéto-calorique du film mince Gd par la mesure du transport électrique de la résistance. Ainsi, au cours de cette thèse, les comportements électriques et surtout magnétiques de $LaCr_2Si_2C$ et de multiferroïques $TbMn_2O_5$ sont décrits en utilisant la méthode ab-initio dans le but d'élargir notre compréhension des caractéristiques électroniques, magnétiques et par conséquent magnétocaloriques de ces composés à base de terre rare.

L'élaboration et la caractérisation des couches minces pour la réfrigération magnétique, le traitement des données correspondantes ont été effectués conjointement au sein du laboratoire de recherche en science des matériaux avec l'équipe nanomagnétisme et électronique de spin à l'institut Jean Lamour à Nancy et au laboratoire de matière condensée et sciences interdisciplinaires à la faculté des sciences de Rabat.

Mots clés : Couche mince, multiferroïques, terre rare, magnétisme, spintronique, effet magnetocalorique.

Abstract

The search for materials with a giant magnetocaloric effect in a massive state and at a temperature close to ambient temperature is of great interest and is mainly obtained by varying the composition of the materials. However, the first-order transition in these materials exhibits considerable thermal hysteresis, making them difficult to handle in applications for refrigerators operating cyclically. Much effort has been made in recent years to reduce this hysteresis, but the performance obtained with these massive materials does not meet the requirements of efficient magnetic refrigeration. Magnetocaloric materials have been largely unexplored on the nanoscale. However, nanostructuring is a well-known and used approach to disrupt the developed structure-property relationships, hence the interest in manufacturing new nanoscale materials. This will improve their magnetic and magnetocaloric characteristics by varying the size and shape. On the other hand, the magnetocaloric effect in magnetic thin layers is particularly interesting for micro-refrigeration. It is therefore important to study the magnetocaloric properties of materials in the form of thin layers in order to eliminate thermal hysteresis.

In this sense, few studies have been done to show the potential of thin film materials for magnetic refrigeration and magnetic properties (saturation magnetization, variation of magnetic entropy and relative cooling ratio ...) measured so far limited remains. In this thesis project, we studied metallic gadolinium, which is the preferred choice as a magnetic refrigerant for most prototypes of active magnetic regenerator (AMR) in the form of a thin layer. The magnetocaloric (MCE) and electrocaloric (ECE) properties of the manufactured gadolinium films (Si / Ta / Gd (100 nm) / Pt (3nm)) are measured, in order to obtain more information on the physics behind the interesting electronic and magnetic properties of this material we demonstrate the magneto-caloric effect of the thin film Gd by measuring the electrical transport of the resistance. Thus, during this thesis, the electrical and especially magnetic behaviors of $LaCr_2Si_2C$ and multiferroics $TbMn_2O_5$ are described using the ab-initio method, in order to broaden our understanding of the electronic, magnetic and therefore magnetocaloric characteristics of these compounds based on rare earth.

The development of thin layers for magnetic refrigeration was carried out in the materials science research laboratory with the nanomagnetism and spin electronics team at the Jean Lamour Institute in Nancy and the theoretical calculations are made in the material laboratory condensed and interdisciplinary sciences at the Faculty of Sciences of Rabat.

Keywords: Thin film, multiferroic, rare earth, magnetism, spintronics, magnetocaloric effect.

Résumé étendu

La réfrigération magnétique est une technologie écologique contrairement aux systèmes de réfrigération conventionnels qui utilisent des gaz polluants. Elle utilise un matériau solide comme liquide de refroidissement et un fluide caloporteur, généralement de l'eau ou de l'huile, pour transférer la chaleur entre les sources chaudes et froides. C'est une technologie qui englobe plusieurs disciplines telles que le magnétisme, les matériaux, la mécanique, la thermodynamique, la thermique, la mécanique des fluides, toutes ces disciplines sont couplées entre elles pour faire fonctionner un système de réfrigération magnétique. Aujourd'hui, les recherches sur le thème de la réfrigération magnétique s'orientent vers 3 grands domaines de recherche, elles concernent le matériau magnétocalorique (plus efficace, CEM géant et moins cher), la source de champ magnétique (forme et géométrie) et le système de réfrigération magnétique (conception et production). La réfrigération magnétique devient de plus en plus fiable, ce qui lui permettra de remplacer les systèmes de réfrigération conventionnels, un changement qui est souhaitable en raison des avantages de l'utilisation de l'effet magnétocalorique (MCE) pour les applications de réfrigération magnétique, ce qui conduit à une efficacité de réfrigération élevée, à un faible volume requis, à un faible coût , respect de l'environnement, pas de pollution sonore et de meilleures performances. La recherche de matériaux à effet magnétocalorique géant à l'état massif proche de la température ambiante présente un grand intérêt et s'obtient principalement en faisant varier la composition des matériaux. Les recherches actuelles sur la réfrigération magnétique sont orientées vers l'étude des matériaux nanométriques. Morelli et al sont le premier groupe travaillant sur l'effet magnétocalorique dans des couches minces de films de manganite de lanthane dopés fabriqués en utilisant la technique de décomposition organométallique. Ils ont montré que la morphologie et la composition du film peuvent fournir une augmentation supplémentaire de la magnétisation et de l'entropie totale. Récemment, de nouveaux résultats ont été publiés dans ce domaine. Par exemple, Gd nanostructuré a un comportement magnétocalorique différent par rapport aux homologues en vrac.

Dans ce travail de recherche, nous avons étudié les propriétés structurales, magnétiques et magnétocaloriques des matériaux à base d'éléments de terres rares, $LaCr_2Si_2C$, le multiferoique $TbMn_2O_5$, et la couche mince de Gadolinium afin de montrer les principales caractéristiques recherchées pour la réfrigération magnétique, c'est à dire un grand effet magnétocalorique et une grande capacité de refroidissement. Le problème clé que nous avons abordé après la caractérisation et la simulation de ces différents matériaux est le potentiel des matériaux en couches minces pour le refroidissement des circuits électroniques. Chaque atome d'un matériau a un moment magnétique qui est la somme du spin de ses électrons. La somme du moment magnétique de tous les atomes contenus dans une unité de volume du matériau magnétique représente la magnétisation. L'application d'un champ magnétique faible à un matériau paramagnétique entraîne une variation d'aimantation suffisante pour générer une augmentation notable de la température. Sous le point de Curie, le matériau adopte un comportement ferromagnétique et passé le point de Curie, il adopte un comportement paramagnétique. Ce type de transition est souvent classé dans le second ordre. Le comportement ferromagnétique s'explique par le concept d'énergie d'échange qui représente l'interaction des charges électroniques d'atomes voisins. L'agitation thermique s'oppose à l'effet d'alignement de l'énergie d'échange et l'ordre local qui définit les domaines magnétiques s'estompe à température plus élevée. L'aimantation subit donc une variation brutale à la température de Curie générant une valeur maximale de l'effet magnétocalorique (EMC). L'effet magnétocalorique associé à une transition de phase n'est suffisamment élevé qu'à des températures proches du point de Curie où se produit la variation d'aimantation. Le comportement magnétique de $LaCr_2Si_2C$ est étudié en utilisant les premières méthodes de principe, la simulation de Monte Carlo et l'approximation du champ moyen. Les propriétés structurelles, électroniques et magnétiques sont décrites à l'aide de la méthode ab-initio dans le cadre de l'approximation de gradient généralisée (GGA) et de la méthode d'onde plane augmentée à potentiel complet linéarisé (FP-LAPW) implémentée dans les packages WIEN2K. Nous avons également calculé les termes de couplage entre les atomes magnétiques qui sont utilisés dans le modèle Hamiltonien. Une étude théorique réalisée par approximation du champ moyen et simulation de Monte Carlo dans le modèle d'Ising est utilisée pour mieux comprendre les propriétés magnétiques de ce composé. Ainsi, nos résultats ont montré un ordre ferromagnétique des moments magnétiques Cr en

dessous de la température de Curie de 30 K dans $LaCr_2Si_2C$. D'autres paramètres sont également calculés comme: l'aimantation, l'énergie, la chaleur spécifique et la susceptibilité. De plus, le calcul prédit que le composé $LaCr_2Si_2C$ possède un caractère métallique et l'analyse de l'énergie de différence entre les états FM et AFM a confirmé que le FM est plus stable avec la température de Curie inférieure à 30K. Les travaux futurs sur ce matériau peuvent être orientés vers l'amélioration de T_c pour les applications spintroniques.

Le deuxième composé étudié est le $TbMn_2O_5$, Récemment, un effet magnétocalorique rotatif réversible et géant a été signalé dans le monocristal multiferroïque $TbMn_2O_5$, ouvrant la voie à de nouvelles conceptions de refroidissement magnétique à basse température. Dans cette étude, nous rapportons un travail théorique préliminaire dans le but d'élargir notre compréhension sur les caractéristiques électroniques, magnétiques et donc magnétocaloriques du composé $TbMn_2O_5$. En particulier, l'anisotropie magnétique $TbMn_2O_5$ est analysée en termes de spectres de dichroïsme circulaire magnétique aux rayons X (XMCD) et de spectroscopie d'absorption des rayons X (XAS).
Le composé $TbMn_2O_5$ a une structure orthorhombique constituée d'octaèdres de $Mn^{4+}O_6$ et de bipyramides de $Mn^{3+}O_5$ liés par leurs bords et leurs coins. Une parfaite connaissance des ordres magnétiques des ions Mn^{3+} et Mn^{4+} est essentielle pour une bonne compréhension du caractère multiferroïque du composé $TbMn_2O_5$. Ce matériau possède plusieurs transitions magnétiques. En dessous de 10K, l'ordre magnétique des spins de l'ion Tb apparaît et adopte un ordre antiferromagnétique. Compte tenu de la complexité de ces ordres magnétiques, nous simplifierons le schéma de ces configurations en regardant le plan ab, dans lequel les ions spins Mn sont presque confinés. La vue de face du plan ab montre que la structure cristalline de $TbMn_2O_5$ est formée par deux boucles d'ions manganèse. Chaque boucle est constituée d'une chaîne d'ions manganèse Mn^{4+} - Mn^{3+} - Mn^{3+} - Mn^{4+} - Mn^{3+} qui forme une boucle pentagonale. Les deux boucles partagent deux pyramides $Mn^{3+}O_5$ voisines. Cependant, si un couplage antiferromagnétique entre deux spins voisins est établi, il doit favoriser une disposition antiparallèle sur toute la chaîne. Cependant, ce n'est pas le cas. En effet, géométriquement, on ne peut pas former un ordre antiferromagnétique le long d'une boucle formée par cinq ions manganèse. Cela crée une structure magnétique frustrée qui donne lieu à des ordres magnétiques plus complexes. L'intérêt de ce composé réside dans le couplage entre les ordres magnétiques et électriques, avec la possibilité, d'un

point de vue statique, de manipuler l'aimantation en appliquant un champ électrique. Dans le $TbMn_2O_5$ les excitations hybrides, appelées électromagnons, peuvent être comprises comme des magnons excités par la composante électrique d'une onde électromagnétique. Comprendre les mécanismes derrière ces nouvelles excitations était notre objectif, et la possibilité de moduler ces excitations via un champ électrique et / ou magnétique est également une piste explorée pour des applications futures à définir dans le domaine du transport d'informations, de la réfrigération magnétique et des dispositifs spintroniques pour exemple, ainsi le magnétisme et la ferroélectricité dans $TbMn_2O_5$ sont couplés. D'autre part, le matériau multiferroïque $TbMn_2O_5$ se caractérise également par différentes interactions d'échange impliquant des sous-réseaux d'ions Mn^{4+}, Mn^{3+} et de terres rares R^{3+}, conduisant à un caractère de magnétisme complexe. En conséquence, $TbMn_2O_5$ révèle diverses transitions de phase magnétiques et électriques. Récemment, un effet magnétocalorique rotatif réversible et géant a été mis en évidence dans le monocristal multiferroïque $TbMn_2O_5$, ouvrant la voie à de nouvelles conceptions de refroidissement magnétique à basse température. Nos calculs préliminaires utilisant l'étude de la théorie fonctionnelle de la densité de $TbMn_2O_5$ révèlent qu'il est possible de déterminer certains paramètres clés tels que les moments magnétiques, l'anisotropie magnétique et les structures électroniques qui sont d'un grand intérêt pour l'étude de son comportement entropique (MCE). En particulier, les moments magnétiques obtenus ainsi que les énergies anisotropes sont en bon accord avec les rapports expérimentaux. Cependant, le principal défi reste la simulation de certains paramètres magnétothermiques importants du $TbMn_2O_5$ tels que la chaleur spécifique, l'entropie et les changements de température adiabatiques.

Les techniques de réfrigération développées et potentiellement commercialisables nécessitent des matériaux de réfrigération efficaces qui répondent à de nombreux autres critères tels que la stabilité structurelle, la résistance à l'oxydation ou une bonne conductivité électrique. L'effet magnétocalorique a été largement étudié au cours des quarante dernières années et de nombreuses données expérimentales ont été rapportées dans la littérature. La majorité des études se sont concentrées sur les terres rares et les composés à base de terres rares et de métaux de transition. Pour les applications de réfrigération autour de la température ambiante, l'élément de référence est le gadolinium pur. A sa température de Curie d'environ 292K, ses propriétés

magnétocaloriques ΔS_m et ΔT_{ad} sont d'environ -10 $J.kg^{-1}.K^{-1}$ et 12 K, respectivement avec une variation de champ magnétique de 0 à 5T.

Le troisième composé de cette thèse est le film mince de gadolinium. Le gadolinium métallique est le choix préféré en tant que matériau réfrigérant magnétique pour la plupart des prototypes de régénérateurs magnétiques actifs (AMR) qui ont été développés jusqu'à présent, car il affiche un grand changement d'entropie magnétique parmi les ferromagnets élémentaires avec une température de Curie élevée proche de la température ambiante lorsqu'il subit une seconde ordre de transition de phase magnétique. Dans ce manuscrit, les propriétés magnétocaloriques (MCE) et électrocaloriques (ECE) des films de gadolinium fabriqués (Si / Ta / Gd (100nm) / Pt (3nm)) sont mesurées, dans le but d'obtenir plus d'informations sur la physique derrière l'intéressant électronique et propriétés magnétiques de ce matériau.

Notre film de gadolinium est cultivé à température ambiante sur un substrat de silicium (Si) en utilisant une disposition de pulvérisation avec une pression de base inférieure à 10^{-7} Torr. Une couche tampon de 5 nm de tantale (Ta) a été utilisée ainsi que 3 nm de couche de recouvrement de platine (Pt) pour éviter l'oxydation de la terre rare de gadolinium. L'épaisseur magnétique totale des échantillons est maintenue constante et égale à 100 nm. Les mesures électriques que nous avons effectuées sur cette couche de gadolinium à l'aide d'un PPMS-7T montrent que l'augmentation de la température provoque une légère augmentation de la résistivité électrique. Par conséquent, pour chaque étape de température, la résistance électrique a été mesurée en faisant varier le champ magnétique, et à partir de la variation d'entropie maximale, nous avons trouvé la quantité de chaleur donnée ou retirée de notre couche mince.

Ce manuscrit est divisé en cinq chapitres. Le premier chapitre consiste en un état de l'art de la réfrigération magnétique et des avancées récentes. Le deuxième chapitre présente les méthodes théoriques utilisées pour simuler les différents composés étudiés dans cette thèse basée sur les terres rares. Le troisième chapitre s'intéresse aux outils expérimentaux utilisés à l'Institut Jean Lamour à Nancy pour effectuer les mesures nécessaires de ces travaux. Le quatrième chapitre présente les résultats théoriques obtenus à l'aide de la théorie fonctionnelle de la densité DFT et des calculs ab-initio pour étudier les propriétés électriques et magnétiques des terres rares. Enfin, le cinquième chapitre est réservé aux résultats expérimentaux de notre couche mince de gadolinium.

Table of Contents

Introduction

Magnetic refrigeration is becoming more reliable which will enable it to replace conventional refrigeration systems, a change which is desirable due to the advantages of using the magnetocaloric effect (MCE) for magnetic refrigeration application which leads to high refrigeration efficiency, small volume requirement, low cost, environmental friendliness, no noise pollution and better performance. The search for giant magnetocaloric effect materials in the bulk state close to room temperature are of great interest and are primarily obtained by varying the composition of materials. The current research on magnetic refrigeration is oriented towards the study of nanoscale materials. Morelli et al are the first group working on the magnetocaloric effect in thin layers of doped lanthanum manganite films fabricated using the metalorganic decomposition technique. They showed that the film morphology and composition may provide a further increase in the magnetization and total entropy. Recently, some new results have been published in this area. For example, Gd nanostructured has different magnetocaloric behavior when compared with the bulk counterparts.

In this thesis, three types of compounds have been studied. The First one is $LaCr_2Si_2C$. The magnetic behavior of this compound is investigated, using first principle methods, Monte Carlo simulation (MCS) and mean field approximation (MFA). The structural, electronic and magnetic properties are described using ab initio method in the framework of the Generalized Gradient Approximation (GGA), and the Full Potential-Linearized Augmented Plane Wave (FP-LAPW) method implemented in the WIEN2K packages. We have also computed the coupling terms between magnetic atoms which are used in Hamiltonian model. A theoretical study realized by mean field approximation and Monte Carlo Simulation within the Ising model is used to more understand the magnetic properties of this compound. Thereby, our results showed a ferromagnetic ordering of the Cr magnetic moments below the Curie temperature of 30 K ($T_c < 30$ K) in $LaCr_2Si_2C$. Other parameters are also computed as: the magnetization, the energy, the specific heat and the susceptibility. This material shows the small sign of supra-conductivity; and future researches could be focused to enhance the transport and magnetic properties of this system. The second compound is $TbMn_2O_5$, Recently, a reversible and a giant rotating magnetocaloric effect has been pointed out in the multiferroic $TbMn_2O_5$ single crystal, opening the way for new designs of low-temperature magnetic cooling. In this study, we report a preliminary theoretical work with the aim of enlarging our understanding on the electronic, magnetic and accordingly magnetocaloric features of the $TbMn_2O_5$ compound. Particularly, the $TbMn_2O_5$ magnetic anisotropy is analyzed in terms of X-ray magnetic circular dichroism (XMCD) and X-ray absorption spectroscopy (XAS) spectra. The third compound in this thesis is Gadolinium thin film. Metallic Gadolinium is the favorite choice as a magnetic refrigerant material for most active magnetic regenerator (AMR) prototypes that have been developed so far because it displays a large change in magnetic entropy among

elemental ferromagnets with high Curie temperature near room temperature when it undergoes a second order magnetic phase transition. In this manuscript, the Magnetocaloric (MCE) and electrocaloric (ECE) properties of fabricated Gadolinium films (Si/Ta/Gd(100nm)/Pt(3nm)) are measured, aiming to get more insight about the physics behind the interesting electronic and magnetic properties of this material.

This manuscript is divided into five chapters. The first chapter consists in a state of the art of magnetic refrigeration and recent advances. The second chapter presents the theoretical Methods used to simulate the different compounds studied in this thesis based on rare earth. The third chapter focuses on experimental tools used at the Jean Lamour Institute in Nancy to make the necessary measurements of this work. The fourth chapter, the fourth chapter presents the theoretical results obtained using the Density Functional Theory DFT and ab-initio calculations to study the electrical and magnetic properties of rare earth materials. Finally, the fifth chapter is reserved for the experimental results of our thin layer of Gadolinium.

Chapter I

Magnetocaloric effect and magnetic refrigeration: General and recent advances

I.1 Introduction

Magnetic refrigeration is an ecological technology unlike conventional refrigeration systems which use polluting gases. It uses a solid material as a coolant and a heat transfer fluid, usually water or oil, to transfer heat between the hot and cold sources. In this first chapter we present the potential of magnetic refrigeration, it is a technology which encompasses several disciplines such as magnetism, materials, mechanics, thermodynamics, thermics, fluid mechanics, all these disciplines are coupled together to operate a magnetic refrigeration system. Today, research on the theme of magnetic refrigeration is oriented towards 3 main areas of research, it concerns the magnetocaloric material (more efficient, giant EMC and less expensive), the source of magnetic field (shape and geometry) and system magnetic refrigeration (design and production).

I.2 Rare earth elements

The lanthanum and the lanthanides form a series of fifteen metallic elements of very similar chemical properties, which are also more commonly known by the name, moreover improper, “rare earths” (because they were first extracted as oxides resembling alkaline earth, from uncommon minerals).

In the classification periodical of the elements, the lanthanides occupy, with the lanthanum, one and the same box of the table; this peculiarity results from their electronic structure, which is identical for the layers and differs from one element to the next only by adding an electron in the layer deep 4f (hence the name 4f elements that physicists sometimes give them).

The rare earths have an electronic configuration of the form [Xe] $4f^n5d^16s^2$, with $1 \le n \le 13$ (in some cases, it is possible to have [Xe] $4f^n5d^16s^2$ with: $1 \le n \le 14$). As a rule, they lose three electrons to give triplicate ionized ions (with some exceptions, such as europium which exists in the form Eu^{2+}) and therefore empty electrons from layers 5d and 5s making the outermost electrons. Given the small spatial extension of the 4f orbitals, the rare earths will therefore have very close properties in terms of physical bonding and reactivity, which explains why it is so difficult to separate them.

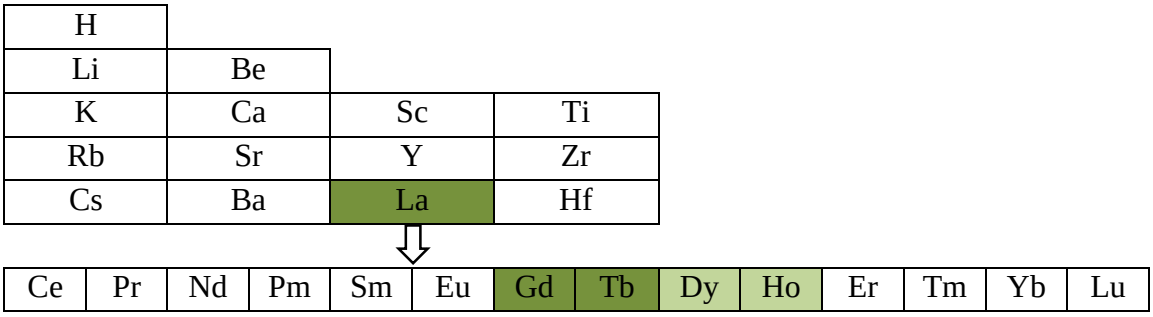

FIGURE 1.1 Position of the lanthanides in the periodic table with their atomic number.

Lanthanides are still associated in minerals, although in fairly high proportions variables. They are also associated with yttrium, their counterpart located above them in the column III A of the periodic table, and scandium in the designation of rare earths. Thorium, which is part of actinides, has properties similar to lanthanides and is often obtained at the same time as them. The predominance in minerals of either light lanthanides or yttrium and heavy lanthanides, led to subdivide the family into a “ceric group” (from lanthanum to gadolinium) and an “yttrique group” (from gadolinium to lutetium). Nevertheless, the similarity of the chemical properties of lanthanides has long been the major obstacle to the development of their study and their industrial use. It's only with the development of the nuclear industry and the development of new separation techniques (ion exchange, solvent extraction) that the lanthanide compounds are become more common chemicals. The lanthanides are then considered to be important industrial materials by the specificity of their characteristics, all the more so than their minerals have turned out to be much more abundant than previously assumed. The “rare earths”, contrary to their name, are fairly widespread elements: their overall concentration in the earth's crust is around 0.016%, that is to say as high than that of zinc, ten times more than that of lead, a thousand times more than that of silver; the most abundant element in the family, cerium, is between copper and tin, two rarer, thulium and lutetium, between mercury and cadmium. But, because of their widely dispersed on the surface of the globe, their relative abundance has only been demonstrated gradually, as detection and analysis methods have developed and that the search for their minerals has grown. The lanthanide minerals are very numerous, among the main ones, we can mention carbonates and fluocarbonates, phosphates and silicates.

The annual global production of lanthanides, expressed in oxides, in 2000, amounted to around 50 000 tons, mainly from the United States and from China. The lanthanides have become in a few years important elements by the originality of their properties and the specific applications that one could draw from it in advanced techniques (electronics, magnetism, catalysis…).

I.3 From magnetocaloric material to refrigeration

Magnetic refrigeration at room temperature is an alternative solution to conventional cooling technology that uses CFC and HCFC, allowing achieve more efficient and less polluting systems. It relies on effect materials "EMC" magnetocaloric which can heat up or cool down when magnetized or disarming them. This effect is maximal around the Curie temperature of the material and can be exploited to make a thermomagnetic cycle equivalent to the thermodynamic cycle classic compression and expansion of a gas. This is a recent topic and multidisciplinary because even if the EMC has been known for more than a century, research in this domain only really started about 15 years ago [1-2], since then, advances important and multiple were carried out on the fundamental and applicative scale in the material and magnetocaloric system (see statistics). This first chapter first describes the history and the principle of EMC, considering an approach thermodynamic. Then the application aspect is treated by explaining how to use the EMC to make cold, describing the different refrigeration cycles as well the cycle magnetothermic of active regenerative magnetic refrigeration. Then the main families of materials at giant EMC are presented with an emphasis on their structural, thermodynamic and magnetic properties by identifying the criteria allowing the development of new, more efficient materials.

I.3.1 Historical

EMC is the change in temperature or entropy of a magnetic material subjected to a variable magnetic field. This phenomenon was discovered by Emil Warburg, professor at the Strasbourg University, in 1881 [3]. By placing iron in a magnetic field, he observed a rise in temperature and a fall in temperature while removing it. In 1918, a theoretical explanation by a thermodynamic approach was given to the Paris Academy of Sciences by Pierre Weiss and Auguste Piccard [4]. It was not until 1926-1927 that the physicist Peter Debye [5] and the chemist William Giauque [6] were able to explain this phenomenon thermodynamically and suggested its use in processes allowing reaching low temperatures by a process called adiabatic magnetization/demagnetization. Shortly after this discovery, a first prototype produced by William Francis Giauque and P.D. McDougall experimentally verified this mechanism. By using the paramagnetic salt of

gadolinium $Gd_2(SO_4)_3$, $8H_2O$, this device under a field of 0.8 Tesla made it possible to reach a temperature of 0.25 K starting from an initial temperature of 1, 5 K [7-8]. Thanks to this powerful and profound research, W. F. Giauque received the Nobel Prize in chemistry in 1949 (68 years after the discovery of the magnetocaloric effect by Emil Warburg). It was for his contributions in the field of thermodynamic chemistry, in particular regarding the behavior of substances at extremely low temperatures.

"*The adiabatic demagnetization method of producing low temperatures was an unexpected by-product of our interest in the third law of thermodynamics. […]. By means of appropriate thermodynamic equations it was possible to calculate the change of entropy when a magnetic field is applied. I was greatly surprised to find, that the application of a magnetic field removes a large amount of entropy from this substance, at a temperature so low that it had been thought that there was practically no entropy left to remove.*"

Speech on reception of the Nobel Prize in Chemistry by William Giauque,
"Some consequences of low temperature research in chemical thermodynamics",
Nobel Lecture,
December 12, 1949 [9].

I.3.2 Principle of the magnetocaloric effect

EMC is defined as the change in temperature of certain magnetic materials due to the variation of an external magnetic field. He is the result of the variation of the magnetic entropy of the solid from the coupling between magnetic moments and the external magnetic field. From a thermodynamics point of view, the total entropy S of a magnetocaloric compound is a combination of magnetic entropy S_M, network entropy S_R, and electronic entropy S_E. The total entropy S is a function of the temperature T and the induction B in a magnetocaloric material, it is given by:

$$S_{(T,B)} = S_M + S_R + S_E \tag{I.1}$$

Magnetic entropy S_M derived from the distribution of spins in the material. Network entropy S_R relates to the crystal lattice of atoms and electronic entropy S_E is associated with the thermal contribution of electrons in the material. The latter can be considered negligible in certain materials. Network entropy and electronics entropy are independent of the applied magnetic field H while the magnetic entropy strongly depends on the magnetic field. If the magnetization process is adiabatic, without heat exchange with the outside, the total entropy remains constant $(\Delta S = 0)$, then the network entropy $(S_E \to 0)$ must compensate for the loss of magnetic entropy $(\Delta S_M = -\Delta S_R)$. Otherwise the loss of magnetic agitation of spins is compensated by the

increase of the thermal agitation of the network. Thus, when a magnetic field is applied, the magnetic moments are aligned (thus reducing their disorder, therefore magnetic entropy), this having the consequence increased network entropy (increased disorder in the atomic arrangement), so the temperature of the compound. Conversely, when deleting the field, magnetic entropy increases (disorder of magnetic moments), thereby reducing network entropy and the temperature of the system [9]. Adiabatic magnetization results in a temperature variation called the variation of the adiabatic temperature ΔT_{ad} (figure I.2). If the process is isothermal, i.e. without temperature variation, the application of a magnetic field on a compound generates a variation of magnetic entropy.

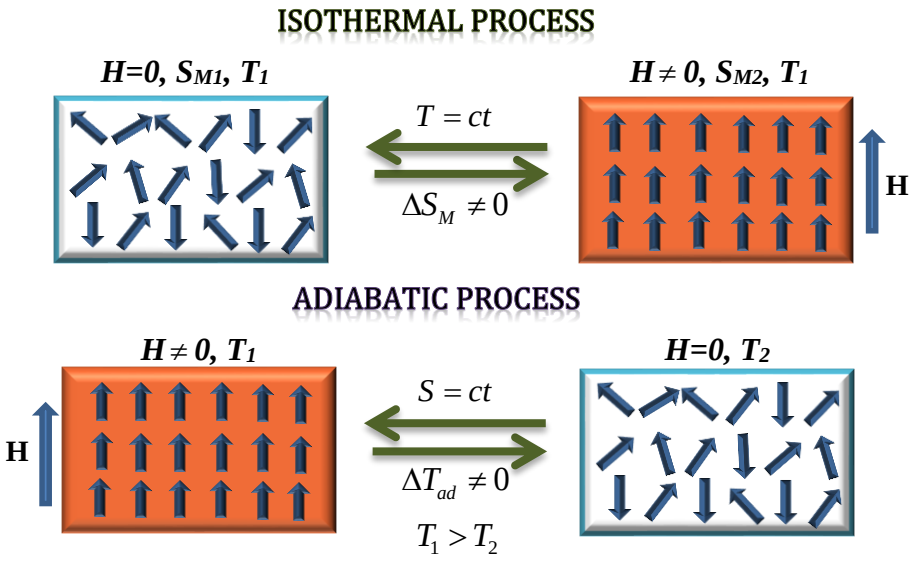

FIGURE I.2 Principle of the magnetocaloric effect.

Energy is instantly transferred as heat. Magnetic entropy variation isotherm following the variation of a magnetic field is noted ΔS_M (figure I.2).
The two parameters ΔS_M and ΔT_{ad} are characteristic values of the magnetocaloric effect, as a function of the initial temperature T_1 and the value of the strength variation of the magnetic field.

Figure (I.3) presents the diagram of the two curves of total entropy as a function of the temperature for two different magnetic fields (H_1 and H_2 with $H_1 < H_2$). The curve entropy with lower magnetic field has higher entropy values than at larger magnetic field. The two previously mentioned processes are represented by blue and green lines. The ΔS_M represents the variation of entropy in the isothermal process (T = Cst, blue line) of magnetic field variation and the ΔT_{ad} represents the temperature variation during the adiabatic process (S=Cst, read line). These processes are all the more

important as the difference between the two curves is big. To maximize this difference, the field H_1 is chosen null (H_1=0) and the field H_2 is high (H_2 > 1T).

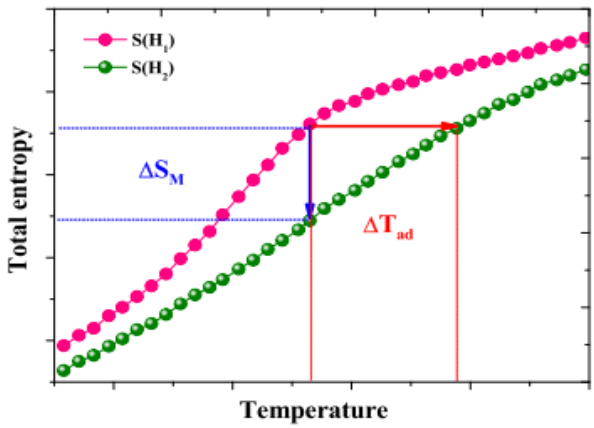

FIGURE I.3 Diagram of total entropy as a function of temperature for two different magnetic fields H_1 and H_2 (H_1 <H_2)

Figure (I.4) shows the variation of magnetic entropy as a function of the temperature. The variation of magnetic entropy passes through a maximum at the temperature of magnetic transition (T_C). It rapidly decreases above (paramagnetic phase) and below (ferromagnetic phase) of the magnetic transition.

The EMC is maximum near the magnetic transition temperature (Curie temperature in the case of ferromagnetic materials) and depends on the nature of the transitions (Figure I.4 below). During a transition of the 1st order the magnetization evolves very quickly with the temperature, the variation of entropy is therefore very large at the transition temperature. On the other hand, the peak of variation of entropy is very narrow. The range of use of a material having a first order transition, for magnetic refrigeration, would therefore be very limited in temperature. In addition, there is often a thermal hysteresis which interferes with the cooling cycle when applying these materials for magnetic refrigeration [10-11]. For the 2nd order transitions, the magnetic transition is much wider, the variation of the maximum magnetic entropy ΔS_M^{Max} remains high over a wider temperature range. In addition, thermal hysteresis is nonexistent, unlike 1st order transitions.

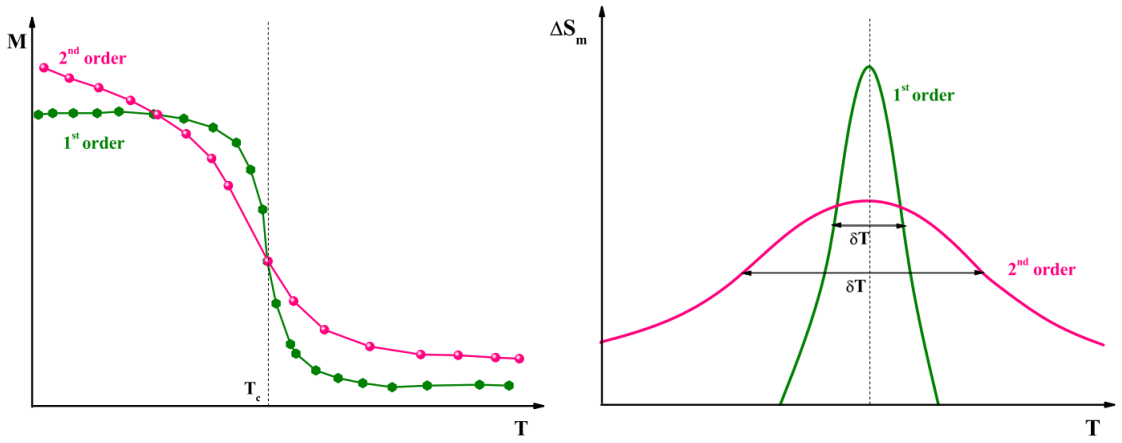

FIGURE I.4 Relationship between the magnetic transition (left) and the entropy variation (right)

To better understand the physical origin of the magnetocaloric effect, it is useful to recall the thermodynamic properties of a magnetic material under an applied magnetic field, as well as the various parameters which intervene in magnetic refrigeration.

I.3.3 Analysis and thermodynamic relationships

To analyze the magnetocaloric effect, it is useful to understand the thermodynamics of the system. A thermodynamic system is characterized by extensive state variables (depend on the size of the system considered) and intensive variables (do not depend on it). For a magnetic material, the extensive variables are the volume V, the internal energy U and the entropy S. The intensive variables are the pressure p, the temperature T and the amplitude of the magnetic field H (or equivalently the amplitude of the magnetization M). The internal energy U is a thermodynamic function which characterizes the energy of a closed system and the entropy S characterizes its disorder.

The internal energy for a magnetic material can be written as follows:

$$U = U(S,V,H) \tag{I.3}$$

Its differential is described as follows:

$$dU = TdS - PdV - MdH \tag{I.4}$$

The thermodynamic potential adapted to the description of such a system is the free enthalpy G (Gibbs energy) which derives from internal energy. For a magnetic system, it is defined at constant pressure by a function of temperature T, pressure P and field H. It is given by:

(I.5)

$$G = U - TdS + PV - MH$$

Its derivative total is written:

$$dG = VdP - SdT - MdH \tag{I.6}$$

The entropy, the magnetization and the volume are given by the partial derivatives of Gibbs free energy:

$$S(T,H,P) = -\left(\frac{\partial G}{\partial T}\right)_{P,H} \tag{I.7}$$

$$M(T,H,P) = -\left(\frac{\partial G}{\partial H}\right)_{\mathrm{T,P}} \tag{I.8}$$

$$V(T,H,P) = \left(\frac{\partial G}{\partial P}\right)_{\mathrm{T,H}} \tag{I.9}$$

So:

$$dG = \left(\frac{\partial G}{\partial P}\right)_{T,H} dP + \left(\frac{\partial G}{\partial T}\right)_{P,H} dT + \left(\frac{\partial G}{\partial H}\right)_{\mathrm{T,P}} dH \tag{I.10}$$

As the materials are generally in solid form, the effects due to pressure and volume are therefore negligible (P = Cst, dP = 0). After simplification, the exact total differential of G can be written:

$$dG = \left(\frac{\partial G}{\partial T}\right)_{P,H} dT + \left(\frac{\partial G}{\partial H}\right)_{T,P} dH \tag{I.11}$$

Mathematically, the second crossed derivatives of the function are identical, then:

$$\frac{\partial}{\partial T}\left(\frac{\partial G}{\partial T}\right) = \frac{\partial}{\partial H}\left(\frac{\partial G}{\partial T}\right) \tag{I.12}$$

By simplifying the equation (I.12) we find the famous relation of “Maxwell”:

$$\left(\frac{\partial M}{\partial T}\right)_{P,H} = \left(\frac{\partial S}{\partial H}\right)_{P,\mathrm{T}} \tag{I.13}$$

Thanks to equation (I.13), we can determine the variation of the entropy associated with the EMC at constant temperature corresponding to the variation of the isothermal entropy of figure (I.3).

It can be determined as follows:

$$\int_{H_1}^{H_2}\left(\frac{\partial M}{\partial T}\right)_H dH = \int_{H_1}^{H_2}\left(\frac{\partial S}{\partial H}\right)_T dH = \Delta S\left(T, H_1 \to H_2\right)$$
$$\Delta S\left(T, H_1 \to H_2\right) = \int_{H_1}^{H_2}\left(\frac{\partial M}{\partial T}\right)_H dH \qquad \text{(I.14)}$$

The variation $\Delta S\left(T, H_1 \to H_2\right)$ is often called the variation of magnetic entropy ΔS_M. Experimentally this variation is determined from the data $M_B(T)$ or $M_T(B)$. Digital data processing is carried out in the form:

$$\Delta S = \sum_i \frac{M_{i+1} - M_i}{T_{i+1} - T_i}\Delta H_i \qquad \text{(I.15)}$$

S being a variable of P, H and T, its differential takes its form:

$$S = S\left(P, H, T\right)$$

$$dS = \left(\frac{\partial S}{\partial P}\right)_{T,H} dP + \left(\frac{\partial S}{\partial T}\right)_{P,H} dT + \left(\frac{\partial S}{\partial H}\right)_{T,P} dH \qquad \text{(I.16)}$$

The heat capacity of a material is defined as the amount of energy to be provided by heat exchange to raise its temperature by one degree. At constant pressure the specific heat is given by:

$$C_{P,H} = \left(\frac{\delta Q}{dT}\right)_{P,H} \qquad \text{(I.17)}$$

According to the second principle of thermodynamics, the variation of entropy can be written as:

$$dS = \frac{\delta Q}{T} \qquad \text{(I.18)}$$

In a constant magnetic field and at constant pressure, the expression of the specific heat can be written as:

$$C_{P,H} = T.\left(\frac{\partial S}{\partial T}\right)_{P,H} \qquad \text{(I.19)}$$

Using the Maxwell relation (equation I.12) and the heat capacity thus defined, and considering the system at constant pressure, the equation (I.14) is given as follows:

$$dS = \frac{C_{P,H}}{T} dT + \left(\frac{\partial M}{\partial T} \right)_{P,H} dH \tag{I.20}$$

From the equation (I.20), in the case of an isothermal environment (dT= 0), dS is the variation of entropy corresponding to the infinitesimal variation dH. We find the variation of the entropy defined in figure (I.3) and the equation (I.14) with a variation of magnetic field $\Delta H = H_2 - H_1$.
The variation of the entropy does not only depend on the variation of the external magnetic field, but also on the variation of the magnetization as a function of the temperature. This effect is maximum when $(\partial M/\partial T)$ is significant in the vicinity of the magnetic phase transition.

For $(dH = 0)$, thanks to equation (I.20) the entropy can be determined from the heat capacity:

$$dS = \frac{C_{P,H}}{T} dT \tag{I.21}$$

$$S(T,H) = \int_0^T \frac{C_{P,H}}{T} dT \tag{I.22}$$

By considering a variation of magnetic field $\Delta H = H_2 - H_1$, the variation of the entropy due to ΔH can also be written:

$$\Delta S(T, H_1 \to H_2) = \int_0^T \frac{C_{P,H_2} - C_{P,H_1}}{T} dT \tag{I.23}$$

Then we can determine the variation of entropy from calorific measurements. The equation (I.23) shows that the variation of the entropy which depends on the inverse of the temperature increases when approaching absolute zero. Considering an adiabatic environment ($dS = 0$), the expression of the temperature variation at constant pressure corresponding to the adibatic temperature variation ΔT_{ad} is determined from equation (I.19):

$$dT = -\frac{T}{C_{P,H}} \left(\frac{\partial M}{\partial T} \right)_{P,H} dH \tag{I.24}$$

$$\Delta T\left(T, H_1 \to H_2\right) = -\int_{H_1}^{H_2} \frac{T}{C_{P,H}} \left(\frac{\partial M}{\partial T}\right)_{P,H} dM \qquad \text{(I.25)}$$

Specific heat measurements are longer and more difficult to implement than the field-based magnetization measurements. For these reasons, measurements of ΔT_{ad} are less frequent in the literature and are generally carried out after the determination of ΔS_M and C_P at a given field H using the equation below derives from equation (I.25):

$$\Delta T_{ad}\left(H\right) = -\frac{T \times \Delta S_M\left(H\right)}{C_P\left(H\right)} \qquad \text{(I.26)}$$

The magnetocaloric effect is maximal around the Curie temperature T_C of magnetic materials, which corresponds to the transition from the ferromagnetic or ferrimagnetic phase (ordered state) to the paramagnetic phase (disordered state). We therefore seek to use magnetocaloric materials at a temperature close to T_C (in general close to ambient temperature for ambient applications) having a maximum magnetocaloric effect.

I.3.4 Magnetocaloric effect and Magnetic refrigeration

Magnetic refrigeration around room temperature is a promising new technology for manufacturing cold because it makes it possible to produce refrigeration or air conditioning systems with high energy efficiency and not using gas to greenhouse effect or destroyers of the ozone layer. It is based on materials with a giant magnetocaloric effect. EMC is an intrinsic property of magnetic materials which results in an increase or a decrease in their temperature during their adiabatic magnetization or demagnetization. It is maximum around the order / disorder temperature (Curie temperature for ferromagnetics). We therefore have the possibility of carrying out, using a magnetic cycle, the equivalent cycle of a conventional thermal machine, all the more so since certain materials have a giant magnetocaloric effect around room temperature.

In compression refrigeration, the refrigerant gas is compressed and its temperature increases. The induced heat is then dissipated towards the hot source. During its expansion, the refrigerant gas cools allowing to absorb the heat from the cold source or the space to be cooled. This is the operating cycle of conventional compression refrigeration. This cycle is repeated n times during the operating time. In the case of magnetic refrigeration, it is the material which undergoes the cycle, and not the gas. The magnetization of the material ensures its heating and vice versa with its demagnetization. The energy contained in the material is extracted by a heat transfer fluid, generally water. In order to understand the thermodynamics of magnetic refrigeration, it is important to define the different existing magnetic cycles.

I.4 Thermodynamic cycles

To produce cold, conventional refrigeration systems are based on compression-decompression (expansion) cycles of a refrigerating gas mechanism which is comparable to that used in magnetic refrigeration systems (Magnetization-demagnetization of magnetocaloric materials). The magnetic refrigeration cycle is made possible by coupling the solid magnetic material, seat of the EMC, to a fluid ensuring thermal transfer. To reach higher temperature differences the system must operate on a magnetic refrigeration cycle. Many magnetic refrigeration cycles exist, with their equivalents in conventional thermodynamics. These are the Carnot, Brayton, Ericsson cycles. Among which, the Ericsson and Brayton cycles are the only ones applicable at room temperature, they use a regenerator to obtain a large temperature range and they are easy to handle [12].

To increase the temperature variation, regenerative cycles AMRR (Active Magnetic Regenerative Refrigeration) can be used [2]. The magnetocaloric material is then subjected to a series of magnetization and demagnetization cycles. The different magnetic cycles will be briefly explained in the following section.

I.4.1 Carnot's magnetic cycle

The Carnot cycle is composed of two isentropic processes and two isothermal processes. It has a potentially ideal efficiency because the heat transfer is done there during isothermal steps, but the implementation of this cycle is complex and difficult because it requires the use of four different amplitudes of magnetic field. The T-S diagram of the magnetic Carnot cycle is illustrated in Figure (I.6). It is made up of four steps:

- Adiabatic magnetization (A→ B): the material is magnetized and its temperature increases, it heats up instantly without exchanging heat with the outside.

- Isothermal magnetization ($B \rightarrow C$): the applied magnetic field is increased. The magnetization is isothermal ($T = Cst$), that is to say that all the heat previously produced is transferred to the hot source (Q_{Hot}).

- Adiabatic demagnetization ($C \rightarrow D$): the applied magnetic field is reduced. The material cools instantly without exchanging heat with the outside.

- Isothermal demagnetization ($D \rightarrow A$): the material is demagnetized and the temperature is kept constant. The material absorbs heat from the cold source (Q_{cold}).

An important criterion for evaluating systems is the coefficient of performance COP (Coefficient Of Performance). In the application of refrigeration, it represents the ratio of the energy taken from the cold source (Q_{cold}) and the work provided to the system W:

$$COP = \frac{Q_{cold}}{W} = \frac{T_{cold}.(S_A - S_D)}{T_{Hot}.(S_B - S_C) - T_{cold}.(S_A - S_D)} \quad (I.27)$$

From figure (I.5), we notice that $S_A - S_D = (S_B - S_C)$, then the relation of the COP becomes:

$$COP = \frac{Q_{cold}}{W} = \frac{T_{cold}}{T_{Hot} - T_{cold}} \quad (I.28)$$

This COP value constitutes the theoretical limit of the refrigeration system that it will be impossible to overtake. However, in practice, magnetization and demagnetization areothermal are very difficult to achieve.

The EMC has a very fast kinetics, it would therefore be necessary dissipate energy extremely quickly or magnetize extremely slowly to keep the temperature constant.

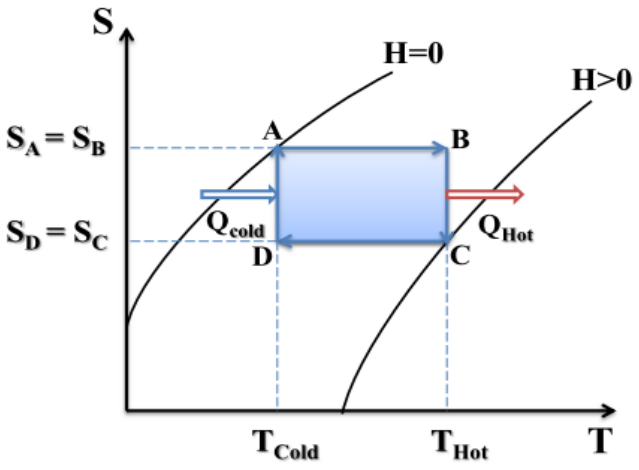

FIGURE I.5 Carnot magnetic cycle

I.4.2 Ericsson magnetic cycle

The Ericsson magnetic cycle (Figure I.6) consists of two isothermal processes and two isofield processes [13]. In practice, it is advantageous to have a temperature difference between the sources which is independent of the adiabatic temperature difference. This cycle provides this temperature difference between the heat sources. It requires a thermal regenerator for its operation (accumulating the heat of the hot fluid and heating the cold fluid). It is composed of four stages:

- Isofield process 1 ($A \rightarrow B$): the material absorbs the heat stored in the heat transfer fluid during the isofield process ($H = Cst$).
- Isothermal process 1 ($B \rightarrow C$): the material is magnetized and gives up heat to the hot source (Q_{Hot}) while keeping the same temperature (T_{Hot}).
- Isofield process 2 ($C \rightarrow D$): the material loses heat (isofield cooling) to the benefit of ($A \rightarrow B$). The heat is discharged to the heat transfer fluid.
- Isothermal process 2 ($D \rightarrow A$): the material is demagnetized, it will reabsorb the heat from the cold source (Q_{cold}) to keep the isothermal process (T_{cold}).

The coefficient of performance is given by the following relation:

$$COP = \frac{Q_{cold}}{W} = \frac{T_{cold}.(S_A - S_D)}{T_{Hot}.(S_B - S_C) - T_{Hot}.(S_A - S_D)} \tag{I.29}$$

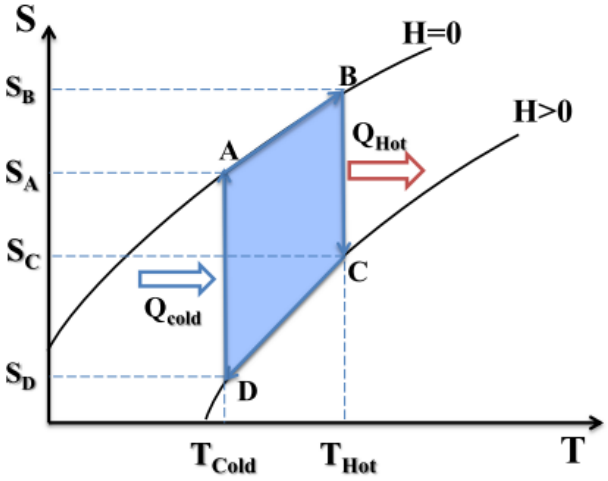

FIGURE I.6 Ericsson magnetic cycle

I.4.3 Brayton magnetic cycle

The Brayton cycle is one of the most basic cycles of magnetic refrigeration. Figure (I.7) shows the mechanism of the Brayton cycle. The latter is based on two processes: isofield (constant magnetic field) and adiabatic (constant total entropy) [14]. The four cycle stages are described as follows:

- Adiabatic magnetization ($A \rightarrow B$): the material is magnetized ($H > 0$) and its temperature increases by $\Delta T = (T_B - T_A)$.
- Isofield cooling ($B \rightarrow C$): The already magnetized cooling material is cooled under constant field. The heat transfer fluid circulates through the refrigerant, it absorbs part of this thermal charge and discharges it to the hot source (Q_{Hot}).
- Adiabatic demagnetization (C → D): the magnetic field is suppressed and the temperature of the material decreases by $\Delta T = (T_D - T_C)$.
- Isofield heating (D → A): this process is at zero magnetic field. The refrigerant can then absorb a thermal load from the cold source (Q_{cold}).

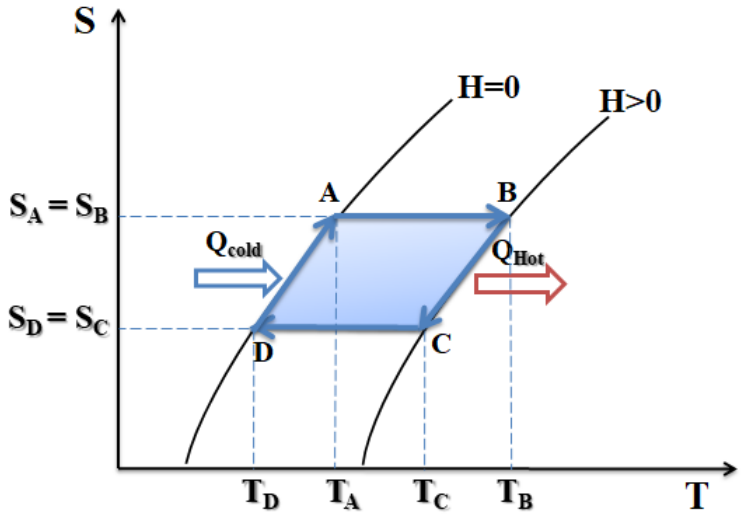

FIGURE I.7 Brayton magnetic cycle

The coefficient of performance (COP) is given by the general formula described below:

$$COP = \frac{Q_{cold}}{W} \tag{I.30}$$

I.4.4 AMRR cycle (Active Magnetic Regenerative Refrigeration)

The AMRR cycle is the most promising and effective for applications near ambient temperature. The first AMRR cycle was described in 1983 by J. A. Barclay [15-16]. The latter has shown that it is possible to reach temperature differences much greater than the adiabatic temperature variation of the refrigerant material by using it simultaneously as a regenerator and as the active magnetic component. The magnetic material is both the seat of the magnetocaloric effect and the thermal regenerator. Each slice of regenerator produces its own magnetic Brayton refrigeration cycle and transports the thermal load over a few degrees, from one slice to another, in the direction of fluid flow, from the cold source to the source hot. It is therefore not a single cycle, but an infinity of simultaneous cycles.

The AMRR cycle is used in most prototypes of magnetic refrigeration at neighborhood of the room. Regeneration in magnetic refrigeration systems allows the heat rejected by the network in a stage of the cycle to be restored and returned to the network in another stage of the same cycle [12]. So the capacity used for cooling the network load can be used effectively to increase the effective variation of entropy and the resulting temperature difference [17]. Indeed, this cycle makes the best use of the magnetocaloric effect in order to obtain differences in high temperatures between the hot and cold source of a heat production system cold.

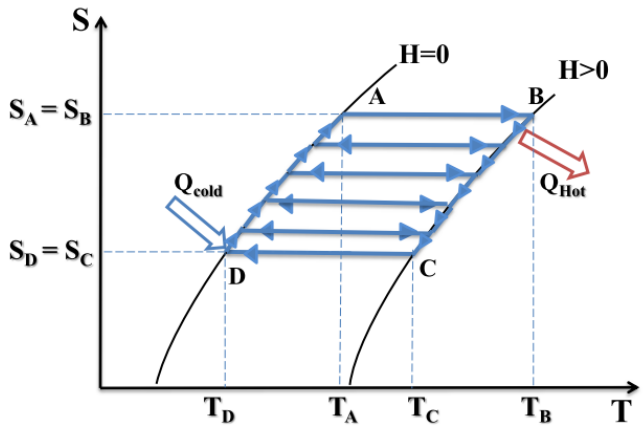

FIGURE I.8 AMRR magnetic cycle

The figure (I.8) represents the thermodynamic cycles of the AMRR cycle. The AMRR cycle consists of four steps, two adiabatic (magnetization / demagnetization) and two isofield (cooling and heating: flow of heat transfer fluid ensuring heat exchange between the cold zone and the hot zone).
AMRR has four steps which are:

- Magnetization of the material, the temperature then increases all along the bed regenerative by magnetocaloric effect. The temperature of the material, hot side, becomes greater than that of the hot tank.

- Fluid flow from the cold tank to the hot tank. This leads to bed temperature to drop in contact with the initially cold fluid (coming from the tank cold). As for the fluid, its temperature will increase. During this step, the bed rejects its heat to the fluid and if this phase is long enough, the material returns to its initial temperature.

- Demagnetization of the material resulting in a drop in its temperature.

- Fluid flow in the opposite direction from the hot tank to the cold tank. This fluid, initially warm, will exchange with the bed, which will allow it to return to its initial temperature.

Moreover, the regenerating bed can be produced by superimposing several composition materials different in order to widen the range of temperature variation and therefore to widen the range system usage. The coefficient of performance (COP) is given by the general formula described below:

$$COP = \frac{Q_{cold}}{W} \tag{I.31}$$

The amount of heat absorbed at the cold source between T_A and T_D is given by:

$$Q_{clod} = \int_D^A T.dS \tag{I.32}$$

I.5 Magnetocaloric materials: reference material

The magnetocaloric effect appears in all magnetic materials. As we have seen previously, the variation in entropy is greater the greater the variation in magnetization ($\partial M / \partial T$). Its value is a maximum at the Curie temperature, temperature at which a material changes magnetic order (ferromagnetic-paramagnetic transition). The so-called “first order” phase transition implies a large variation in magnetic entropy (increases the EMC) but to the detriment of a low temperature range over which the effect is significant (Figure I.4). Coçnversely, the so-called “second order” transitions imply a small variation in magnetic entropy but over a large temperature range T. There are a very large number of magnetocaloric materials which have been studied since the discovery of the giant EMC. Many experimental data concerning different

magnetocaloric materials have been reported in the literature. The majority of studies have focused on rare earths and compounds based on rare earths and transition metals. For applications of magnetic refrigeration around room temperature, the material must have a giant magnetocaloric effect well extended around room temperature. By giant EMC, we mean high temperature variations (a few degrees to a few tens of degrees) for magnetic inductions accessible by permanent magnets (1 to 2T) or superconductive electromagnets. In the following section, examples of magnetocaloric materials already studied in the literature will be cited.

I.5.1 Gadolinium "Gd"

Gadolinium (Gd) is the reference material used in most prototypes of magnetic refrigeration at room temperature (see the section: review on prototypes of magnetic refrigeration). It was the first material which made it possible to validate the principle of magnetic refrigeration [2, 18]. It belongs to the Lanthanide family with a second order magnetic transition (ferromagnetic-paramagnetic) at 292 K with an absence of magnetic hysteresis (spin-orbit coupling is zero (L = 0)) [19]. Given its high magnetic moment (7μB/Gd atom from the valence layer $4f^7$), it can generate a relatively high magnetocaloric effect (≈ 2 K/T) with a variation of magnetic entropy ΔS_M^{Max} around 4J/Kg.K to a magnetic field of 2 Tesla [20].

Gadolinium (Gd) also has the advantage of being an easy to obtain compound (pure element) and easy to use due to its great ductility and malleability. However, in despite its intrinsic properties and its magnetocaloric performance at room temperature, this rare earth presents multiple disadvantages including its oxidation like other earths rare, its prohibitive price (up to 5000€/Kg), and its limited reserves, something which discards its use in refrigeration systems for the general public. It is therefore important to find other magnetocaloric materials with interesting properties. This problem has pushed scientists to look for other alternative materials with interesting and motivating properties (low cost and significant magnetocaloric effect). Among the most commonly cited materials at present are the families $Gd_5(Si_xGe_{1-x})_4$, $MnFeP_{1-x}As_x$, MnAs and its derivatives, Ni-Mn-Ga, $LaFe_{13-x}Si_x$ and manganite perovskites.

I.5.2 Selection criteria for magnetocaloric materials

As already described in the analysis and thermodynamic relationships section, the two important criteria describing the magnetocaloric properties of a material are the maximum variation of magnetic entropy ΔS_M and the variation of adiabatic temperature ΔT_{ad}. However, these two criteria do not make it possible to obtain a complete estimate of the magnetocaloric performances of materials. Two other characteristic values, which

include a combination of ΔS_M and ΔT, make it possible to more precisely assess and compare the magnetocaloric refrigerant materials: the refrigeration capacity (RC) and the relative cooling power (RCP, Relative Cooling Power) [28, 29].

The figure (I.9) represents a graphic diagram of the refrigeration capacity RC(a) and the relative cooling power RCP(b). The refrigeration capacity RC is the quantity of heat which can be transmitted during a thermodynamic cycle, taking into account the shape and the width of the peak of $\Delta S_M(T)$. It is a better criterion for the evaluation of the technological interest of a material. By integrating the curve of variation of entropy between two temperatures framing the maximum of the variation of magnetic entropy $\Delta S_M(T)$ (generally at temperatures within $\pm\ 30K$ of the transition temperature), we obtain the refrigeration capacity RC:

$$RC = -\int_{T_1}^{T_2} \Delta S_M(T)\, dT \tag{I.33}$$

The relative cooling power (RCP) can be evaluated either from the variation of magnetic entropy and the width at half height of the variation of entropy ΔT_{LMH} (Equation I.34), or from the variation of the adiabatic temperature and the width at half-height of the variation of the temperature ΔT_{LMH} (Equation I.35).
It is given by RCP(S) or RCP(T):

$$RCP(S) = \Delta T_{ad}^{MAX} \times \Delta T_{LMH} \tag{I.34}$$

$$RCP(T) = -\Delta S_M^{MAX} \times \Delta T_{LMH} \tag{I.35}$$

The refrigeration capacity RC and the relative cooling power RCP represent the refrigeration capacity in the broad sense, in general $RC = \frac{3}{4} RCP$ for conventional magnetocaloric responses (Figure I.9). The higher the values of RC and RCP, the more magnetic cooling is effective and important.

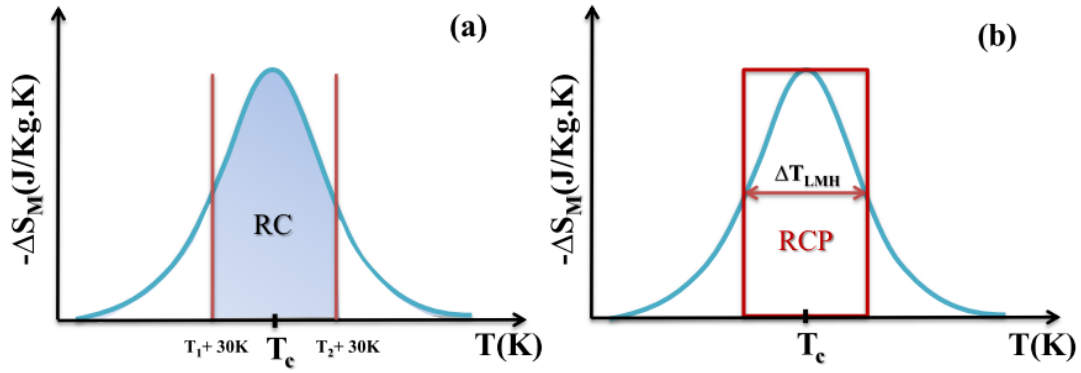

FIGURE I.9: Graphical representations of the RC refrigeration capacity (a) and the relative cooling power RCP (b).

In summary, a magnetocaloric material to be considered efficient for magnetic refrigeration must have several properties such as:

- A Curie temperature T_C close to the operating temperature, depending on the intended application (T_C is close to ambient temperature for applications ambient).

- A large variation in magnetic entropy ΔS_M and in the adiabatic temperature ΔT_{ad} for low values of the intensity of the magnetic field.

- A wide temperature range T (second order transition). This allows to work on a wider temperature range, and therefore to target more variable applications.

The material must also have other interesting physical properties:

- Very low or zero values of thermal and magnetic hysteresis.
- High electrical resistivity (to limit joule losses).
- Good thermal conductivity (to improve heat transfers with the heat transfer fluid and ensure a thermal gradient within the regenerator).

In addition, the material must meet the manufacturing and operating constraints:

- Ease of processing (ore purity)
- Ease of shaping (malleable and ductile)
- Resistant (corrosion, oxidation, mechanical durability)
- Non-toxic

Finally, the material must have good technical and economic characteristics:

- Low manufacturing cost
- Abundance

Chapter II

Theoretical Physics: Concepts and Methods

II.1 Introduction

Among first-principles approaches, density-functional theory (DFT) is most often employed, as it currently represents the best compromise between accuracy and computational effort. Despite the inherent demands of DFT calculations, contemporary advances both in methods and hardware are continuously extending the range of systems to which these approaches can be successfully applied using available computational resources, and nowadays electronic structure simulations are routinely conducted using one of the several black-box packages available. These efforts have brought about a wealth of basic knowledge on metal nanoclusters and nanoalloys, furnishing a deeper – sometimes novel – interpretation of experiments and significantly increasing our understanding of these systems. Many specific features of the metallic bond at the nanoscale have been highlighted, especially in the range of sub-nanometer to few-nanometer particles. Exotic morphologies and unusual structural arrangements have been rationalized and their link to peculiar properties of metal particles have been proposed. In this chapter, after a brief introduction to the basics of DFT (and other wave function approaches for comparison), examples of first-principles predictive computational science in the field of the structure of metal nanoclusters and nanoalloys will be reviewed with the aim of providing some understanding of basic concepts and of present capabilities and limitations.[30]

The last two decades have witnessed tremendous progress in the development of methods for ab-initio calculations of materials properties and for simulations of processes in materials [31]. The cornerstone of this development was laid by density-functional theory (DFT), which casts the intractable complexity of the electron–electron inter- actions in many-electron systems into an effective one-electron potential, which is

a functional of the electron density only[32, 33]. Although the form of this functional which would make the reformulation of the many-electron Schrödinger equation (the Kohn–Sham equations) exact is not known, starting with the pioneering work of Perdew, Becke, and coworkers a hierarchy of approximate functionals has been developed, which allow to predict many properties of solids with increasing accuracy [34,35].

II.2 Ab-initio methods

II.2.1 Hamiltonian Molecular

At the beginning of the 20th century, physicists discovered that the laws of classical mechanics did not allow the behavior of small particles such as electrons [36], nuclei or molecules to be described. These are in fact governed by the laws of quantum mechanics which will make it possible to calculate and predict the physical properties of atomic and molecular systems. These properties have their origin in the behavior of electrons present in such systems and can be assessed using molecular dynamics calculations, statistical mechanical calculations and electronic structure calculations. The latter use various mathematical formalisms in order to solve the fundamental equations of quantum mechanics described in the following part. During this first chapter, we will first present generalities regarding the non-relativistic quantum processing of several systems composed of several particles, then we will approach the two main families of quantum calculations: the Hartree-Fock approximation and the processing of electronic correlation on the one hand, and densit theory on the other hand theory on the other hand y functional theory on the other hand.

The state of a system with M nuclei and N electrons is described in quantum mechanics by a wave function Φ satisfying Schrödinger's equation [37]:

$$H\Phi = i\hbar\frac{\partial\Phi}{\partial t} \tag{II.1}$$

In a large number of cases, the Hamiltonian H has no explicit time dependence and the wave function can then be written as the product of two functions: one depends on $\vec{R}$ of the nuclei and $\vec{r}$ of electrons and the other depends only on time:

$$\Phi = \Psi\left(\vec{R}_A, \vec{R}_B, ..., \vec{R}_M, \vec{r}_1, \vec{r}_2, ..., \vec{r}_N\right)\Theta(t) \tag{II.2}$$

In this case, we are led to solve a stationary equation:

$$H\left|\Psi\right\rangle = E\left|\Psi\right\rangle \tag{II.3}$$

The temporal evolution of the wave function of the system only introduces a phase:

$$\Theta(t) = e^{-\left(\frac{iEt}{\hbar}\right)} \tag{II.4}$$

The transition from a classical to a quantum approach leads to define a Hamiltonian (here not relativistic). In the case of an isolated aggregate, it is written in units atomic $\left(\hbar = e^2 = m_e = 1\right)$, as follows:

$$H = -\sum_{A=1}^{M} \frac{\nabla_A^2}{2M_A} - \sum_{i=1}^{N} \frac{\nabla_i^2}{2} + \sum_{A=1}^{M} \sum_{B<A}^{M} \frac{Z_A Z_B}{r_{AB}} - \sum_{i=1}^{M} \sum_{A=1}^{N} \frac{Z_A}{r_{iA}} - \sum_{i=1}^{N} \sum_{i<j}^{N} \frac{1}{r_{ij}} \tag{II.5}$$

Where A, B, …, denote the nuclei and i, j, ..., denote the electrons.

The first two terms of the equation are the kinetic energy operators of the nuclei T_n and electrons T_e; the other terms are Coulomb interaction terms for each pair of charged particles: nucleus-nucleus repulsion term $V_{n\text{-}n}$, term electron-nucleus attraction $V_{e\text{-}n}$ and electron-electron repulsion term $V_{e\text{-}e}$. An exact solution to equation II.3 is impossible for systems polyelectronic. It is therefore necessary to implement simplifying procedures associated with some mathematical tips in order to make it possible to obtain a solution approached.

The Born-Oppenheimer Approach

This approach is today the basis of many calculations in matter physics [38]. Starting from the simple observation that the electrons are much lighter than the nuclei, we can classically say that their movement is much faster. Therefore, we consider that the electrons evolve in a potential created by fixed atoms. Function electronic wave $\Psi_e\left(\vec{r}, \vec{R}\right)$ then explicitly depends on the coordinates $\vec{r}$ and parametrically of $\vec{R}$. Schrödinger's equation is solved in two stages: first, we solve the electronic equation by setting the fixed nuclei and then we solve the equation nuclear in the potential created by electrons. The Born-Oppenheimer approximation is only valid when the couplings of electronic and nuclear movements are negligible, i.e. when the function wave Ψ_e does not undergo abrupt variations when the nuclei vary. She reaches her limits when dealing for example with collision problems or potential energy surface crossings. However, a large part of the studies of aggregates are done within the framework of this approximation.

The Hartree-Fock Approximation

This approximation is very important because it is the basis of almost all methods ab initio (based on the wave function). There are no exact solutions to equation II.3 that for trivial systems such as the hydrogen atom. This is related to the complexity intrinsic to polyelectronic systems and in particular to the presence of repulsion terms coulombian -

terms of the form ($1/r_{ij}$) - which couple the movement of electrons between them. In order to get around this difficulty, a first approximation consists in bringing the problem with a single particle moving within an average potential caused by the presence of its other partners. The electron-electron repulsion is therefore included as a medium effect. This approximation is called the mean field method. The Hartree-Fock approximation (HF) takes advantage of this simplification by applying it to the electrons of a molecule.

In order to take into account the principle of antisymmetry imposing on the wave function Ψ to change of sign during the permutation of two electrons, a good approximation of this one is obtained in the form of a Slater determinant [39]. This determinant is made up of monoelectronic functions called spin-orbital and applies to "closed" layer systems - corresponding to the case where all electrons are paired. Each spin-orbital is the product of a space function ϕ_i (orbital) dependent on the spatial coordinates of the electron and a spin function can take two opposite values: $\alpha(S)=1/2$ and $\beta(S)=(-1/2)$. Spin density being zero for a closed layer system, the system is thus symmetrical with respect to these two values which makes it possible to describe a pair of electrons as a function of same orbital ϕ_i. In this way, the polyelectronic determinant associated with the N electron system is consisting of N/2 orbital $\{\phi_1 \quad \phi_2 \quad ..., \quad \phi_{N/2}\}$ knowing that two spin-orbitals of the determinant with the same spatial function have different spin functions. This thus makes it possible to verify the principle of Pauli [40] which postulates that two electrons of the same state spin cannot be in the same region of space.

The polyelectronic wave function is therefore written:

$$\Psi(1,...N)=\frac{1}{\sqrt{N}}\begin{vmatrix} \phi_1\alpha(1) & \phi_1\beta(1) & ... & \phi_{N/2}\alpha(1) & \phi_{N/2}\beta(1) \\ \phi_1\alpha(2) & \phi_1\beta(2) & ... & \phi_{N/2}\alpha(2) & \phi_{N/2}\beta(2) \\ & & ... & & \\ ... & ... & ... & ... & ... \\ & & ... & & \\ \phi_1\alpha(n) & \phi_1\beta(n) & ... & \phi_{N/2}\alpha(n) & \phi_{N/2}\beta(n) \end{vmatrix} \quad \text{(II.6)}$$

The formalism based on such a wave function Ψ is called Hartree-Fock Restricted [41,42]. The HF model provides a starting point for making additional approximations as in the case of semi-empirical methods, either to add additional determinants generating solutions that converge to a solution as close as possible of the exact solution of the electronic Schrödinger equation.

Hartree-Fock theory uses the variational principle [43] to assert that, for the ground state, the value of the energy associated with any wave function standardized and asymmetrical Ψ will always be greater than or equal to the energy associated with the exact wave function Ψ_0 hence $\langle\Psi|H|\Psi\rangle \geq E_0$, E_0, representing the lowest eigenvalue

associated with the exact Eigen function. For a non-degenerate system, equality is only achieved when Ψ is identical to Ψ_0. The energy of the exact wave function can thus serve as a lower limit of energy calculated for any other standard asymmetric wave function. So the determinant of optimal Slater is obtained by seeking the minimum energy and by minimizing the term $\langle \Psi | H | \Psi \rangle$.

From the wave function defined in II.6, we arrive at equations for the orbitals monoelectronics of the form:

$$\begin{cases} f(1)\phi_i(1) = \varepsilon_i \phi_i(1) \\ f(1) = h(1) + v_{eff} = h(1) + \sum_a^{N/2} 2J_a(1) - K_a(1) \end{cases} \quad \text{(II.7)}$$

The 1 Index refers to the position of an electron and emphasizes the monoelectronic nature of different operators. The term v_{eff} represents the average potential in which the electrons move. It is consisting of a sum of Coulomb operators J_a and of exchange K_a defined as follows:

$$\begin{cases} J_a(1) = \int dr_2 \phi^*{}_a(2) \frac{1}{r_{12}} \phi_a(2) \\ K_a(1)\phi_i(1) = \left[\int dr_2 \phi^*{}_a(2) \frac{1}{r_{12}} \phi_i(2) \right] \phi_a(1) \end{cases} \quad \text{(II.8)}$$

The Coulomb operator $J_a(i)$ represents the potential linked to the average load distribution electrons. The exchange operator $K_a(i)$ has no physical interpretation in the classical sense of the term but it is present because elementary particles, such as electrons, are not discernible. In addition, a significant part of the exchange operator will be a correction to the auto-interaction error present in Coulomb's term.

It will therefore be possible to write the expression of electronic energy as a function of h, J and K:

$$E^{RHF} = \langle \Psi_{HF} | H | \Psi_{HF} \rangle = 2\sum_{i=1}^{N/2} h_{ij} + \sum_{i,j=1}^{N/2} \left(2J_{ij} - K_{ij} \right) \quad \text{(II.9)}$$

Hartree-Fock equations II.9 are too complex to solve direct by numerical analysis techniques. It is therefore necessary to carry out an additional transformation which will be more suitable. To do this, a new approximation is to express molecular orbitals (MO) as combinations linear of predefined sets of monoelectronic functions (χ_H): this is the LCAO approximation (Linear Combination of Atomic Orbitals). These basic functions are generally centered on the nuclei of the different atoms of the molecule. Thus, orbitals can be written in the form:

$$\phi_i = \sum_{\mu=1}^{K} C_{\mu i}\chi_\mu \qquad \text{i=1,2,...,K} \tag{II.10}$$

The calculation of MO therefore boils down to the determination of $C_{\mu i}$ coefficients. The determinant of Slater, solution of the equation with N electrons, is constructed from N/2 more orbital low energies.

From the previous equation, it is possible to rewrite the equality II.7 in the form:

$$\sum_{v} C_{vi}\int dr_1 \chi_\mu^*(1)\, f(1)\,\chi_v(1) = \varepsilon_i \sum_{v} C_{vi}\int dr_1 \chi_\mu^*(1)\,\chi_v(1) \tag{II.11}$$

We thus end up with the equations of Roothaan and Hall [44, 45] which are written as follows:

$$\sum_{v=1}^{K}\left(F_{\mu v} - \varepsilon_i S_{\mu v}\right)C_{vi} = 0 \quad \mu\text{=1,2,..., K} \tag{II.12}$$

With as definition of $F_{\mu v}$ and $S_{\mu v}$:

$$\begin{cases} F_{\mu v} = \int \chi_\mu^*(1)\, f(1)\,\chi_v(1)\, dr_1 \\ S_{\mu v} = \int \chi_\mu^*(1)\,\chi_v(1)\, dr_1 \end{cases} \tag{II.13}$$

The matrix form of expression II.13 therefore becomes:

$$Fc = SC\varepsilon \tag{II.14}$$

Where each element is a matrix:

- ε is a diagonal matrix of orbital energies: each of these ε_i elements represents the orbital energy of a MO electron ϕ_i .
- F is the Fock matrix representing the average effect of the field created by all electrons on each orbital.
- S is the overlap matrix representing the overlap between each orbital.
- C is the matrix made up of the coefficients of the molecular orbitals on the functions basic.

Since the Fock matrix F depends on the coefficients of the matrix C, the equation II.14 is not linear and must be resolved iteratively using the procedure called Self-Consistent Field or SCF Method (Self-Consistent Field). When this procedure converges, the energy is at its minimum and the orbitals generate a field producing the same orbitals hence the name of the technique. The solutions produce a set of orbital spaces that are either occupied or empty and the total number of orbital spaces is equal to the number of basic functions used.

The HF method has two variants: the restricted Hartree-Fock approach (RHF) and the unrestricted Hartree-Fock approach (UHF) [46-47]. This approach is more costly in calculation time because it doubles the number of integrals to be calculated, the orbitals no longer being doubly occupied. It should also be noted that, in the context of the HF method, the electrons are considered independent of each other and each move into a potential means created by all of the nuclei and other electrons. So there is no instant electron-electron interaction hence the development of certain methods to try to remedy this problem of lack of correlation.

II.2.2 Basic functions

The ab-initio methods make it possible to obtain information from the resolution of the Schrödinger equation without smoothing experimental data. However, one of the inherent approximations to these methods is the introduction of a set of basic functions. Hartree-Fock molecular orbitals are defined from Equation II.8 as linear combinations of predefined monoelectronic functions. The choice of these functions is the result of a compromise between the quality of the results and the speed of the calculations.

There are four basic types of functions also called atomic orbitals, commonly used for the calculation of electronic structure:

- Slater Type Orbitals STO [48]
- Gaussian Type Orbitals GTO [49]
- Basic digital functions
- The plane waves.

The STO, in spherical coordinates, are of the form:

$$\chi_{\varsigma,n,l,m}(r,\theta,\varphi) = NY_{l,m}(\theta,\varphi)r^{n-1}e^{-\varsigma r} \qquad \text{(II.15)}$$

Where N is a normalization factor

ς is the orbital exponent

n, l, m are the numbers quantum

$Y_{l,m}$ is an usual spherical harmonic function.

It should be noted that an STO does not have radial nodes as might be expected for the description of an atomic orbital. These nodes will therefore be introduced through linear combinations of STO. These functions have a correct decay, of the type exponential with r and have good behavior near the nucleus.

Gaussian type orbitals can be formulated as follows:

(II.16)

$$\chi_\mu(r-R_A)=P(r-R_A)\sum_p d_{p\mu}g_p\left(\alpha_{p\mu},|r-R_A|\right)$$

Where g_p and $P(r)$ are defined by:

$$g_p(\alpha,r)=e^{-\alpha r^2}$$
$$P(r)=cx^n y^m z^l \qquad \text{(II.17)}$$

Each function is centered on an atom defined by its position RA. She has some resemblance to atomic orbitals (AO) corresponding to the solutions of the equations HF for isolated atoms. The angular part P(r) of the function consists of a polynomial of varying degree. Depending on the degree of this polynomial (0, 1, 2, ...), it will be possible to define Gaussian type s, p, d, e ... The radial part of the function is defined, for its part, as a linear combination of primitive Gaussians, gp. The different parameters necessary for the expression of GTO (the coefficients and exponents of the polynomial, the coefficients $d_{p\mu}$ exponents $\alpha_{p\mu}$ and contraction) are fixed.

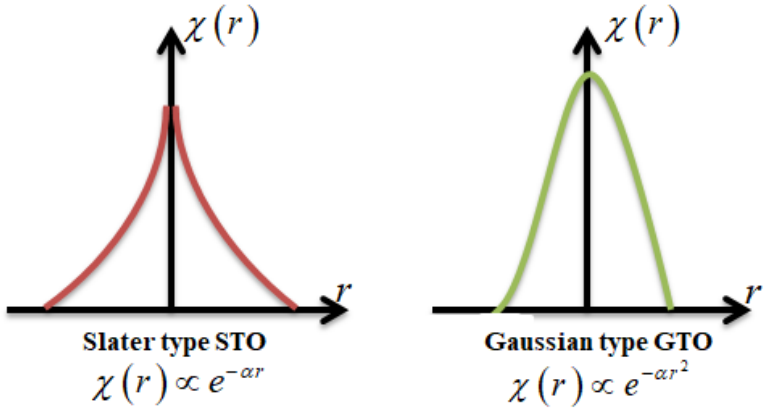

Figure II.1 Comparison between STO and GTO

Generally speaking, small exponent primitives (which are diffused) are not contracted while the others are distributed in contractions, grouped initially to reproduce the STOs [50].

Formulation of Electronic Correlation

A wave function represented by a single Slater determinant will never be equal to the exact wave function. So this means that the EHF quantity is necessarily higher to the exact energy of the ground state. Indeed, the Hartree-Fock theory does not take into account of all the correlation effects between the movements of electrons within a

system molecular. The correlation between two electrons of parallel spins (called Fermi) is in part described in Hartree-Fock methods. In addition to this Fermi correlation, there exist, by elsewhere, the Coulomb correlation due to the electrostatic repulsion between the electrons. The difference between the results obtained in HF and that resulting from the exact solution of Schrödinger's equation is called correlation energy, defined by:

$$E_{corr} = E_0 - E_{HF} < 0$$

E_{corr} is a measure of the error introduced by the HF approximation and it is mainly due to the almost instantaneous repulsion of electrons which does not take into account the effective potential HF, V_{eff}. In a diagram of this type, we can consider that the electrons are often close to each other because the electrostatic interaction is only treated by terms averaged. The term of interelectronic repulsion is therefore too large and the energy E_{HF} is greater than the exact energy E_0. This difference can be of great importance, it is necessary to take it into account account for the calculation of the properties of a molecular system (containing, in particular, metal ions) and to be able to integrate it into an electronic structure calculation.

The term dynamic correlation is used to refer to the repulsion between two electrons during their respective displacements. The term static correlation is related to the existence of Slater determinants degenerate (or almost) into energy. This effect is present when the ground state of an electronic system cannot be described by a single Slater determinant, a case encountered by example when separating a pair of electrons in space, especially when dissociative processes between two atoms.

II.3 The Post-Hartree-Fock Methods

These methods deal with correlation effects that are not taken into account in an HF type approach. They fall into two categories: the disruptive methods and the multi-configurational methods. These methods call a function of correlated wave, solution of the problem with N electrons, which is described in the form of a linear combination of Slater determinants.

The most economical Post-HF method is the Møller-Plesset perturbative theory at second order. This method can also be used at higher orders, which require more IT resources. It is, moreover, not possible to say that results are improved with increasing order disturbance. Among the multi-configurational methods, we can cite the Configuration Interaction method or CI and the Multi-Configuration Self-Consistent Field MCSCF.

II.3.1 The Møller-Plesset Perturbative Method

The Møller-Plesset perturbations theory [51] is expressed in the context of the development of Raleigh-Schrödinger type, often called Many-body perturbation theory. This theory applies when the Hamiltonian H of the system can be decomposed into two terms: a Hamiltonian of zero order H_0 whose proper functions Ψ_i^0 are known and whose proper values E_i^0 are not too far from the desired proper values of H and a disruptive term λ.V assumed small before H_0.

In quantum mechanics, perturbative methods can be used for the purpose add corrections to solutions using particle independent approximation.

So we have:

$$\begin{cases} H = H_0 + \lambda.V \\ H_0 \left| \Psi_i^0 \right\rangle = E_i^0 \left| \Psi_i^0 \right\rangle \qquad i = 1, 2, ..., \infty \end{cases} \tag{II.18}$$

E_i^0 Energies are the solutions, chosen orthogonal or not, of the non-Hamiltonian disturbed for a full basis. λ is a parameter determining the size of the disturbance.

The total energy corrected to order two is given by:

$$E_0 = 2\sum_i^{N/2} h_{ii} + \sum_i^{N/2} \left(2J_{ij} - K_{ij}\right) + \sum_{ij,rs}^{N/2} \frac{2\left(ir\middle|js\right)\left(ri\middle|sj\right) - \left(ir\middle|js\right)\left(rj\middle|si\right)}{\varepsilon_i + \varepsilon_j - \varepsilon_r - \varepsilon_s} \tag{II.19}$$

The three terms constituting the equation 1.A.19 are respectively the corrections order 0, order one and order two. The i and j indices relate to the occupied orbitals and the r and s indices correspond to the virtual orbitals in Ψ_{HF}. According to the definition of correction to second order, the total energy thus calculated will always be less than the HF energy. It should also be noted that these methods only take into account dynamic correlation and that you have to use multi-configurational methods to include correlation static.

II.3.2 Multi-Configuration Methods

The Hartree-Fock method determines, for a given base, a mono-determinantal wave function. To improve the HF result, it is possible to use a wave function containing several determinants. Multi-configurational methods therefore use the HF wave function as a starting point. The general form of the multi-configurational wave function is:

$$\Psi = a_0 \Psi_{HF} + \sum_{i \neq 0} a_i \Psi_i \tag{II.20}$$

Where a_0 is generally close to 1.

These methods differ in the way they calculate the coefficients a_i who weight Ψ_i, a_0 being determined by the normalization conditions.

The Interaction of Configuration

The most comprehensive method for describing the electronic correlation is the interaction of configuration [52, 53]. It is based on the variational principle. In this approach, the wave function is described as a linear combination of several determinants and the coefficients of this combination are obtained by minimizing energy.

$$\Psi_{CI} = a_0\Psi_{HF} + \sum_{ia} a_i^a \Psi_i^a + \sum_{ijab} a_{ij}^{ab}\Psi_{ij}^{ab}$$
$$\Psi_{CI} = a_0\Psi_{HF} + \sum_{S} a_S \Psi_S + \sum_{D} a_D \Psi_D \qquad \text{(II.21)}$$

Or Ψ_{HF} is the Hartree-Fock configuration, Ψ_S and Ψ_D are, respectively, the excitations single and double.

The electrons of the occupied orbitals i and j are excited in the vacant orbitals a and b. The MO used to construct the excited Slater determinants come from an HF calculation and are kept afterwards. It is possible to consider only the Double excitations (CID calculations (Configuration Interaction Doubles)) - or Single and Double Excitations (CISD calculations (Configuration Interaction Simples and Doubles)).

However, if this multi-configurational method is complete and efficient for the description of electronic systems, it requires IT resources substantial. It is therefore little used and limited to small molecules because of the significant number of determinants that it generates regardless of the size of the database used.

II.4 The Density Functional Theory (DFT)

The detailed study of the electronic and the magnetic properties of a molecular system requires taking into account for electronic correlation effects, especially if it contains metals. We have seen that Post Hartree-Fock methods make it possible to integrate these effects but are often heavy and limiting as to the size of the systems studied. This is why, over the past thirty years, the Density Functional Theory has been considerably developed for the study of physical systems and has become an effective alternative to Post HF methods. Initially designed and applied to solid state problems, several reasons have contributed to its popularity for physical applications:

- This theory includes in its formalism a large part of electronic correlation.
- The method can be applied to any type of system: covalent, ionic or metallic.

Whereas Hartree-Fock methods lead to expressing the energy of the system as a functional of its wave function Ψ, for DFT methods, the energy is a functional of electronic density (ρ) of the system. One of the great attractions of the methods DFT is to solve Schrödinger's equation by only involving the observable ρ defined in physical space R^3 which therefore replaces the 3N configuration space variables in which the wave function (Hartree-Fock) is defined. However, this possibility of avoiding the N-particle problem by using electronic density collapses when it is necessary to give an analytical expression of energy as density functional.

Before tackling the foundations of the Density Functional Theory, it seems essential to define the central quantity of this theory: the electronic density (ρ).

II.4.1 Electronic density

In the previous part, we defined electrons as particles inseparable and indistinguishable. Indeed, an electron cannot be located as individual particle [25], on the other hand its probability of presence in an element of volume can be estimated and corresponds to the electronic density (ρ). The electrons must therefore be considered in their collective aspect (electron cloud) and the electronic density allows know the regions of space where electrons are most often found.

The electronic density $\rho(r)$ is a positive function depending only on the 3 coordinates of space (x, y, z). This quantity is infinitely canceled and is worth N (Total number of electrons) when integrated all over space.

$$\begin{cases} \rho(r \mapsto \infty) = 0 \\ \int \rho(r) dr = N \end{cases} \qquad \text{(II.22)}$$

$\rho(r)$ Therefore represents, by definition, the probability of finding an electron in a volume unitary dτ defined by r.

Thus, we can notice that $\rho(r)$ seems to contain enough information to describe the system while Ψ has a lot more information, some of which is not necessary for the description of the physical interaction. All of these arguments seem to indicate that the electronic density is sufficient for the complete determination of the properties of an atomic system and it is for this reason that several attempts to set up a quantum formalism based on this quantity have been offered. But it is to Hohenberg and Kohn

that we owe the proposal for an exact formalism (free from any approximation) stated in the form of two theorems.

First Hohenberg-Kohn theorem

Recall that for an electronic system described by the Hamiltonian Hel (Equation II.17), the energy and the wave function of the ground state are determined by the minimization of the functional $E[\Psi]$. For a system with N electron, the external potential $v_{ext}(r)$ fixed completely the Hamiltonian Hel. This means that if we know the number of electrons N of the system as well as the external potential $v_{ext}(r)$, we can uniquely determine the Hamiltonian and thus access the energy and the wave function of the ground state. The external potential therefore perfectly reflects the different characteristics of a compound. There are two ways of looking at an atomic system, either with through the nuclei via the potential outside, or through its electron cloud via electronic density. It appears very clearly a relationship between these two quantities, one appearing to be the image of the other.

The first theorem of Hohenberg and Kohn [55] consists in giving a theoretical justification to the idea that a given electronic density corresponds to an unique external potential. The potential $v_{ext}(r)$ is, in fact, determined, to within a constant, by the electronic density $\rho(r)$. Since ρ fixes the number of electrons, it follows that the electron density $\rho(r)$ also uniquely determines the wave function and all electronic properties of the system. So for a system defined by a number of electrons (N), positions (R_α) and nuclear charges (Z_α), by adding electronic density (ρ) , we can build the corresponding Hamiltonian and thereby access the wave function (Ψ_{fond}) and fundamental energy of this system (E_{fond}):

$$\rho \Rightarrow \{N, Z_\alpha, R_\alpha\} \Rightarrow H \Rightarrow \Psi_{fond} \Rightarrow E_{fond} \tag{II.23}$$

The total energy of the system is therefore a density Functional $\rho(r)$, $E = E[\Psi]$, that we can rewrite by distinctly separating the parts which depend on the system (N, v_{ext}) of those who are not.

$$\begin{cases} E[\rho(r)] = F_{HK}[\rho(r)] + \int \rho(r) v_{ext}(r) dr \\ E[\rho(r)] = T_{el}[\rho(r)] + V_{el\_el}[\rho(r)] + V_{el-noy}[\rho(r)] \\ F_{HK}[\rho(r)] = T_{el}[\rho(r)] + V_{el\_el}[\rho(r)] \end{cases} \tag{II.24}$$

The terms independent of the system are then grouped within functional Hohenberg-Kohn (FHK). This new functional contains the kinetic energy electronic $T_{el}[\rho]$ and $V_{el-el}[\rho]$, the potential energy due to the interaction between electrons. The explicit expressions of these two functional are not known. However, we can extract from V_{el-el} the classic part, Hartree energy $V_{el-el}^{cla}[\rho]$.

$$V_{el-el}^{cla} = \frac{1}{2}\int \frac{\rho(r)\rho(r')}{|r-r'|} dr dr' \qquad \text{(II.25)}$$

Second Hohenberg-Kohn theorem

We have just established that the density of the ground state is sufficient to obtain all the interesting properties of an electronic system. Only how can we be sure that a given density is that of the desired fundamental state?

Hohenberg and Kohn answer this question through a second theorem [55] that we can state in the following way: the energy $E[\rho_{test}]$, associated with any test density, satisfying the necessary boundary conditions $\rho_{test}(r) \geq 0$ and $\int \rho_{test}(r) dr = N$ and associated with an external potential v_{ext}, is greater or equal to the energy associated with the electronic density of the fundamental state $E[\rho_{fond}]$.

This theorem is nothing other than the variational principal expressed for energies of a density, $E[\rho]$ and not of a wave function $E[\Psi]$ [56, 57]. However, according to first theorem, a density of test defines its own Hamiltonian and similarly its own test wave function.

From there, we can have a correspondence between the variational principle in its wave function version and in its electronic density version such as:

$$\langle \Psi_{test} | H | \Psi_{test} \rangle = E[\rho_{test}] \geq E_{fond} = \langle \Psi_{fond} | H | \Psi_{fond} \rangle \qquad \text{(II.26)}$$

In summary: all the properties of a system defined by an external potential v_{ext} can be determined from the electronic density of the ground state. The energy of system $E(\rho)$ reaches its minimum value if the electronic density is that of the basic state. The use of this variational approach is limited to the search for the energy of the ground state and, to be more precise, this reasoning is limited to the state fundamental for a given symmetry.

II.4.2 Kohn-Sham equations: Orbital approach

The two theorems of Hohenberg and Kohn therefore offer a theoretical framework allowing to consider solving the Schrödinger equation via electronic density as main variable. The energy of a system of N electrons interacting is therefore a density functional and ground state energy research can be performed iteratively based on a variational law. During these various treatments of the total energy of the system, we therefore have introduces a new functional, called universal because it does not depend on the electronic system, FHK, the Hohenberg and Kohn functional. As we have seen previously, this functional includes two terms (T_{el} and $V_{el\text{-}el}$). Only, their analytical expression for the system of N interacting electrons is unknown.

Kohn and Sham [58] approached this problem from another angle. The same way as the exact expression of classical potential energy is known (Hartree Energy), they introduced the notion of a fictitious electron system without interaction with same density $\rho(r)$ as the interacting electron system. Based on this reference system, it is then possible to give an exact expression to the energy kinetics of a non-interacting N electron system as a density functional $\rho(r)$. This correspondence between electron systems in interaction and without interaction, actually, has many consequences:

- Passage of a description based on the wave function with N electrons (Ψ) at N wave functions to an electron (ϕ_i) ;
- Determination of the electronic density through the summation of $|\phi_i|^2$ on all occupied states instead of considering the integral of $|\Psi|^2$ on all the variables of space except one, defined by r;

- The kinetic energy (T_{el}) and potential energy (V_{el-el}) of N electrons in interaction are both split into two parts which we can call classic and no-classic.

- The classical kinetic energy $\left(T_{el}^{ind}\right)$ comes from the electron reference system independent and classic Coulomb energy $\left(V_{el-el}^{cla}\right)$ is none other than Hartree energy. The rest (kinetic energy and no-classical potential) were grouped in a quantity called exchange-correlation energy, E_{xc} [59-61]. One way to define this new functional is to say that it contains everything which is not exactly known:

$$E_{xc} = \left(T_{el} - T_{el}^{ind}\right) + \left(V_{el-el} - V_{el}^{cla}\right) = T_{el}^{dep} + V_{el-el}^{ncla} \qquad \text{(II.27)}$$

- This exchange-correlation term is found in the expression of the functional model of (Hohenberg and Kohn (FHK). So we go from one expression for which we do not know the mathematical form of the two functional $T_{el}[\rho]$ and $V_{el-el}[\rho]$ to an expression where the functional $T_{el}^{ind}[\rho]$ and $V_{el-el}^{cla}[\rho]$ are known and where the term E_{xc} represents what is not known, that means, exchange-correlation energy. AT through this approach, Kohn and Sham therefore transferred what is not known in the smallest term, E_{xc}. Therefore, the error committed will be made on a small contribution to the total energy of the system.
- The total energy of the system then passes from independent contributions (FHK) and dependent on potential (v_{ext}), to the sum of the kinetic energy of the independent particles (T_{el}^{ind}) with a term depending on the effective potential.
- This effective potential (v_{eff}) contains the external potential (v_{ext}), the contribution classical to the potential energy of particles without interaction and the exchange-correlation potential (v_{xc}) defined as:

$$v_{xc} = \frac{\delta E_{xc}}{\delta \rho} \tag{II.28}$$

Kohn and Sham's choice to refer to a fictitious system of N electrons without interaction involves solving N "monoelectronic" Schrödinger equations. This brings us to rewrite the problem in the form of three independent equations, the Kohn- Sham equations:

- The first gives the definition of the effective potential:

$$\rho(r) \to v_{eff}[\rho(r)] = v_{ext}(r) + \int \frac{\rho(r')}{|r-r'|} dr + v_{xc}[\rho(r)] \tag{II.29}$$

- The second uses this effective potential in the N monoelectronics Schrödinger equations in order to obtain the ϕ_i :

$$v_{eff}(r) \to \left(-\frac{1}{2}\nabla^2 + v_{eff}(r)\right)\phi_i(r) = \varepsilon_i \phi_i(r) \tag{II.30}$$

- The third shows how to access the density from the N monoelectronics wave functions:

$$\phi_i(r) \to \rho(r) = \sum_{i=1}^{N} |\phi_i(r)|^2 \tag{II.31}$$

II.5 Processing of the exchange and correlation

The density functional theory applied in the context of the Kohn and Sham orbital approach remains exact in its formalism. Gradually, the unknown part in the functional $E[\rho]$ has been reduced to a universal functional $F_{HK}[\rho]$ and finally to an exchange energy and correlation $E_{xc}[\rho]$. It is necessary to approach the expression of this functional exchange and correlation, to offers a description as precise as possible of the system.

The energy of exchange-correlation gathers the kinetic and no-classics electrostatic terms $\left(T_{el}^{dep}\right.$ and $\left.\mathrm{V}_{el-el}^{ncla}\right)$. Indeed, the electrons as fermions (half-integer spin) have a collective behavior governed by two large principles. On the one hand, two electrons of the same spin state cannot be in a same region of space: this is the Pauli Exclusion Principle (electrons of the same spin repelling each other). On the other hand, two electrons with opposite spin moments can occupy the same region of space. These inter-electronic interactions with purely order quantum.

The choice of Kohn and Sham is more judicious because the approximation is made on the most small contribution to total energy [62, 63].

II.5.1 Local density approximation (LDA)

Now we need to give an algebraic form to E_{xc} which allows to take into account satisfactorily the correlations between the movements of the different electrons. The first approximation which was considered goes in the continuity of the Kohn and Sham approach and consists of defining a reference for which we also have an expression specifies as possible to the functional in question. The idea of local density approximation is to consider the exchange-correlation potential as a local quantity defined at r point, weakly dependent on the variations of the density around this same r point. The local density approximation or LDA must therefore reproduce as well as possible the physical characteristics of the spherical mean of the hole exchange-correlation.

This approximation is the basis of all modern exchange-correlation functionalities and can be defined as follows:

$$\begin{cases} E_{xc}^{LDA}[\rho] = \int \rho(r)\,\varepsilon_{xc}\left(\rho(r)\right)dr \\ E_{xc}^{LDA}\left[\rho_{\alpha},\rho_{\beta}\right] = \int \rho(r)\,\varepsilon_{xc}\left(\rho_{\alpha}(r),\rho_{\beta}(r)\right)dr \end{cases} \qquad \text{(II.32)}$$

It is the functional for which an exact form is almost known. The approximation of $E_{xc}[\rho]$ is based on the uniform electron gas model where the term $\varepsilon_{xc}(\rho(r))$ is the exchange-correlation energy by particle of uniform electron gas of density $\rho(r)$. Moreover, $\varepsilon_{xc}(\rho(r))$ can be considered as the sum of an exchange contribution and correlation:

$$\varepsilon_{xc}(\rho(r)) = \varepsilon_x(\rho(r)) + \varepsilon_c(\rho(r)) \tag{II.33}$$

The exchange term, commonly called "Dirac exchange" [64] (symbolized by S because that this expression was taken up by Slater) is known exactly:

$$\varepsilon_x^s(\rho(r)) = -\frac{3}{4}\left(\frac{3\rho(r)}{\pi}\right)^{1/3} \tag{II.34}$$

The correlation part $\varepsilon_c(\rho(r))$ cannot be expressed exactly. The approximation of this term established by Vosko, Wilk and Nussair (VWN) [65] has been most successful. She is based on an interpolation of the results of very precise quantum Monte-Carlo calculations on the uniform electron gas made by Ceperley and Alder [66].

The basic idea of the LDA is that it is possible to estimate the exchange-correlation energy of an inhomogeneous system using on infinitesimal portions the results of an homogeneous electron gas density equal to the local density of the inhomogeneous system. This approximation is reasonable for a system where the density varies slowly but this condition is not met in practice. However, LDA is surprisingly effective and its application to atoms and molecules is justified by the success of its digital applications.

II.5.2 Generalized gradient approximation (GGA)

The biggest source of LDA error comes from the exchange energy which is often underestimated while the correlation energy is often overestimated even if, in value absolute, its contribution to the total energy is smaller. These two errors tend to cancel. To improve the accuracy of DFT calculations, we need better approximations for the exchange-correlation functional. Some authors have had the idea of define a density functional that they have associated with its own derivatives in order to take into account the inconsistency of the system. At first, LDA was treated as the first term in a Taylor series development:

$$E_{xc}^{GEA}[\rho] = \int \varepsilon_{xc}^{GEA}(\rho(r))\rho(r)\,dr + \int C_{xc}(\rho(r))\frac{|\nabla\rho(r)|}{\rho^{4/3}(r)}dr + \ldots \tag{II.35}$$

This functional form is the gradient approximation (GEA or Gradient Expansion Approximation). Unfortunately, this gives worse results than the LDA. Indeed, the exchange-correlation hole does not satisfy the conditions which ensured LDA some physical sense. In order to correct these problems, the above functional has been modified to force it to comply with the main boundary conditions. We then get the generalized gradient approximation (GGA) behind the success of the DFT:

$$E_{xc}^{GGA}\left[\rho;\nabla\rho\right]=\int\varepsilon_{xc}^{GGA}\left(\rho(r),\nabla\rho(r)\right)dr \tag{II.36}$$

Often the contributions for exchange and correlation are developed separately:

$$E_{xc}^{GGA}\left(\rho,\nabla\rho\right)=E_{x}^{GGA}\left(\rho,\nabla\rho\right)+E_{c}^{GGA}\left(\rho,\nabla\rho\right) \tag{II.37}$$

The major problem of the LDA coming from the exchange, a very particular attention was focus on the development of this part:

$$E_{x}^{GGA}\left(\rho,\nabla\rho\right)=E_{x}^{LDA}-\int F\left(s(r)\right)\rho^{4/3}(r)\,dr \tag{II.38}$$

Where F is a function of the reduced gradient density (dimensionless):

$$s(r)=\frac{\left|\vec{\nabla}\rho(r)\right|}{\rho^{4/3}(r)} \tag{II.39}$$

We can thus cite the functions of Becke (B88) [67], that of Perdew (PW86) [68] and that of Handy and Cohen (OPTX) [69].

- **B88**

The B88 exchange functional is based on a dimensional analysis and on a correct asymptotic behavior of the exchange energy density:

$$F^{B88}(s)=\frac{\beta s^{2}}{1+6\beta s\times\sinh^{-1}(s)}\ \text{avec}\ \beta=0.0042\ \text{u.a} \tag{II.40}$$

β is an empirical parameter determined by a least squares analysis of the exchange energies of the six gas rare atoms (from He to Rn). The functional of Perdew and Wang (PW91) [70] comes from a modification of this functional to meet certain scaling conditions.

- **PW86**

This functional is based on an analysis of the expansion of the hole correlation exchange gradient around its LSDA form.

$$F^{PW86}(s)=\left[1+1.296\left(\frac{s}{p}\right)^2+14\left(\frac{s}{p}\right)^4+0.2\left(\frac{s}{p}\right)^6\right]^{1/15} \quad \text{avec p}=\left(24\pi^2\right)^{1/3} \qquad \text{(II.41)}$$

The functional of Perdew, Burke and Ernzerhof (PBE) [71] is a modification of this functional. It is interesting to note that neither PW86 nor PBE contain empirical parameters.

- **OPTX**

This functional is an improvement of the exchange functional of Becke [72] in which the authors have not only optimized the enhancement factor F but also the Dirac exchange coefficient in the LDA part obtaining so:

$$E_{xc}^{GGA}(\rho,\nabla\rho)=1.051\times E_x^{LDA}-\int F^{OPTX}\left(s(r)\right)\rho^{4/3}(r)dr \qquad \text{(II.42)}$$

$$With:\ \mathrm{F}^{\mathrm{OPTX}}(s)=1.43169\left(\frac{\gamma s^2}{1+\gamma s^2}\right)^2 \text{ with } \gamma=0.006 \qquad \text{(II.43)}$$

The three coefficients were obtained by reproducing the Hartree-Fock energy of the fundamental state of the first 18 atoms (H-Ar).

- **The correlation functionals**

Corrections to the correlation term are much more complex to formulate than those regarding the term of exchange. In addition, even if their influence on the structural and electronic properties of the systems studied is much less significant than that of the exchange, the fact remains that their taking into account turns out to be absolutely essential for obtaining quantitatively satisfactory results.

So the analytical expression of these corrections, particularly complicated, does nothing to help a better understanding of the physical principles on which they are based and cannot be understood using simple physical reasoning. These are mostly expressions satisfying known mathematical properties. We can cite, among others, the functional of Lee, Wang and Parr (LYP) [73], of Perdew (P86, counterpart of the functional exchange of PW86) [68] and that of Perdew and Wang (PW91) [70]. The exchange-correlation functional GGA represents a very significant improvement LDA, the main reason being the modification of the exchange part.

- **The functional meta-GGA**

In order to further improve the performance of GGAs, the exchange correlation functional meta-GGA (mGGA) take into account the kinetic energy density of Kohn-Sham orbitals:

$$\tau=\frac{1}{2}\sum_i^{occ}\left|\nabla\Psi_i\right|^2 \qquad \text{(II.44)}$$

In addition to the dependence on the density gradient already included in the GGAs.

The term of exchange E_x^{mGGA} can be written:

$$E_x^{mGGA} = -\frac{3}{4}\left(\frac{3}{4}\right)^{1/3} \int f\left(\rho, \nabla\rho, \tau\right) \rho^{4/3}\left(r\right) dr \qquad \text{(II.45)}$$

The dependence of the exchange term on the Laplacian density greatly improves the accuracy of these functional. However, the dependence on the kinetic energy density poses implementation problems of these functionalities in a self-consistent scheme for the exchange-correlation potential, making the SCF procedure more time-consuming.

On the other hand, physical precision has not yet been achieved and the main part to improving is the exchange. The question is therefore: why use an exchange functional approximate when we know how to calculate the exchange exactly?

II.5.3 The hybrids Functional

When they proposed their approach in 1965, Kohn and Sham had already mentioned the interest of an exact processing of the exchange. They had already established an expression formal of the exchange-correlation energy based on the Hartree-Fock approximation for the exchange, the correlation term remaining unchanged from the LDA. They had also noted that the effective potential would have, through the use of this hybrid functional, a correct asymptotic behavior (in 1/r) far from the atom.

In the overwhelming majority of cases, the GGAs achieved better accuracy. The reason for this failure is the artificiality of the separation of exchange correlation terms: by combining a non-local exchange hole (Hartree-Fock) with a local correlation (LDA). Becke therefore chose to use the exact exchange differently by including only a part of it in the energy of exchange-correlation [74]. He proposed an expression to three parameters which will be designated by [75]:

$$E_{xc} = E_{xc}^{LDA} + a_0\left(E_x^{axact} - E_x^{LDA}\right) + a_x \Delta E_x^{B88} + a_c \Delta E_c^{PW91} \qquad \text{(II.46)}$$

Where the a_0, a_x and a_c coefficients are determined semi-empirically by fitting to experimental data. E_{xc}^{exact} here represents the exact exchange energy obtained from Hartree-Fock calculation. In the first corrective term, the value of the a_0 coefficient can be linked to the "independent particles" character of the system. The following two terms allow to optimize gradient corrections, for the exchange and for the correlation. As such, the above equation represents the simplest way to take into account the exact exchange and find the limit of uniform electron gas. Because of this approximation, the accuracy of the energies is even better than when we use generalized gradient corrections.

A variation of this approach, calling the Lee's approximation, Yang and Parr (LYP) and Perdew and Wang [76], known as B3LYP, which is the most popular.

$$E_{xc}^{B3LYP} = a_0 E_x^{LDA} + (1 - a_0) E_x^{exact} + a_1 \Delta E_x^{B88} + E_c^{LDA} + a_2 \left(E_c^{LYP} + E_c^{LDA} \right) \qquad \text{(II.47)}$$

Where $a_0 = 0.80$, $a_1 = 0.72$ and $a_2 = 0.81$. The a_0, a_1 and a_2 parameters are semi-empirical quantities. This functional gives remarkably precise results for a large number of systems [77]. It has also been shown that she permits, unlike GGA, to correctly describe the magnetic properties of molecular compounds of transition metals and ligands. However, it is far from putting an end to the exchange and correlation problems in DFT [78, 79]. A number of avenues are currently being explored in order to get the most out of benefits of the exact exchange. On the one hand, Becke has built new functionalities taking into account both the exchange and the correlation. According to him, the functional based on GGAs and incorporating a fixed proportion of exact exchange has reached a limit.

Chapter III

Experimental tools and samples

III.1 Introduction

In this third chapter, we introduce the main experimental techniques used in this thesis for the sample elaboration and the study of different properties of thin film materials. First, we report in section III.2 on the Physical vapor deposition technique (PVD) used to elaborate the studied thin metallic film. Second, we introduce in section III.3 technique used for the Magnetic characterization of our thin layer of gadolinium and in section III.4 we have detailed the Measuring principles of Thermoelectric characterizations of Gd Thin film using Physical Properties Measurement System (PPMS).

III.2 Thin film deposition techniques

III.2.1 Liquid phase deposits - sol-gel deposits

Thin film deposits can be carried out in reaction chambers, either in liquid or vapor phase.

The TiO_2 particle fixation tests according to conventional methods are generally made from solutions of titanium precursors or particles of TiO_2 in suspension.

The fixation of TiO_2 particles in liquid phase on the substrate (glass plates, metal sheets, fabrics, ...) can be produced according to two possibilities[80-82]:

- PMTP (Previously Made Titanium Powder)

The TiO_2 particles previously prepared are put in colloidal solution to then be deposited on the substrate.

- In-situ preparation

The liquid phase deposition is carried out according to the so-called sol-gel method which is the most used in this fixing mode. The metal precursor salts (Ti) used are generally alkoxides[83-86]. The TiO_2 particle deposition process according to the sol-gel method is described as follows:

- Dissolution of the precursor salt of Ti in an organic solvent.
- Hydrolysis of the Ti precursor salt solution leading to the formation of the gel.
- Quenching of the substrate in the gel formed.

Fixing can be done either by quenching (dip-coating) or by spinning (spin-coating). [89]

- Drawing of the substrate plate.
- Evaporation of the organic solvent.
- Calcination of the layer deposited on the substrate.

The fixing of the catalyst carried out from titanium precursor solutions according to the aforementioned methods leads to deposits, the fixing and thickness of the layer particles of the catalyst (TiO_2) are difficult to produce according to the specifications desired (thickness and adhesion of the catalyst layer).

III.2.2 Vapor phase deposits

Physical vapor deposition (PVD), Chemical vapor deposition (CVD) and especially Atomic Layer Deposition (ALD) vapor phase fixation techniques are currently in development given the best adhesion and catalyst layer thickness control, compared to the methods carried out in liquid phase or the sol-gel method. A deposit produced by PVD or CVD is a thin coating ($\approx$ 10 µm thick) performed at low pressure in an enclosure under partial vacuum ($< 10^{-1}$ mbar).

In general, this technology uses three components:

- a source

This is where the material to be deposited (metal plate, gas bottle, ...) is concentrated. It is the seat of the dispersion of the element (Ti) in the form of atoms, ions, and more generally steam.

- a substrate

This is the part to be coated according to the phenomenon of condensation of the material from the source to form germs that will grow to lead to the formation of layer.

- a medium

It is the seat between the source and the substrate where the transfer of the matter. It is also the site of chemical reactions taking place between the atoms of material to be deposited and a gas (reactive deposits). We differentiate between chemical deposits in the vapor phase (CVD) and physical deposits in the Steam phase (PVD) by the means used to produce the steam.

- CVD: it results from a chemical reaction or from the decomposition of the molecule.

- PVD: it is produced by a purely physical phenomenon (vaporization by Joule effect, spraying, etc.).

The vapor deposition processes are described below.

III.2.2.1 CVD techniques

The chemical vapor deposition process consists in bringing a volatile compound of the material to be deposited in contact, either with another gas near the surface of the substrate, or with the surface itself. One or more chemical reactions are caused to give a solid product. The other reaction products must be gaseous in order to be removed from the reactor. The deposits are made at variable pressure and require an energy supply to promote these reactions. CVD techniques are differentiated by the type of energy used to activate the chemical reaction.

- **Thermal CVD**

In this case, it is the temperature of the substrate which supplies the energy necessary for the activation of the reaction as well as the diffusion in the substrate of the atoms brought to the surface.

This temperature can be obtained by:

- Direct heating by passing an electric current through the substrate.
- Heating by high frequency induction: limits the choice of substrate since it must be electric and thermal conductor.
- Heating by thermal radiation: can be applied to bad substrates electrical conductors.

- **LCVD (Laser CVD)**

This technique consists in irradiating, thanks to a continuous or pulsed laser beam, either very locally the surface of the substrate (in which case the chemical reaction takes place by simple thermal activation), i.e. the vapor phase so as to excite the molecules and thus increase the reactivity of gaseous species.

This technique is also used to obtain deposits in very localized, especially in microelectronics, but very limited industrially due to its cost.

- **PECVD (Plasma-Enhanced CVD)**

In this process, the plasma, generally induced by a high-frequen cy field (microwave or radio frequency), interacts with the gas phase to form species chemically active, such as ions and free radicals. This process allows the lowest deposition temperatures (25-400°C) allowing then the use of any type of substrate. In addition, the deposition rates reached are superior to those of a conventional CVD process. However, due to the temperatures very low, elimination of parasitic reaction products is difficult, and we observe sometimes incorporating them into growing films. In addition, the bombing of the substrate by energetic particles can cause microstructural defects and significant residual stresses.

III.2.2.2 PVD techniques

There are different PVD techniques, depending on the nature of the following three components:

1) The mode of steam production

2) The electrical state of the substrate

3) The nature of the gas constituting the medium.

Influence of the mode of production of the vapor

- Evaporation under vacuum

The evaporation of the source material can be obtained, either by Joule effect, by induction of heat, by ionic or electronic bombardment or by laser beam. The deposits are made under high vacuum so as to give the layers great purity. The lower the pressure, the more the trajectories of the vaporized particles will be rectilinear. In this case, only the parts of the substrate directly opposite the source will be covered. This technique requires the use of sufficient power to vaporize the most refractory compounds. In addition, the energy of particles torn from the source is relatively low, which results in poor adhesion. Industrially, the evaporation technique is widely used in optics (filters, lighthouse dishes, etc.), in decoration, for the coating of sheet substrates (packaging, capacitors, etc.);

- Cathode sputtering

A sufficient electrical voltage is applied between the two electrodes causing the ionization of the atmosphere (usually composed of argon) and the creation of a glow discharge plasma. The ions present are then accelerated to the cathode (the target or

source of the material to be deposited). The vapor phase is done according to a purely mechanical process, by transferring the kinetic energy of the ions to the atoms of the target which will be ejected.

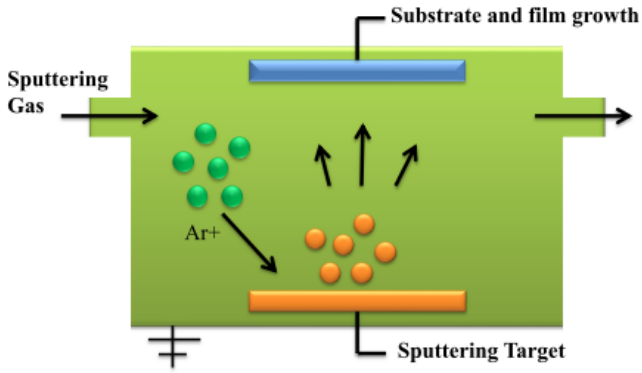

FIGURE III.1: Scheme of a magnetron sputtering system.

- Arc processes Metal

Vapor is obtained by the erosion of one or more cathodes by means of very high intensity electric arcs. The ejected atoms are mostly ionized, then accelerated towards the substrate. There are several variants of this process: multiple arcs, ion deposition by arcs, evaporation by arcs, evaporation by thermionic arcs, etc. These techniques, which have many advantages, in particular high deposition rates and good homogeneity of the coatings, are increasingly no longer used industrially, among other things for coating high-speed steel tools or for friction parts.

- Spray by ion beam

As before, the vapor results from the interaction between the target (source) and ions with high kinetic energy. The ions are not generated around the source, but come from an ion gun. This slightly more flexible technique than the previous one, allows the use of more energetic ions than in sputtering.

Influence of the electrical state of the substrate

The polarization of the substrate will allow, whatever the vapor phase technique used, to increase the relative density of the deposit by means of a sputtering phenomenon of the atoms least attached to the surface of the deposit, then redeposition. The crystallization of deposits will also be greatly improved. In addition, if this discharge is created before the vaporization of the material to be deposited, the Argon ions will directly spray the substrate, which makes it possible to rid it of its surface impurities (oxides, water vapor, etc.) and improve the adhesion of the deposit. When we couple

the polarization of the substrate with the evaporation under vacuum, we speak of ion plating.

Influence of the nature of the medium

The deposition of layers of oxide, carbide, or nitride is obtained by introduction into the enclosure of reactive gas (Oxygen, nitrogen, methane, etc.) capable of combining with the metal vapors to form the compound. This spraying or reactive evaporation technique offers a very wide choice of different compounds, but results in a significant drop in the deposition rate.

FIGURE III.2: The Physical Vapor Deposition – IJL Nancy.

The deposition of thin layers by PVD method [Physical Vapor Deposition] uses the energy of a plasma source under low pressure conditions of a neutral gas (10^{-2} to 10^{-4} mbar) to tear off the atoms […] a physical target in order to deposit them on the surface of the material located in the enclosure.

This technique makes it possible to produce thin and dense layers on the sample (substrate) and thus to modify certain surface properties. The thickness of the deposited layers generally varies from a few nanometers to several micrometers depending on the uses among which one can cite the properties of resistance to wear, in tribology, optics, electrical, wettability...

The vapor phase deposits are exploited industrially for their properties:

- Mechanical - resistance to erosion, abrasion and friction

- Optics-: reflection, transmission, radiation detection

- Electrical-conduction, insulation

- Physico-chemical - diffusion barrier, corrosion resistance, catalysis

Vapor deposition techniques are generally carried out at very high temperatures thus limiting the choice of substrate to be used and the field of application. To this end, the ALD (Atomic Layer Deposition) technique is used to overcome the severe temperature and pressure conditions for vapor deposition.

III.2.2.3 The ALD technique

The ALD process, developed in the 1970s, is a special technique vapor deposition or CVD. In CVD processes, the precursors gaseous elements to be deposited are mixed, transported together and so constant during the deposition of a thin layer. However, in the processes ALD, they are each introduced in turn in contact with the surface of the substrate.

In the ALD process, the growth of the monolayer is ensured by the succession of pulses of the metal precursor to be deposited on the surface of the substrate. The reactor is purged after each deposition to eliminate all the species which have not reacted and are physiologically sorbed, as well as any by-products of the chemisorption reaction. The cycle is repeated as many times as necessary to produce the desired thickness.

III.2.3 Advantages and disadvantages different processes

PVD techniques, mainly ionic and collimated sprays, are successfully used to deposit layers of sizes above 70 nm [90]. For smaller sizes, compliance and thickness control are no longer satisfactory by PVD.

CVD methods have several strong points compared to PVD:

- Better conformity of films due to the active participation of the surface of the substrate in the deposition process.
- Better control of the composition.
- Deposits can be selective under certain conditions.
- Annealing is not always necessary.
- Significant processing capacity which lowers production costs.

Table III.1: Characteristics of CVD and ALD processes

CVD	ALD
The precursors react at the same time on the substrate.	The precursors react separately on the substrate (elimination of phase reactions nitrogen purge).
Preferred less reactive precursors (high temperature).	Preferred highly reactive precursors (low temperature).
Uniformity of deposit requires uniformity of flow reactant and temperature control.	Uniformity is ensured by the saturation (self-limited growth).
Thickness controlled by time.	Thickness controlled by the number of cycles of reaction.
Controlled growth speed.	Low growth speed.

Very good uniformity of thicknesses (excellent compliance), elimination of uncontrolled deposits and parasitic reactions in the gas phase are the advantages of ALD compared to CVD. Thin film deposits on substrates depend on the type of application longed for. Soft magnetic materials deposited by PVD. The increase in operating frequencies in the GHz range requires the use of soft magnetic materials combining a strong magnetization at saturation, a weak coercive field and magnetic permeability levels high. We can identify three main families of alloy meeting these requirements:

- **Polycrystalline metal alloys:** Iron-based Permalloys and of nickel present a null magnetocrystalline anisotropy for the composition Fe_{25} Ni_{75} and a coefficient of null magnetostriction for $Fe_{17}Ni_{83}$. So, he is possible to control the intensity of magnetic anisotropy via the composition. Their low resistivity is a negative point for applications micro-layer thin film microwaves.

- **Amorphous metal alloys:** These alloys do not exhibit magnetocrystalline anisotropy and have a low coercive field due to absence of defects (the defects serve as anchor points for the walls of magnetic field). The amorphous state is formed from a certain threshold concentration by the addition of an amorphizing element which has the e ff and of inducing disorder.

III.3 Magnetic characterization of samples

III.3.1 Magnetization measurements:

Several techniques which allowed us the magnetic characterization of samples will be described later. These techniques can be divided into two main categories:

a) Techniques which allowed us to determine the behavior of the magnetization function of the applied magnetic field. In this category there are: VSM, SQUID, MOKE. For each technique, the mode of operation, its sensitivity, its advantages or disadvantages.

b) Techniques which allowed us to determine the magnetic configuration of the samples. This part contains a detailed description of the magnetic force microscope (MFM).

III.3.2 Vibrating Sample Magnetometer - VSM

The operating principle of a vibrating sample magnetometer is based on the Faraday's law, which says that the variation over time of the induction flow passing through a coil induces a potential difference across the coil. In a VSM the variation flux is created by the variation of the magnetization of a magnetic sample which vibrates near detection coils [91].

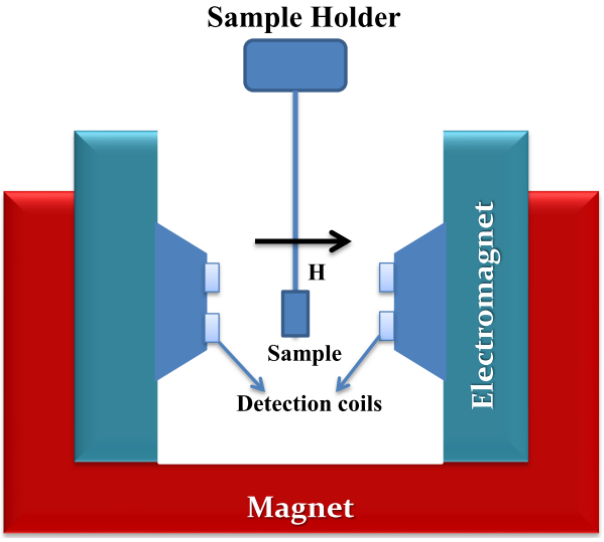

FIGURE III.3: Schematic image of a vibrating sample magnetometer (VSM).

The sample is connected by a sample holder to a vibration source and it is placed in the middle of the detection coils. An electromagnet surrounds the sample and detection coils [92]. It is used to vary the field applied to the sample in order to measure the variation of the magnetization as a function of the field. The sample holder in our case allows rotation of the sample with an amplitude of 360° relative to the direction of the applied field.

III.3.3 Superconducting Quantum Interferometer Device - SQUID

The magnetic properties of thin films have been studied using the vibrating sample magnetometer (VSM) and SQUID (Superconducting Quantum Interferometer Device). The magnetization curves were measured by different methods on a Vibrating Sample Magnetometer (VSM), and SQUID magnetometer (Superconducting Quantum Interference Device). We offer a brief description of the devices used to identify the advantages and disadvantages of the different devices as well as the specific information given by each of the methods. The SQUID also allows us to determine the magnetic moment of the sample based on the external field. Compared to VSM it presents some advantages like for example a greater measurement sensitivity or the possibility of making low temperature measurements. Another advantage of SQUID is the possibility of making measurements at larger fields, up to 7T. The main parts that make up a SQUID are shown in the following figure.

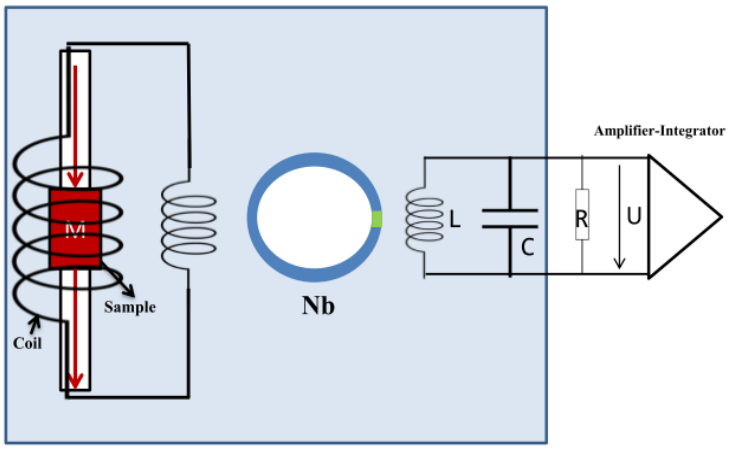

FIGURE III.4: SQUID magnetometer diagram.

The sample to be measured is installed on a rod which performs a movement similar to a unidirectional extraction along the axis of 4 turns in series mounted in opposition and looped on a reel. The flux variations in the coil are proportional to those obtained in the 4 turns and therefore to the magnetization of the sample. The coil will in turn induce a flux variation in a superconductive SQUID ring of Nb, interrupted by a Josephson junction (Nb / insulator / Nb). This allows you to measure the very precise variation in the amount of material flow [93]. In principle, by injecting into the ring a current slightly higher than the critical metal transition current normal superconductor / metal, the output voltage VS is periodic with the flux intensity which crosses the ring: the period of the oscillations corresponds to the "passage" of a quantum of elementary flux ($\Phi_0 = 2.07 * 10^{-15}$ Wb).

The SQUID ring used in this study is coupled inductively to an RF oscillating circuit which, using synchronous detection, gives a voltage proportional to the integrated number of oscillations observed by V_s during the extraction time. The precision on the variation of the flux is a few percent of Φ_0 and the sensitivity of $5 * 10^{-7}$ emu [Jenks_97]. The sample and the detection coils are placed in a liquid He cryostat this which allows measurements at low temperatures up to 4K. The SQUID measurements were carried out at the Jean Lamour in Nancy on a device MPMS Quantum Design. The SQUID allows us to make measurements of hysteresis cycles at several temperatures and zero field cooled –field cooled (ZFC-FC) cycles which will be detailed later. The Magnetism and Cryogenesis competence center in Institut Jean Lamour, currently groups together 7 devices enabling various physical measurements to be made according to a magnetic field and temperature, as well as a complete chain of helium reliquefaction.

Table2: Devices allowing various magnetic measurements to be made at the Jean Lamour Institute

	Squid magnetometer		Modular cryostats		Vibrating Sample Magnetometer	
Devices	MPMS	SQUID-VSM	PPMS		VSM LakeShore	VSM-DMS
Magnetic field	Superconducting coil				Electromagnet	
	7 T		7 T	9 T	2 T	3 T
Temperature	2- 400K	2 - 1000 K	2 – 350 K		300 K	77 -300 K
Magnetic measurements	M (10^{-8} emu)	M + χ (10^{-8} emu)	M + χ + R	M + χ + C	M (10^{-6}emu)	
Benefits		Quick	Resistance, Hall effect, specific heat			Rotating field

Experimental protocol

Two quantum design brand SQUID magnetometers (MPMS and SQUID-VSM) are used to measure weak magnetic signals with a resolution of less than 10^{-8} emu. They are equipped with a 7 T superconductive coil. The temperature of the sample is controlled from 5K to 400K for one and from 2K to 1000K for the other. These devices are typically dedicated to the study of magnetic materials of which at least one of the dimensions is nanometric or for bulk materials / powders of very weak magnetization.

FIGURE III.5: The VSM Squid at the Jean Lamour Institute-Nancy.

Sample Mounting

If our film of Gadolinium is oriented according to the plan we use the quartz sample rod then we mount the sample to 66 mm from the bottom end of the rod and we used the Kapton tape to secure the sample to the rod.

FIGURE III.6 The quartz sample rod.

Sample Centering

The most important step in sample installation procedure is to center the sample correctly. A sample that is incorrectly centered would yield inaccurate measurement data. For “difficult” samples (weak sample signal, inhomogeneous sample, inhomogeneous background such as Holmium (Ho), Dysprosium (Dy)), this step can be tricky. Furthermore, the MPMS system is susceptible to errors in the centering step. It is

almost like an art to know when something is right, and when something has gone wrong and require troubleshooting.

Using an appropriate magnetic field to center the sample

The appropriate field to apply for sample centering depends on the sample. An ideal sample would have a homogeneous diamagnetic background, and the sample itself has strong signal. For most samples of unknown magnetic properties, start with 1000 Oe field for centering. For weakly magnetic samples, it is possible for the sample signal to get cancelled out by the background diamagnetism at a particular value of field. When centering, one wishes to avoid this region where the sample signal is nulled by the diamagnetism of the sample holder. One way is to apply a very large field, at least 1 T, and then center with the diamagnetic signal. Alternatively, if the sample is ferromagnetic and known to have remanence at zero field, then one can center with the remanence signal. First, saturate the sample with a high field (1T is sufficient for most samples), and then set the field back to a small field of 30 Oe. At this field, the diamagnetism is minimized.

Good sample centering profile (Ex Gadolinium)

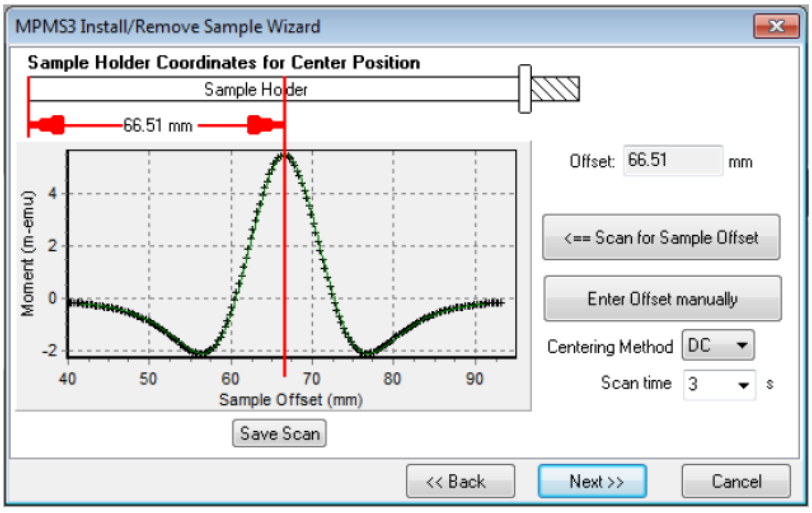

FIGURE III.7: Sample Holder Coordinates for Centre Position

The black cross points are measured signal as a function of position in the detection coil. The green curve is the fitting function, assuming a point dipole source. The red vertical line is the mathematical fit of the sample position from the green curve.

III.4 Thermoelectric characterizations of Gd Thin film

III.4.1 Measuring principles

Electrical resistivity

In order to measure the electrical resistivity of our Gadolinium sample at different temperatures, we opted for a four-contact method. This measurement method is perfectly suitable for our sample which has a low electrical resistance. In addition, this measurement technique makes it possible to overcome parasitic resistances related to electrical contacts and measurement wires and to measure electrical resistivity between 10^{-5} and 10^{-6} W.m. In this method, two wires are used for the passage of an electric current of intensity I connected to the ends of the cut sample in the form of a parallelepiped bar. The two other metal contacts, distant by a distance l, used to measure the voltage resulting ΔV (Figure IV.1).

The electrical resistivity ρ is then simply given by Ohm's law:

$$\rho = \frac{\Delta V}{I}\frac{s}{l} \qquad \text{(III.1)}$$

With “s” The section of the sample.

In order to minimize the experimental error associated with this geometric factor, it is necessary that the sample has a constant section on its entire length and perfectly parallel faces two by two[94].

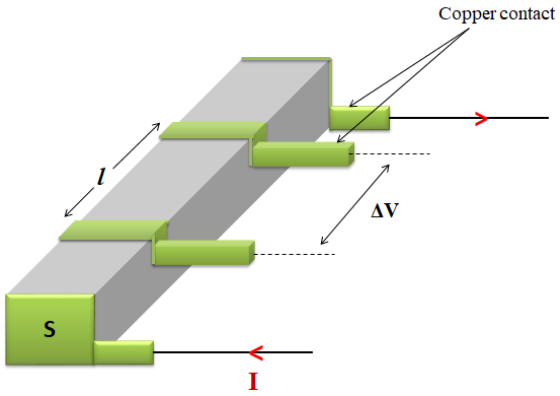

FIGURE III.8: Schematic diagram of the measurement of electrical resistivity by the four-contact method.

Thermal conductivity and thermoelectric power

Thermoelectric power and thermal conductivity were measured simultaneously using a four-contact method derived from the stationary method that we describe here. To carry out stationary measurements, one end of the sample at a fixed temperature through a heat sink. Ideally, the temperature is invariant whatever the energy exchanges with the external environment. Experimentally, this means that its thermal capacity must be high enough to that its temperature variations are negligible [95]. The other end of the sample should be in good thermal contact with a resistive oven. The passage of an electric current in this furnace (of electrical power P) generates a one-dimensional heat flow (if the sample is long in one direction) which flows through the material, creating a gradient thermal. Two temperature sensors connected to the central part of the sample and distant by a length l make it possible to note the drop in temperature ΔT (Figure III. 9). The thermal conductivity K is then given by:

$$K = C\frac{l}{s} = \frac{P}{\Delta T}\frac{l}{s} \qquad \text{(III.2)}$$

With: C [W/K] is the thermal conductance of the sample.

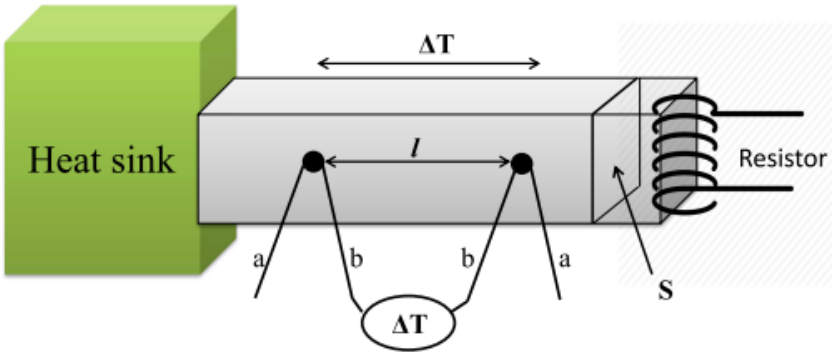

FIGURE III.9: Schematic representation of the principle of measurement of thermal conductivity and thermoelectric power.

The appearance of the temperature gradient also generates tension thermoelectric ΔV due to the Seebeck effect. If the positive terminal of the voltmeter is connected to the hot side of the sample, the thermoelectric power S of the sample is then given by:

$$S = S_{fil} - \frac{\Delta V}{\Delta T} \qquad \text{(III.3)}$$

Where S_{fil} is the thermoelectric power of the tension measurement wires (on figure III.9 wires a) or b). Since the measurement leads are not isothermal, it is necessary to take into account this contribution. The measurement of thermal conductivity by this method

is however very delicate and many experimental precautions are necessary for the heat flux generated by the oven passes completely through the sample. Different heat losses are thus to be avoided such as gas conduction and convection losses, conduction losses in furnace supply thermocouples and the thermocouples connected to the sample for temperature and potential measurements or radiation losses from the furnace and the sample to the coldest parts of the measurement system [96]. Gas conduction and convection losses become negligible if the measurement is carried out under secondary vacuum ($<10^{-5}$ mbar). Losses through measuring thermocouples can be minimized by using metal alloys (such as chromel, constantan or manganin) rather than pure metals. Similarly, thermocouples of low diameter and great length are used so as to make their conductance negligible before that of the sample[97]. Radiation losses, which are mainly significant at temperatures above 150 K, can be reduced by protecting the measuring cell from radiation screen maintained at the temperature of the heat sink.

III.4.2 Physical Properties Measurement System (PPMS)

Experimental protocol

The resistivity measurements were carried out using the PPMS-7T. The cryostat is equipped with a superconductive coil allowing to generate a magnetic field ranging from -7 to 7 Tesla (Figure III.10). The measurements were carried out with alternating current.

FIGURE III.10: The Physical Properties Measurement System 7T at the Jean Lamour Institute-Nancy

The PPMS-7T consists of a low temperature system (340mK to 400K) and an intense magnetic field (0 to 7T) which allows measurements of electrical and thermal transport, specific heat, magnetic susceptibility and dielectric constant. The system includes the cryostat containing the superconducting magnet and operating with liquid helium (4.2K or -269°C). The control module allows to stabilize the temperature, change the magnetic field and make the required measurements dictated by the computer. It is possible to adapt the system to use it with external devices such as very sensitive nanovoltmeters and current sources as small as 1 pA.

The rotator makes it possible to make electrical transport measurements while varying the angle that the sample makes with respect to the magnetic field. This option can be used from 2 to 400K. Measuring the Hall constant is often tricky. Indeed, it requires that two contacts used to measure the Hall V_H voltage are perfectly aligned along a straight perpendicular to the electric field lines. With a 4-contact method, this condition is difficult to achieve, and the measured voltage V_{mes} is in fact the sum of the Hall voltage V_H and a magnetoresistive longitudinal voltage V_{res} (Figure III.11a). For overcome these difficulties, a 5-contact method for accurately measuring the Hall tension was favored (Figure III.11b).

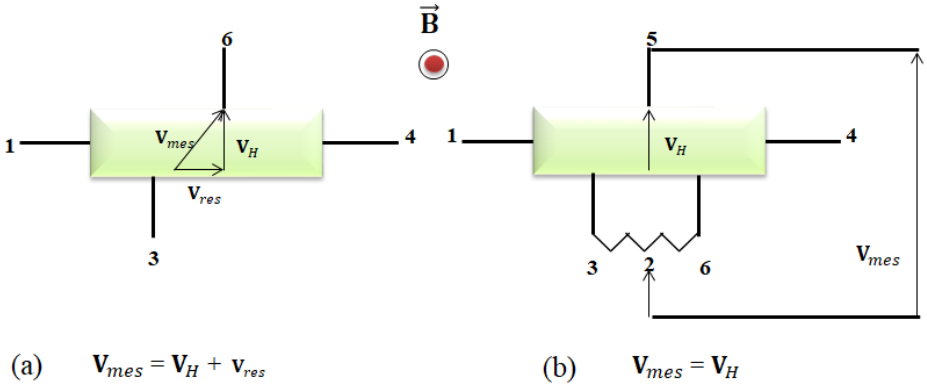

FIGURE III.11. Hall effect measurement with 4 contacts and 5 contacts (b).

Two wires (1 and 4) are used to pass the current and the other three wires (2, 3 and 6) allow measure Hall voltage using a potentiometric method. Under magnetic field zero, a potentiometer between wires 2 and 3 is used to remove the voltage between wires 2 and 5 which corresponds only to the Hall voltage when a non-zero magnetic field is applied (Figure III.12). Consequently, the Hall coefficient corresponds to the slope of the Hall resistivity depending on the magnetic field applied.

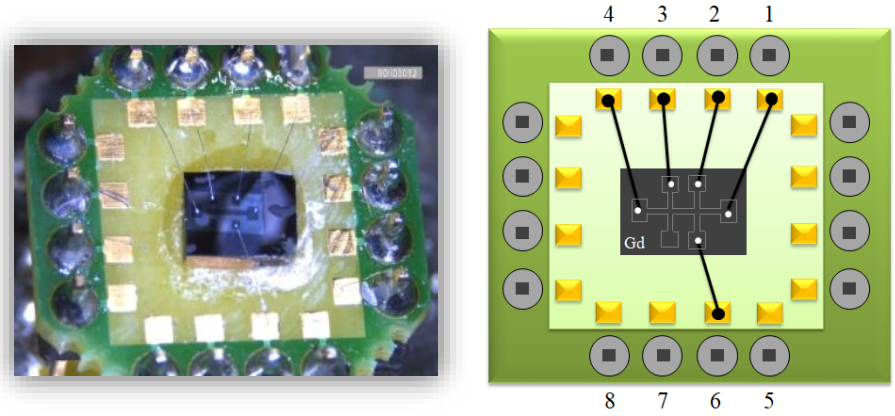

FIGURE III.12. Photo and diagram of the sample holder used for electrical measurements.

Figure III.12 shows the sample holder which was used for the Hall effect measurement from the two available measurement channels. Small diameter tinned copper wires (200 µm) were welded to the bar with a low melting point BiSn solder in order to produce ohmic contacts. Beforehand, gold deposits were made by masking to ensure good wettability of the BiSn solder. The sample is electrically isolated by a film of Kapton® and is then anchored to the support with a thin layer of varnish (GE 7031).

Chapter IV

Theoretical calculations of rare earth materials

IV.1 Introduction

In the fourth chapter of this thesis, we present a theoretical investigation of electronic and magnetic properties of $LaCr_2Si_2C$ and $TbMn_2O_5$, First, we report in section IV.2 an interesting result about the magnetic properties of $LaCr_2Si_2C$, the electric structure and magnetic behavior to improve the experimental work about temperature transition and magnetic ordering, also to show how we can enhance the ferromagnetic behavior of this system. Second, we introduce in section IV.4 the first principles calculations (DFT) of $TbMn_2O_5$ to investigate the electronic and magnetic properties of $TbMn_2O_5$, aim to opening the way for the understanding of the physics behind the RMCE in $TbMn_2O_5$ single crystals and the promising RMn_2O_5 family of multiferroics

IV.2 Study of $LaCr_2Si_2C$ compound

IV.2.1 Introduction

Recently, it becomes possible to compute with a great accuracy an important number of structural, electronic and magnetic properties of solids using first-principles calculations. This kind of development in computer simulations has opened up many of interesting and existing possibilities in condensed matter studies. For example, it is now possible to explain and to predict the properties of solids which were previously inaccessible to experiments [98]. Using different methods of approximation which could be used to describe the magnetic, optical and electronic properties of semiconductor [99-100], insulators [101] or metals. The RCr_2Si_2C compounds have been extensively studied in recent years because of their interesting technology; they can be used in various applications of superconducting materials, the ability of superconductivity to conduct electricity with zero resistance can be exploited in the use of electrical transmission lines.

The experimental results of the X-ray diffraction, magnetic measurements, and neutron powder diffraction show that RCr_2Si_2C compounds crystallize in the tetragonal $CeMg_2Si_2$-type structure (space group P4/mmm). The compounds with R=Pr, Nd, Gd–Dy have a ferromagnetic order at low temperature ($T_C < 35$ K), whereas those with R=Y, La, Ce, and Sm do not exhibit any magnetic ordering below 2 K [102] on the contrary, the parent $ThCr_2Si_2$-type RCr_2Si_2 compounds (R= Y, Sm, Tb–Lu) exhibit strong antiferromagnetic properties ($T_N > 600$K) linked to a large magnetic moment (1.9μB) on the Cr sublattice. The ferromagnetic behavior, is a result of magnetic atoms in connection with nonmagnetic ones, thus to better understand the role played by carbon on structural and magnetic properties in these systems, ab initio electronic structure calculations of RCr_2Si_2 and RCr_2Si_2C compounds with R=Y and La have been performed, using the Korringa Kohn-Rostoker KKR method, in the $ThCr_2Si_2$- and $CeMg_2Si_2$-types as well as their corresponding C-"filled" types, with C atoms located in 001 planes. The results of these studies have allowed elucidating the particular role of carbon in the breakdown of the local magnetic moment on the Cr sublattice [103]. According to these results, and based on our knowledge, there is no theoretical study about the effect of temperature on the magnetic properties, like the magnetization change as function of temperature, magnetic transition ...

IV.2.2 Study of the magnetic stability: Ab-initio calculations

We performed first-principles calculations within the Generalized Gradient approximation (GGA) [104] Based on the full potential linearized augmented plane wave (FP-LAPW) method as implemented in the Wien2k code [105]. The Brillion zone integrations have been carried out using 400 k-points. Well-converged solutions were obtained for R_{MT}*Kmax=7; R_{MT} is the atomic sphere radii and Kmax is the maximum value of the wave vector K=k+G). The self-consistent calculations are considered to converge when the total energy of the system is stable within 10^{-5}Ry.

Structural and Electronic properties

$LaCr_2Si_2C$ [106] has a tetragonal structure (a=b ≠ c and α=β =γ = 90°) with space group P4/mmm settings, standardized atom coordinates are: La ($5d^1\ 6s^2$): 0, 0, 0; Cr ($3d^5\ 4s^1$): 0, 1/2, 1/2; Si ($3s^2\ 3p^2$): 1/2, 1/2, 0.2311; C ($2s^2\ 2p^2$): 0, 0, 1/2 (Figure IV.1) and has a unit cell with lattice parameters a=b= 4.0646 Å, c = 5.4196 Å and c/a = 1.333 [107].

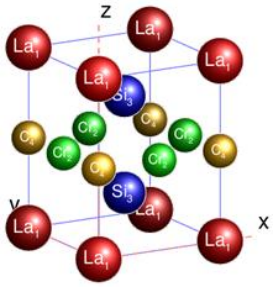

FIGURE IV.1: Tetragonal structure of the $LaCr_2Si_2C$ compound

To determine the nature of $LaCr_2Si_2C$ system and the nature of the distribution of electrons in the valence and conduction band, we calculated the partial and total density of states (DOS) of $LaCr_2Si_2C$ system as displayed in Figure IV.2.

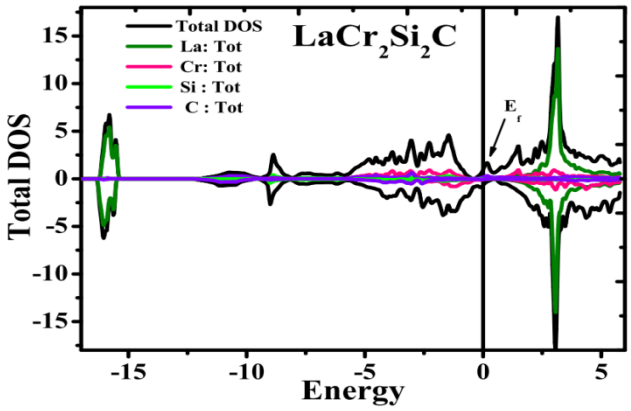

FIGURE IV.2: Density of states total (DOS) by the GGA approximation the $LaCr_2Si_2C$

The valence band consists essentially of Cr -3d orbital, between -5 and 0 eV, the 3d states of Cr are partially filled, whereas the La-5p is located at -15 eV. Figure IV.2 shows the absence of band gap (orbital cross the Fermi level). Accordingly, $LaCr_2Si_2C$ structure has a metallic character. The states in the valence band are dispersive because the bands are very close and thus electrons are easily moved from one band to another. As against the conduction bands are not close, and an electron must have a kinetic energy value for ' jump ' from one band to another and so the states are more localized. The magnetic moment value of Cr is to 0.48 μB, this value is comparable with the magnetic moment given by Ref. [108]: m = 0.5 μB. Cr is the only atom responsible for magnetism in the compound; to interpret the properties of this element we present the following partial DOS in figure IV.3.

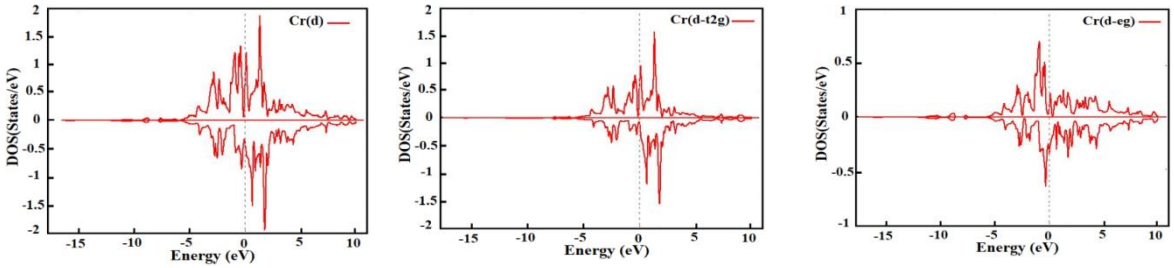

FIGURE IV.3: The density of states of t2g and e2g layers.

Under the effect of the crystal field, 3d band splits into two sub-orbital t2g and e2g, d orbitals have now different energy levels. The normal type is a strong crystal field, and the second type, a weak crystal field in our case, the filling of electrons begins with up-electrons then down-electrons as explained in Figure IV.4, we say in this case that the system has low spin, which explain the value of 0.5 for the effective moment.

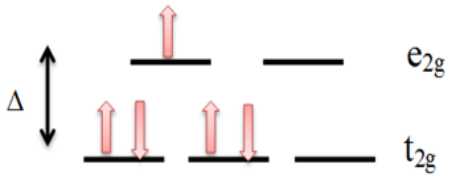

FIGURE IV.4: Simplified diagram of t2g and e2g layers

Stoner criterion: How to stabilize the ferromagnetic order?

The electrons responsible for magnetism become homeless that is highly delocalized, without being totally free. To explain the band of transition metal, a so-called tight-binding approach may be used. In this approach, we consider that the wave function of itinerant electrons is a linear combination of atomic orbitals, this is in perfect agreement with the Stoner criterion which stipulates the existence of ferromagnetism for:

$$I.n\left(E_F\right)>1$$

Where: N (E_F) is the density of states at the Fermi level and I is the exchange integral characterizing the exchange interaction between electrons of the same atomic site. Under the effect of exchange interactions, Δn electrons are transferred from the spin-down band (↓) to the band spin-up (↑) [109].
The bands are shifted in energy with respect to each other by a U-value, resulting in kinetic energy increase for the system (Figure IV.5) Thus, the magnetism results from competition between the energy gain ' exchange interaction I (favoring the movement of gangs and parallel spins) and the increase of kinetic energy (promoting coupling antiparallel spins). According to the Stoner criterion, ferromagnetism is stable only in systems with strong exchange integral and high density of states at the Fermi level.

We want to apply this test to study the stability of ferromagnetism in our system and how it is stabilized by different methods.

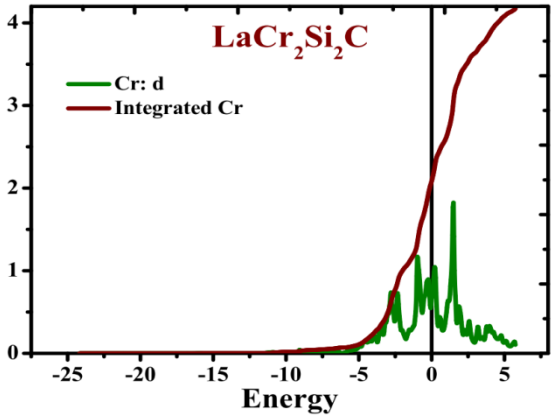

FIGURE IV. 5: The change in the density of states at the Fermi level of Cr and I the integral of exchange which characterizes the exchange interaction between electrons of the same atomic site

- **Defects study (vacancy site) :**

Many lanthanides carbides are reported in the literature, indicating the possibility of chemical bonds between the R and Carbon elements. We can identify the role of carbon in our system by removing carbon atoms and then a comparison is made as shown in Figures IV.6, IV.7 and Table 1.

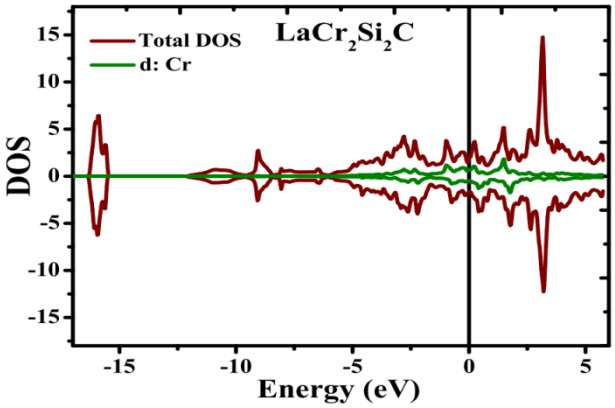

FIGURE IV.6: Total and partial DOS of Cr, $LaCr_2Si_2C$

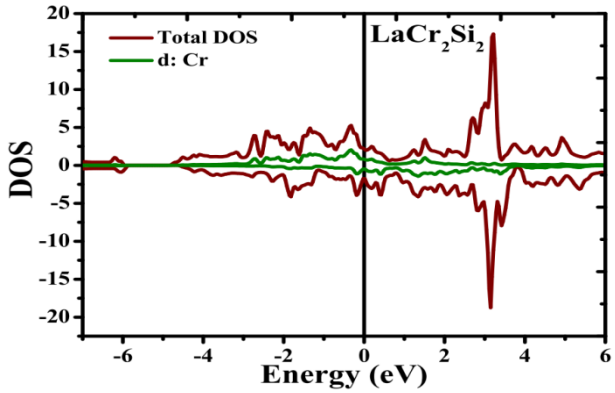

FIGURE IV.7: Total and partial DOS of Cr, $LaCr_2Si_2$

A part of the charge has been moved to the chromium after removal of a Carbon atom, which favored the increase of total and partial magnetic moment of Cr. (Table 1)

Table 1: The Total and partial moments of $LaCr_2Si_2C$ and $LaCr_2Si_2$

	$LaCr_2Si_2$	$LaCr_2Si_2C$
Total moment	4.66	0.85
Partial moment Cr	2.36	0.5
Spin Polarization	31%	13%

According to the following relation $p(\%) = \frac{n_{\uparrow}(E_f) - n_{\downarrow}(E_f)}{n_{\uparrow}(E_f) + n_{\downarrow}(E_f)} \times (100)$, the spin polarization is increased also with Carbon defect.

IV.2.3 Mean field theory

Using ab-initio methods we have compute the value of magnetic coupling Ji and then we can implemented these value in our Hamiltonian of the system is given by:

(IV.1)

Based on the crystal structure of this system (Figure IV.8), we consider 3 types of magnetic coupling in this theoretical study, namely:

J_1: The interaction between the first nearest neighbors of Cr atoms.

J_2: The interaction between second nearest neighbors of Cr atoms.

J_3: The interaction between Cr atoms Cr in different plan.

.

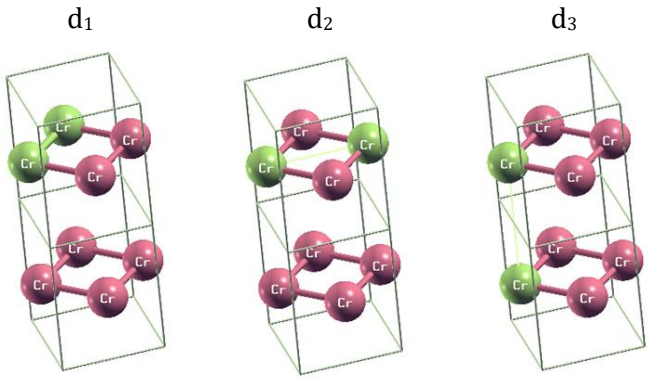

FIGURE IV.8: schematic presentation of magnetic coupling between Cr-atoms

The values of magnetic coupling are computed using the following relation:

$$J = \frac{1}{2zS^2} \Delta E_{FM-AFM} \qquad \text{(IV.2)}$$

The main idea of the mean field theory is to focus on one particle and assume that the most important contribution to the interactions of such particle with its neighboring particles is determined by the mean field due to the neighboring particles, the Hamiltonian of our system can be written as:

$$h_1 = J_1 \sum_j S_j + J_2 \sum_k S_k + J_3 \sum_l S_l \quad \text{(IV.3)}$$

The Gibbs–Bogoliubov inequality, for the free energy per site of an N atom structure, describes the variational principle by Refs. [110, 111, 112]:

$$F \le F_0 = \frac{-T}{N} \ln(Z_0) + \frac{1}{N} \left\langle H - H_0 \right\rangle_0 \quad \text{(IV.4)}$$

With: $$Z_0 = tr\left(e^{-\beta H_0}\right) \quad \text{(IV.5)}$$

H: the Hamiltonian of the structure.

H_0: An effective Hamiltonian in which the interactions of each spin with its neighbors are assimilated to an effective field h.

Z_0: the associated partition function.

With: $$F_0 = -TN \ln\left[2ch\left(\frac{h_1\beta}{4}\right)\right] \quad \text{(IV.6)}$$

$$\left\langle H \right\rangle_0 = -J_1 Z_1 \frac{N}{2} m_s^2 - J_2 Z_2 \frac{N}{2} m_s^2 - J_3 Z_3 \frac{N}{2} m_s^2 \quad \text{(IV.7)}$$

$$\left\langle H_0 \right\rangle_0 = -h_1 N m_s \quad \text{(IV.8)}$$

So: $$F = -TN \ln\left[2ch\left(\frac{h_1\beta}{4}\right)\right] - J_1 z_1 \frac{N}{2} m_s^2 - J_2 z_2 \frac{N}{2} m_s^2 - J_3 z_3 \frac{N}{2} m_s^2 + h_1 N m_s \quad \text{(IV.9)}$$

The free energy Helmotz becomes:

$$F = -TN \ln\left[2ch\left(\frac{h_1\beta}{4}\right)\right] - \frac{N m_s^2}{2}\left(J_1 z_1 + J_2 z_2 + J_3 z_3\right) + h_1 N m_s \quad \text{(IV.10)}$$

Z_1; Z_2 and Z_3 are the first, second and third neibohrs taking the values 4; 4 and 2 respectively.

And by minimizing the energy we found:

$$m_s = \frac{1}{2} th\left(\frac{\beta h_1}{2}\right) \quad \text{(IV.11)}$$

The variation of the magnetization and the susceptibility as a function of temperature with the mean field approximation are shown in figures IV.9 a and b.

(a) (b)

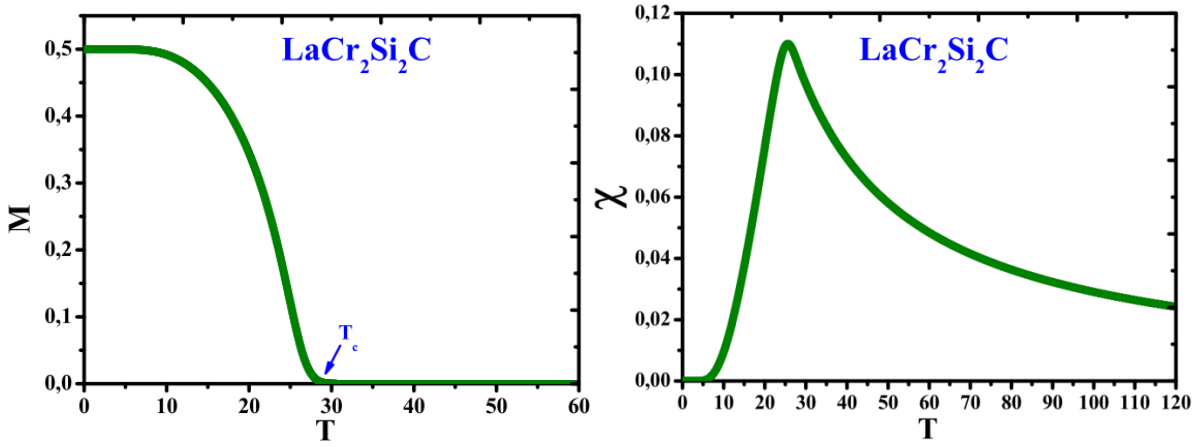

FIGURE IV.9: (a)The variation of the magnetization as a function of T, (b) The variation of the susceptibility as a function of T

We are Using the exchange coupling values obtained by ab-initio calculations (J_1 = 0.95 meV, J_2=0.81 meV and J_3=0.67 meV). The critical temperature as function of the exchange couplings as cited in [113, 114]:

$$T_c = \frac{2}{3}\frac{zJS(S+1)}{K}$$
$$T_c = \frac{2}{3}\frac{(z_1J_1 + z_2J_2 + z_3J_3)}{K} = 31.34K \quad \text{(IV.12)}$$

The approximation of the mean field is known, that it overestimates the value of T_c because, it does not take into account the effects of correlations, so we will apply another approximation to take account of this effect

IV.2.4 Monte Carlo simulation of $LaCr_2Si_2C$

The magnetic properties of $LaCr_2Si_2C$ have been investigated using Monte Carlo simulations. The thermal total magnetization and magnetic susceptibility are found by: [115, 116, 117, 118, 119]

$$m = \frac{1}{N}\sum_{i}^{N}|S_i| \quad \text{(IV.13)}$$

$$\chi = \frac{N}{K_BT}\left(\langle m^2\rangle - \langle m\rangle^2\right) \quad \text{(IV.14)}$$

The critical behavior and the magnetic properties of the $LaCr_2Si_2C$ are analyzed, using Monte Carlo Simulation in combination with the Metropolis algorithm, for systems with linear size L which is varied from 4 to 10.

$$\chi(L) = L^{\frac{\gamma}{\nu}} f_{\chi}\left(tL^{\frac{1}{\nu}}\right) \tag{IV.15}$$

$$\frac{d\langle m\rangle}{d\left(\frac{1}{K_B T}\right)} = L^{\frac{1-\beta}{\nu}} f_m'\left(tL^{\frac{1}{\nu}}\right) \tag{IV.16}$$

$$\frac{d\left(\ln\langle m\rangle\right)}{d\left(\frac{1}{K_B T}\right)} = L^{\frac{1}{\nu}} f_{dm}\left(tL^{\frac{1}{\nu}}\right) \tag{IV.17}$$

$$\frac{1}{K_B T_c(L)} = \frac{1}{K_B T_c} + \alpha L^{\frac{1}{\nu}} \tag{IV.18}$$

The critical behavior of the Ising model is given by ref [120]

$$m\alpha\left(T - T_c\right)^{\beta} \quad ; \quad \chi\alpha\left|T - T_c\right|^{-\gamma} \quad ; \quad Cv\alpha\left|T - T_c\right|^{-\alpha} \tag{IV.19}$$

The changes in physical function of T values are presented in the following figures:

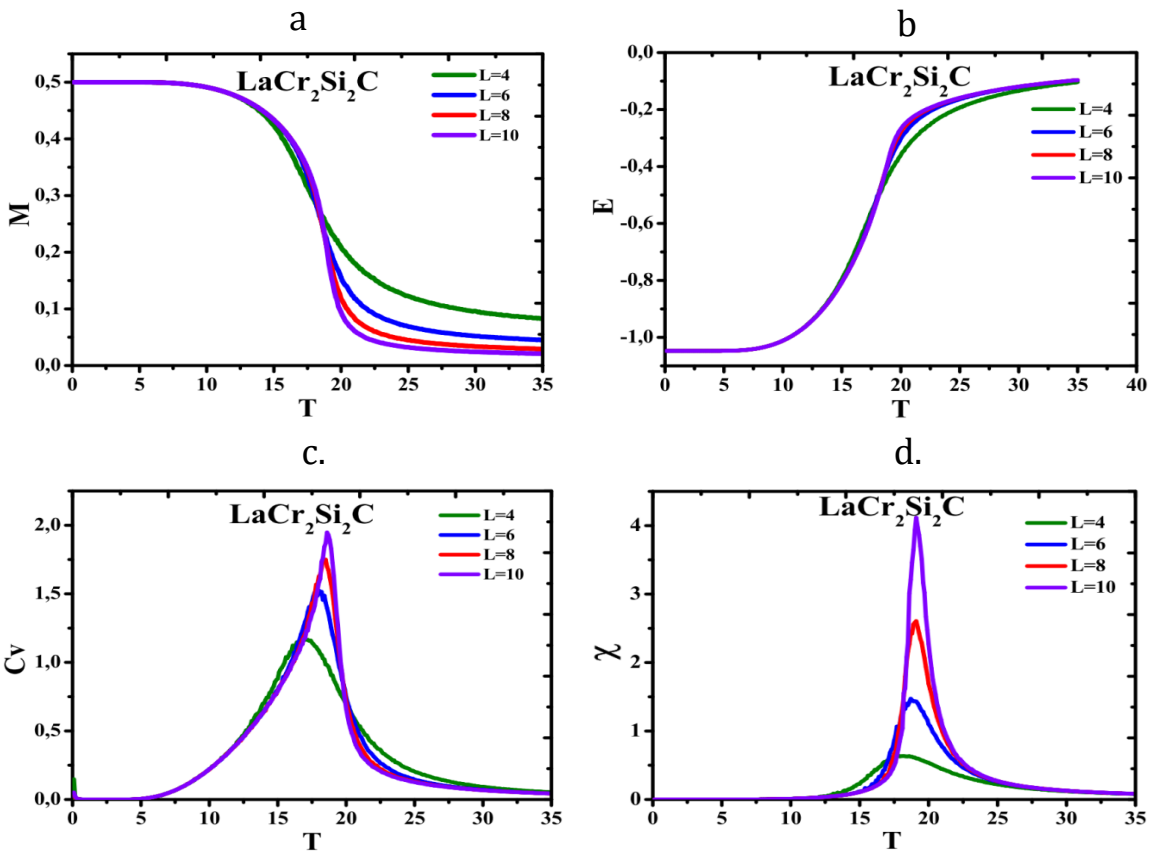

FIGURE IV.10: (a) The magnetization, (b) the energy, (c) the specific heat and (d) the susceptibility as a function of the temperature for L=4 to L=10.

The critical behavior and the magnetic properties of the $LaCr_2Si_2C$ are investigated for systems varying from L = 4 to L = 10. We are Using the exchange coupling values obtained by ab initio calculations (J_1 = 0.95 meV, J_2=0.81 meV and J_3=0.67 meV). In Fig. IV.10 (a)–(d), the variation of the susceptibility and the magnetization for different system sizes is plotted as a function of the temperature, with T_{cMC}=18,5K.

(a) (b)

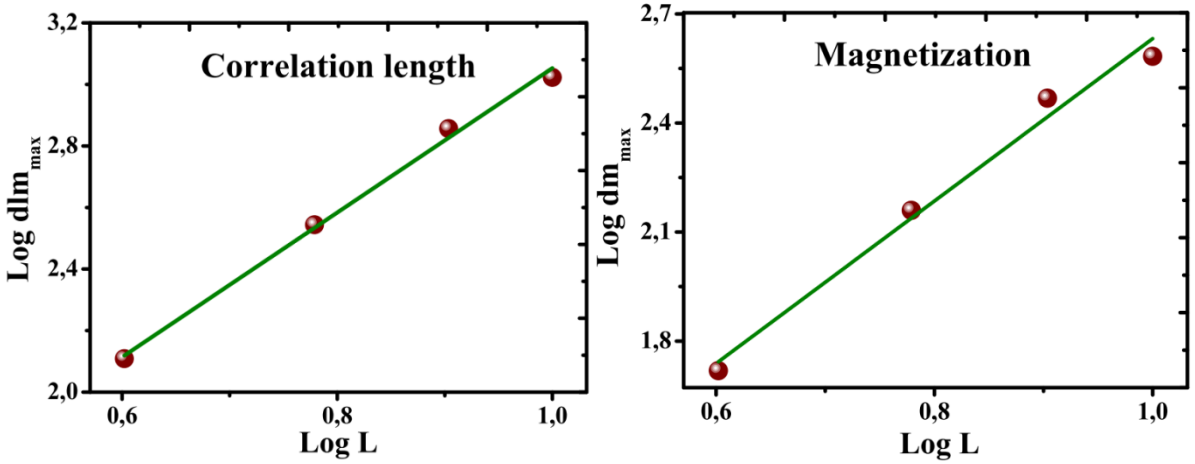

FIGURE IV.11: (a) Log–log variation of the maxima of $\frac{d\left(\ln\langle m\rangle\right)}{d\left(\frac{1}{K_BT}\right)}$ as a function of the system size L, (b) Log–log variation of the maxima of $\frac{d\langle m\rangle}{d\left(\frac{1}{K_BT}\right)}$ as a function of the system size L

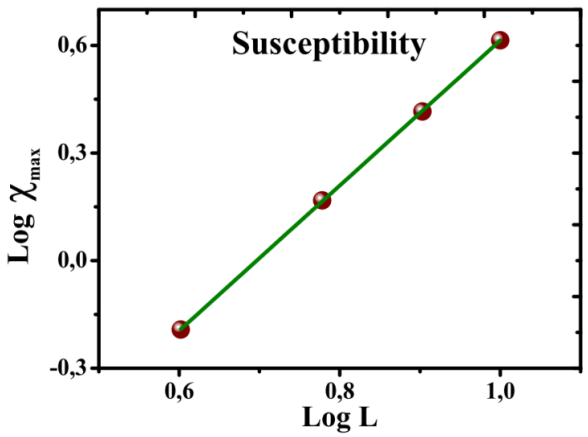

Figure IV.12: Log–log variation of the maxima of the susceptibility as a function of the system size L

For the linear size L, we used the finite size scaling method; this method is used to extracting values for critical exponents by observing how measured quantities vary as the size L of the system studied changes. Indeed for our system, we saw an alignment for L=10.

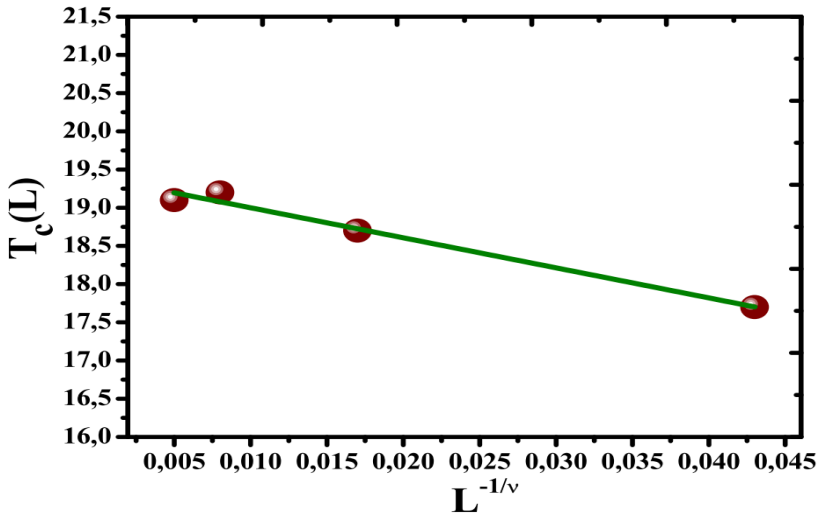

FIGURE IV.13: The transition temperatures of the maxima of $\frac{d\left(\ln\langle m\rangle\right)}{d\left(\frac{1}{K_B T}\right)}$ as a function of $L^{\frac{-1}{\nu}}$

From figures (IV.11 and IV.12) the value of different critical exponents are ν=0.44, β=0.15 and γ=1.012. Now, in order to calculate the critical exponents ν, β and γ and the critical temperature Tc, firstly we take the logarithm of Equation (IV.17) and calculate the critical exponent ν from the slope (1 /ν) of the linear fit as shown in Figure IV. 10. After that, by using the value of the critical exponent ν and taking the logarithm of Equations (15) and (16) we calculate the critical exponents β and γ from the slopes (1−β/ν) and (γ/ν) of the linear fits as seen clearly in Figures IV.11 and IV.12. Finally, from Equation (IV.18), we determine the critical temperature Tc, using the value of the critical exponent ν, which corresponds to the intersection of the linear fit with the axis $T_c(L)$ as shown in Figure IV.13 (T_{cMC}=18,5K), this value is small than the transition temperature found by the mean field approximation, generally $T_{cMFA}=2*T_{cMC}$.

IV.3 Study of $TbMn_2O_5$ compound

IV.3.1 Introduction

The discovery of new multiferroic compounds exhibiting a strong magneto-electric coupling has aroused great interest since the beginning of the century, justified both by the fundamental issues involved and the prospects for technological applications [121]. The interest of these compounds lies in the coupling between orders, magnetic and electrical, with the possibility, from a static point of view, to manipulate the magnetization by applying an electric field [122]. The more recent discovery of magneto-electric excitations has opened up a new field investigation [123]. In multiferroics, these hybrid excitations, called electromagnons can be understood as magnons excited by the electrical component of a wave electromagnetic and are the signature in the dynamic regime of magneto-electric coupling [124, 125]. Understanding the mechanisms behind these new excitations is one of the recent challenges of condensed matter physics, and the possibility of modulating these excitations via a field electric and / or magnetic is also an avenue explored for future applications to be defined in the field of information transport, magnetic refrigeration and spintronic devices for example. These materials in which the magnetism and the ferroelectricity are coupled have been widely studied [126, 127, 128]. Studies on RMn_2O_5 oxides have shown an important magneto-caloric effect (MEE) that is associated with a unique commensurate-incommensurate magnetic transition [121-129]. In this way, by using relatively low magnetic fields a highly reversible switching of electrical polarization was reported in $TbMn_2O_5$ [130]. On the other hand, it was recently shown that the same compound unveils a giant and reversible rotating magnetocaloric effect (RMCE). Habitually, this compound exhibits an insulating behavior. Its crystalline structure consists of edge-shared $Mn^{4+}O_6$ octahedra arranged along the c-axis and linked by pairs of $Mn^{3+}O_5$ pyramids [131-134]. The multiferroic $TbMn_2O_5$ material is characterized also by different exchange interactions involving Mn^{4+}, Mn^{3+} and rare earth R^{3+} ions sublattices, leading to a complex magnetism character. As a result, $TbMn_2O_5$ reveals various magnetic and electric phase transitions [135, 136]. At $T_N = 43$ K, it shows an incommensurate antiferromagnetic (ICM) state with a propagation vector k (0.50, 0, 0.30) that transforms into a commensurate antiferromagnetic (CM) phase at $T_{CM} = 33$ K with k = (0.5, 0, 0.25), while a ferroelectric order takes place at $T_{FE} = 38$ K [135]. Recently, it has been demonstrated that a large thermal effect can be simply produced by rotating the $TbMn_2O_5$ single crystal within the ac-plane in relatively low constant magnetic fields rather than using the conventional magnetization-demagnetization method [121]. Under a constant magnetic field of 2T, the resulting maximum entropy change from the rotation motion is more than 6 J/kg K, while the associated adiabatic

temperature change is found to exceed 8K. Such a large RMCE was attributed to different factors such as strong magnetocrystalline anisotropy, low specific heat as well as the enhancement of the magnetization under magnetic fields lower than 3T.

IV.3.2 Computational method

The $TbMn_2O_5$ compound crystallizes in an orthorhombic symmetry with Pbam space group (number 55). Its lattice parameters are given by: a = 7.2643 Å, b = 8.4768 Å and, c = 5.6700 Å [137]. The electronic and magnetic properties of $TbMn_2O_5$ have been studied using ab-initio calculations with full-potential linearized augmented plane-wave (FP-LAPW) [138] involving the gradient generalized approximation GGA [139], GGA+U and spin-orbit coupling.
Conventional approaches such as the local density approximation (LDA) [140], or that of generalized gradients (GGA) [141], used in density functional theory (DFT), are standards and widely used as an approach to describe the ground state of a large number of insulating, semiconductor and metallic systems. However, it seems to us that they are insufficient to obtain a satisfactory qualitative description of the structure electronics and magnetic properties of correlated systems, so it is necessary to go beyond the DFT to properly treat strong electronic correlations. Several corrections have been developed to provide solutions to this DFT deficiency.
Among those which have been applied, we find the GGA+U method [142, 143], where "U" is the Hubbard parameter which designates the intra-atomic Coulomb interaction applying to localized orbitals (In general d or f) to correct errors in the DFT.

In $TbMn_2O_5$, U is equal to 8eV for Tb and 4eV for Mn while J is assumed to be zero for both atoms [139]. The total and partial electron densities are calculated at equilibrium state. The self-consistent calculations are considered to converge with a convergence criterion fixed by a variation of the sixth decimal place in the electronic charge density and with 7x6x9 Monkhorst-Pack mesh implemented in the code WIEN2k [144]. In this work, calculations are performed on the Pbam orthorhombic structure of $TbMn_2O_5$ reported in Figure 1 using the reported crystallographic parameters in ref [137].

To determine the magnetic anisotropy, we have utilized DIPAN program implemented in WIEN2K code [138] that calculates the magnetic dipolar hyperfine field and the dipolar magneto-crystalline anisotropy. It is theoretically possible to measure the XMCD signal of any compound having at least one paramagnetic moment and for which the spin-orbit coupling is not zero. The analysis of XMCD spectra allows, with the "sum rules", to go back to the moment of spin and orbit of the studied element $TbMn_2O_5$. It is necessary for that, firstly, to have the absorption field in zero field and calculate it's integral, secondly, to make the difference of the two absorptions obtained for the two polarizations, it is the signal XMCD [144]. This signal is employed to estimate the value of the spin and orbital moments in $TbMn_2O_5$ compound. Also, the XMCD spin moment sum rule to the $M_{4,5}$ edges of Tb is used for the calculation of orbital and spin moments. Considering the

transition 3d (c = 2) into 4f final states (l=3) with the number of holes n = 4l+2-n_{4f}, the following equations are obtained [48]:

$$m_L = (\mu_b / \hbar)\langle Lz \rangle = -2((\int_{M_4+M5} d\omega(\mu^+ - \mu^-)) / \int_{M4+M5} d\omega(\mu^+ + \mu^-)) * \left(14 - n_{4f}\right) \quad \text{(IV.20)}$$

$$ms = (\mu_b / \hbar)\langle Sz \rangle =$$

$$((7\int_{M5} d\omega(\mu^+ - \mu^-) - 6\int_{M4} d\omega(\mu^+ - \mu^-)) / (\int_{M4+M5} d\omega(\mu^+ + \mu^-)) * \left(14 - n_{4f}\right)\left(1 + 10(\langle Tz \rangle / \langle Sz \rangle)\right)^{-1} \quad \text{(IV.21)}$$

Where the Sz and Lz are the spin and orbital moment of Tb atoms, respectively.

IV.3.3 Electronic properties results

The compound $TbMn_2O_5$ has an orthorhombic structure consisting of octahedra of $Mn^{4+}O_6$ and bipyramids of $Mn^{3+}O_5$ linked by their edges and their corners. This structure is illustrated in FIG. 1. Perfect knowledge of the magnetic orders of the Mn^{3+} and Mn^{4+} ions is essential for a good understanding of the multiferroic character of the compound $TbMn_2O_5$. This material has several magnetic transitions. Below 10 K, the magnetic order of the Tb ion spins appears and adopts an antiferromagnetic order. Given the complexity of these magnetic orders, we will simplify the diagram of these configurations by looking at the ab plane, in which the ion spins Mn are almost confined.

The front view of the ab plane shows that the crystal structure of $TbMn_2O_5$ is formed by two loops of manganese ions. Each loop consists of a chain of manganese ions Mn^{4+} -- Mn^{3+} -- Mn^{3+} -- Mn^{4+} -- Mn^{3+} which forms a pentagonal loop. The two loops share two neighboring $Mn^{3+}O_5$ pyramids. However, if an antiferromagnetic coupling between two neighboring spins is established, it should favor an antiparallel arrangement along the entire chain. However, this is not the case. Indeed, geometrically, one cannot form an antiferromagnetic order along a loop formed by five manganese ions. This creates a frustrated magnetic structure which gives rise to more complex magnetic orders.

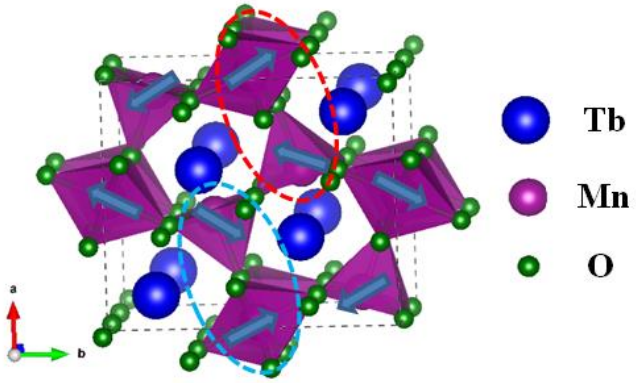

FIGURE IV.14: Orthorhombic structure of $TbMn_2O_5$, the blue arrows indicate the magnetic structure of manganese ions.

Figure IV.14 shows the magnetic configuration of $TbMn_2O_5$ in the commensurable antiferromagnetic phase, the spins of which are ordered antiparallelically along the zigzag chain along the b axis. The neighboring pairs $Mn^{3+} - Mn^{4+}$ are alternately coupled in a quasi-ferromagnetic and quasi-antiferromagnetic manner along the axis a (ellipses in red and blue dotted lines). As we had discussed previously, $TbMn_2O_5$ crystallizes in an orthorhombic structure of space group Pbam, The manganese in this structure have two valences, Mn^{3+} and Mn^{4+}, corresponding to two crystallographic sites, The cations Mn^{4+} have an octahedral environment of six oxygen (Fig IV.15). The octahedra are joined together by a ridge and form continuous chains along the c axis. The Mn^{3+} environment has pyramids with a square base of five oxygen. They are organized in dimers in which the two pyramids share an edge. Octahedra and bipyramids constitute the elementary building bricks. Along the c axis, there is an alternation of planes of pyramids $Mn^{3+}O_5$, octahedra $Mn^{4+}O_6$ and rare earth Tb^{3+}.

The crystallographic sites and the coordinates of the ions in the mesh are given in the following table:

Table 1: Atoms positions in $TbMn_2O_5$

Ion	Name	Position
Tb^{3+}	Tb	(x, y, 0)
Mn^{3+}	Mn1	(0, 0.5, z)
Mn^{4+}	Mn2	(x, y, 0.5)
O	O1	(0, 0, z)
O	O2	(x, y, 0)
O	O3	(x, y, 0.5)
O	O4	(x, y, z)

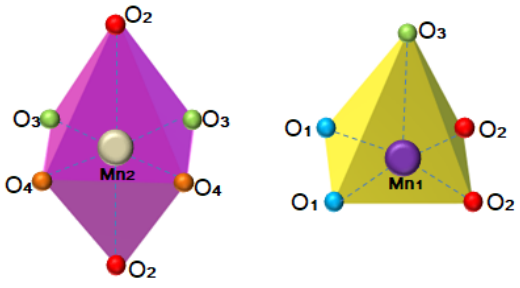

FIGURE IV.15: Basic structural units of distorted $Mn1O_5$ octahedra and $Mn2O_6$ square pyramid

In order to explain the impact of electronic structure on the magnetic properties, we have calculated the total and partial densities of states (PDOS) of $TbMn_2O_5$ with GGA and

GGA+U approximations as they are displayed in Fig.IV.16(a) and Fig.IV.16(b). The lower valence bands situated in the range (-7.0 eV) to (-5.0 eV) is due to the Tb-f states. The main contribution to the magnetism comes from 4f states of Tb atoms.

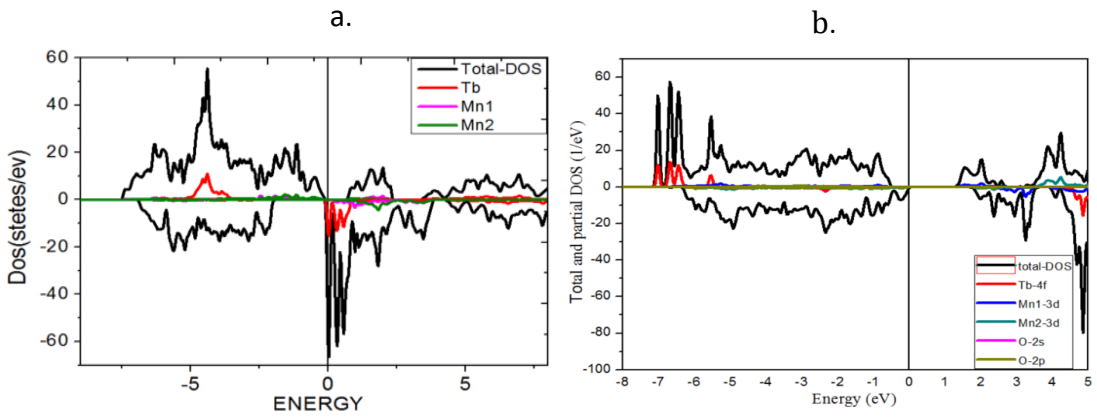

FIGURE IV.16: (a) Total density of states for $TbMn_2O_5$ with the GGA approximation. (b) Total and partial density of states for $TbMn_2O_5$ with the GGA+U approximation.

The detail of the structure strongly depends on the nature of Terbium. It is not only the order of moments of Tb^{3+} which differs from one compound to another of the same family, but also the order of moments of Mn can also be influenced [146, 147]. This indicates the role of Tb in the magnetic ordering of manganese ions. Indeed, with its strong spin-orbit coupling, the Tb^{3+} ion has a strong anisotropy. Since that of manganese ions is much weaker, it is expected that the magnetic order in $TbMn_2O_5$ will depend on the anisotropy of Terbium. The filling of the d orbitals in a pyramidal environment with a square base and in an octahedral environment is done by respecting Hund's rule (the energy of repulsion is minimized by adopting a maximum spin state). The environment of the terbium, having 8 first neighbors, and the nature of the 4f orbitals being more complex, the estimation of the degeneration and the filling of these orbitals requires more detailed calculations based on a precise crystallographic structure. The nature of the occupied 3d and 4f orbitals and the fine crystallographic structure are essential parameters for the calculation of the exchange integrals.

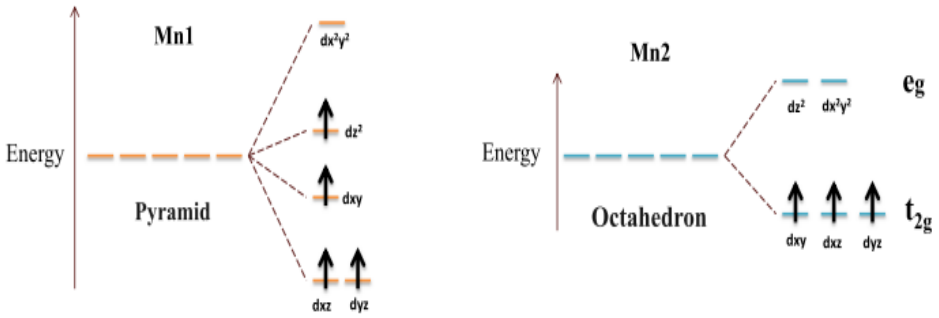

FIGURE IV.17: Energy levels and filling of 3d manganese orbitals in a pyramidal (left) and octahedral (right) environment.

The Pbam symmetry of $TbMn_2O_5$ allows a position freedom of Mn^{3+} ions along the pyramid axis. Such motion alters the Mn-O bonds, and thus the hybridization between the manganese 3d and oxygen 2p states. It is worth noting that the U value is taken from ref [148].

The density of states for Mn1 show that the t_{2g} level gives rise to two levels: a level which remains stable with a pure metallic character dxy and a level formed by the two hybrid molecular orbitals with a metallic character dxz and dyz, this level is a little destabilized because of the decrease in the binding character metal ligand. The level eg generates an undisturbed level formed predominantly of dx^2-y^2, and a dz^2 level which is stabilized (see Fig IV.17 and IV.18).

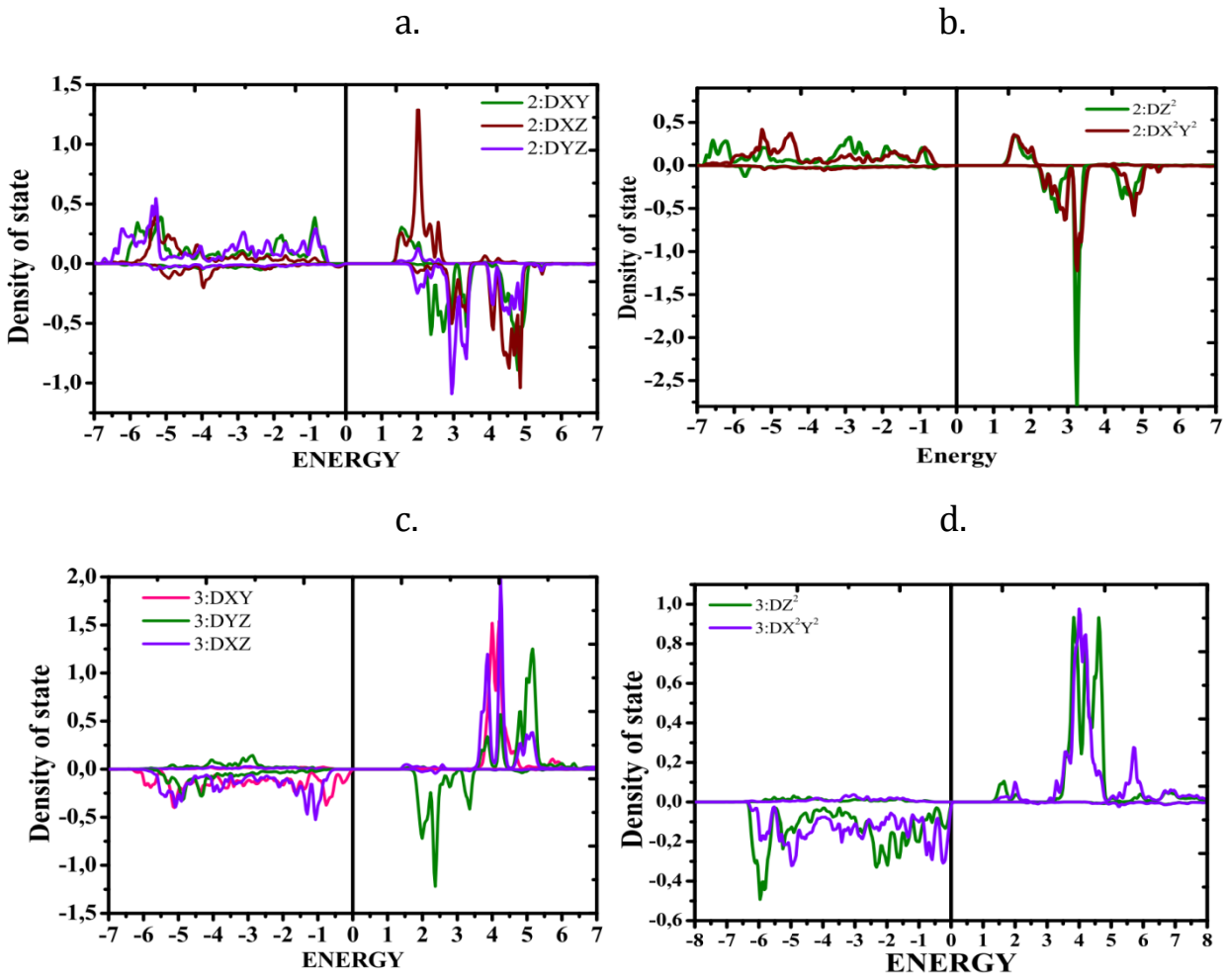

FIGURE IV.18: The density of state as a function of energy (eV), of Mn1 (number 2) and Mn2 (number 3) atoms, (a) dxy, dxz and dyz states, (b) dz^2 and dx^2y^2 states for Mn1 atoms, and (c) dxy, dxz and dyz states, (d) dz^2 and dx^2y^2 states for Mn2 atoms.

IV.3.4 Magnetic properties results

In order to well understand the magnetic interactions in the $TbMn_2O_5$ compound, we have calculated the values of Tb and Mn spins and their orbital magnetic moments [149]. The sign of the XMCD signal and that of its integral give the relative orientation of the magnetic moments between them and with respect to the applied external field. For the total magnetic moment given in The Self-Consistent Field (SCF) calculation, it is difficult to distinguish between the contributions from the spins and orbitals since it is equivalent to the difference between up and down spin densities of state.

For these reasons XMCD can gives more details about the value of spin-orbit coupling and calculate separately the spin and orbital moments. The absorption and dichroic spectra XAS and XMCD of $TbMn_2O_5$ are shown in Fig IV.19(a) and Fig IV.19(b). At the M edge, the absorption spectrum presents a peak situated at 1208.0 eV. At the L_2 edge, the spectrum presents one contribution at 1244.5 eV. The integral of XMCD and XAS allows the calculation of orbital m_{orb} and spin m_s moments.

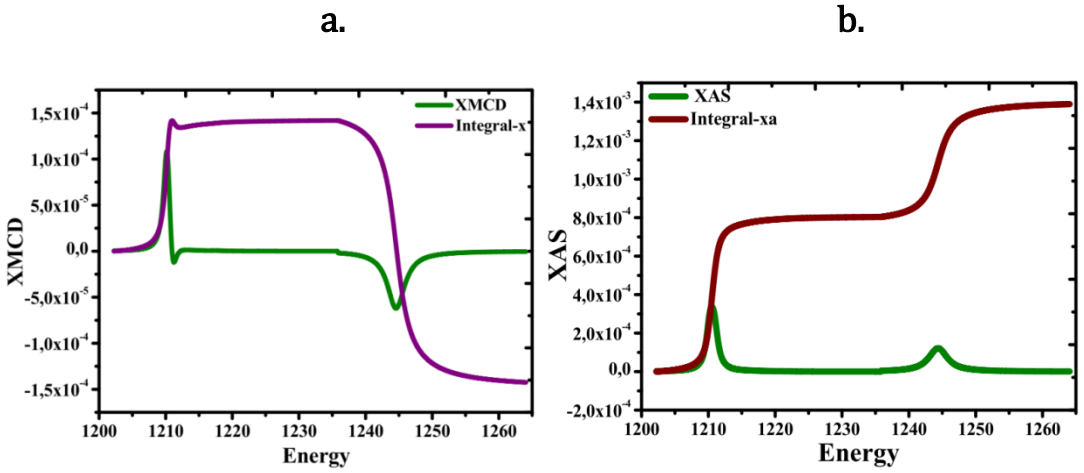

FIGURE IV.19: (a) X-ray magnetic circular dichroism (XMCD) spectra of $TbMn_2O_5$. (b) X-ray absorption spectroscopy (XAS) spectra of $TbMn_2O_5$.

The number of 4f-electrons (3d) is calculated by integrating the 4f projected (3d) density of states inside each atomic sphere. According to the relations (IV.20) and (IV.21) and using GGA approximation, the values of m_{orb} and m_s are given in Table 2 for both Tb and Mn atoms. These values indicate on the strong contribution of Tb ions to the total magnetic moment [150]. On other hand, the obtained moment for Tb compares well with that experimentally reported in Refs. [121] and [151].

Table 2: The orbital and spin moments of Tb, Mn1 and Mn2 atoms for $TbMn_2O_5$.

	XMCD			Experimental
	Tb	Mn1	Mn2	Tb
Spin moment (μB)	6.9	-2.01	1.44	-
Orbital moment (μB)	1.69	-0.15	0.06	-
Total moment (μB)	8.59	-	-	9.34[152]

In $TbMn_2O_5$ compound, giant magnetocrystalline anisotropy is remarked where the magnetization tends to orient preferentially along the a-axis [121, 151] (along the b-axis for $HoMn_2O_5$ [153]).As mentioned before, the DFT calculations using xdipan program enabled us to determine the minimal energy corresponding to the easy-axis of magnetization. Thus, the magnetic anisotropy is defined as:

$$\Delta E = E(\text{easy axis})\text{-}E(\text{hard axis}).$$

The spin-orbit term is included to observe the change in density of states. For 4f states and 3d states, it is known that there is a competition between the spin-orbit effect and the crystal field. The latter is usually strong in the case of 3d states (transition metals). Also, the rare earth elements require a spin-orbit calculation. So, it is highly important to see the charge distribution in 3d and 4f states in the case of spin orbit coupling (SOC). To understand the anisotropy shown by $TbMn_2O_5$, we calculated the energy of the compound following each axis using DIPAN package implemented in WIEN2k program. The calculation consists to compute the total energy for different axes to find the minimal one. For $TbMn_2O_5$, the lower value corresponds to the a-axis, confirming early reported experimental works [121, 154]. The Hubbard U potential makes it possible to localized f and d states or the electrons which are delocalized. The localization of these bands which are responsible for the magnetisms makes it possible to better calculate the magnetic moment and the most stable magnetic phase, as well as the spin orientation of each electron which gives access to the orientation of the magnetization in the compound. In fact we obtain the most probable value of magnetic anisotropy energy (MAE).

Table 3: Magnetic anisotropy of $TbMn_2O_5$ using GGA and GGA+U

Direction	$E_{anj}(J/m^3)$	
	GGA	GGA+U
[001]	$-0{,}8625.10^3$	$-0{,}7853.10^4$
[100]	$-0{,}2985.10^4$	$0{,}1474.10^5$
[010]	$-0{,}7825.10^3$	$-0{,}6890.10^4$
[110]	$-0{,}1311.10^4$	$0.2292.10^4$
[101]	$-0{,}4524.10^3$	$0{,}6133.10^4$
[011]	$-0{,}6167.10^3$	$-0{,}7190.10^4$
[111]	$-0{,}2786.10^3$	$0.19058.10^3$

It seems from the table 3 that the calculations without applying the potential U give the easy magnetization axis on the a axis while the correction U gave a minimum energy on the [011] axis or the (001) plane.

It should be noted that the magnetic anisotropy is given by the Wien2k code using the Dipan package, which just gives an anisotropy contribution, in particular it is the anisotropy created by the network. For the correction U, the easy magnetization axis is located between the z axis and the yz plane, which confirms the non-collinearity of the spins of magnetic atoms [155].

Chapter V

Gadolinium thin films: Theoretical and experimental results

V.1 Introduction

Metallic Gadolinium is the favorite choice as a magnetic refrigerant material for most active magnetic regenerator (AMR) prototypes that have been developed so far because it displays a large change in magnetic entropy among elemental ferromagnets with high Curie temperature near room temperature when it undergoes a second order magnetic phase transition. In this chapter, the Magnetocaloric (MCE) and electrocaloric (ECE) properties of fabricated Gadolinium films (Si/Ta/Gd(100nm)/Pt(3nm)) are measured, aiming to get more insight about the physics behind the interesting electronic and magnetic properties of this material. The physical properties of magnetocaloric materials are decisive for obtaining an important magnetocaloric effect [156]. The refrigeration techniques developed and potentially marketable require efficient refrigeration materials which meet many other criteria such as structural stability, resistance to oxidation or good electrical conductivity [157]. The magnetocaloric effect has been extensively studied in the past forty years, and much experimental data has been reported in the literature [158]. The majority of studies have focused on rare earths and compounds based on rare earths and transition metals [159]. For refrigeration applications around room temperature, the reference element discovered experimentally is pure gadolinium [160, 161]. At its Curie temperature of around 294 K, its magnetocaloric properties ΔS_m and ΔT_{ad} are approximately -10 $J.kg^{-1}.K^{-1}$ and 12 K, respectively with a field variation magnetic from 0 to 5T [162-165]. This important magnetocaloric effect is linked to the high value of its magnetic moment (7 μB / atom) coming from its $4f^7$ electrons and we will take it apart in this chapter. In addition, the absence of spin-orbit coupling (L=0) in gadolinium implies the absence of hysteresis in the magnetization / demagnetization cycles [166, 167]. These excellent properties make gadolinium often the rare earth of choice for the development of materials based on rare earths [168]. More generally, current research focuses on materials in which the magnetic element is a rare earth or a 3d transition metal.

In 1997, Pecharsky and Gschneidner [169, 170] discovered a very important magnetocaloric effect in the compound $Gd_5Si_2Ge_2$, which undergoes a 1st order transition near room temperature. They also showed that with a variation of the applied magnetic field from 0 to 5 T, the peak of ΔS_m, reached almost 273 K, is around -20 $J.kg^{-1}.K^{-1}$ [171]. The fact that this variation in magnetic entropy is so great compared to the gadolinium bulk, earned it the name of giant magnetocaloric effect. Since the discovery of this giant effect, the search for new magnetic materials with high EMC values has seen renewed interest from many scientists around the world [172]. In general, the materials currently available have values of ΔT_{ad} between a few Kelvin and a few tens of Kelvin. Similarly, they reach values of $-\Delta S_m$ between a few $J.kg^{-1}.K^{-1}$ and a few tens of $J.kg^{-1}.K^{-1}$ (or between a few tens and a few hundred $mJ.cm^{-3}.K^{-1}$).

On the other hand, the MCE on magnetic thin films is of particular interest for micro-refrigeration devices [173]. In this particular aspect of the MCE, the intrinsic characteristics of thin films like the strong demagnetization effect becomes of specific research interest. Usually, the characterization of the MCE of a material consists in determining the isothermal entropy change, ΔT_s, as well as the adiabatic temperature change, ΔT_s, which appear as a response of the material to the application of a magnetic field [174]. In a magnetic medium with crystalline or shape anisotropy, as is the case of the Gd films, the work done by the applied magnetics field depends on its orientation relative to the film [175]. This comes from the fact that the magnetization tends to be aligned in the plane of the film, mainly due to the demagnetizing field energy [176]. Therefore, the direction of the resulting magnetization will depend on the applied field strength and orientation. As a consequence, the MCE, expressed through both ΔT_s and ΔT_a, can be obtained by just rotating the film with respect to the field direction. However, the small amount of material is a challenge for the experimental determination of the MCE.

V.2 Study of Gadolinium Bulk and thin film: DFT calculation

V.2.1 Crystal structure and density of state

Gadolinium [Gd] $4d^{10}\ 4f^7\ 5s^2\ 5p^6\ 5d^1\ 6s^2$, has a Hexagonal structure with space group P63/mmc settings, standardized atom coordinates are: Gd_1: 1/3, 2/3, 1/4 and Gd_2: 2/3, 1/3, ¾ (See Figure V.1) and has a unit cell with lattice parameters a = b = 3.639 Å and c= 5.812Å. To determine the nature of Gadolinium system and the nature of the distribution of electrons in the valence and conduction band, we calculated the partial and total density of states (DOS) of Gadolinium system as displayed in Figure V.2.

We performed first-principles calculations within the Generalized Gradient approximation (GGA) Based on the full potential linearized augmented plane wave (FP-LAPW) method as implemented in the Wien2k code. The Brillion zone integrations have

been carried out using 400 k-points. Well-converged solutions were obtained for R_{MT}*Kmax =8; R_{MT} is the atomic sphere radii and Kmax is the maximum value of the wave vector K=k+G). The self-consistent calculations are considered to converge when the total energy of the system is stable within 10^{-5}Ry.

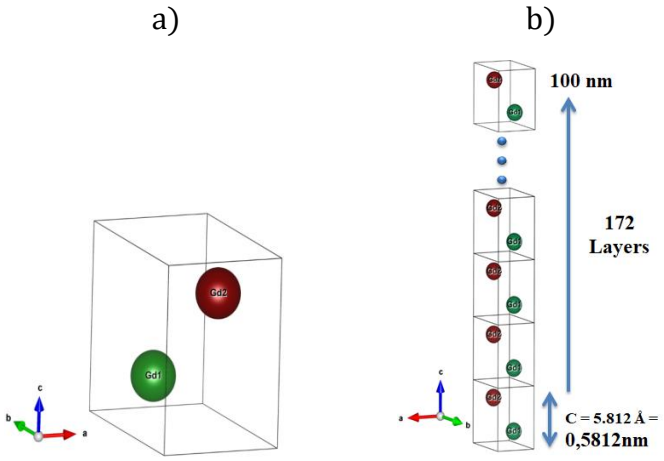

FIGURE V.1: Hexagonal structure of the Gadolinium (Bulk) and b) Simplified diagram of the layer simulated by the Wien2K code.

In order to explain the impact of electronic structure on the magnetic properties, we have calculated the total and partial densities of states (PDOS) of Gadolinium Bulk and Thin film(2nm) with GGA approximation as they are displayed in Figure V.2 (a)and figure V.2(b). The lower valence bands situated in the range (−5.0 eV) to (−4.0 eV) are due to the Gd-f states. The main contribution to the magnetism comes from 4f states of Gd atoms. The density of the states shows the distribution of the electrons in the conduction band and the valence band of gadolinium. We can see that the electrons of the valence band are in localized states. They cannot participate in the phenomena of electrical conduction. Conversely, the electrons in the conduction band are delocalized (free electron of 4f). It is these electrons that participate in electronic conduction. From the figure V.2 The magnetic moment value of Gd Bulk and Gd thin film is to 6,863 µB and 7,17641 µB, respectively.

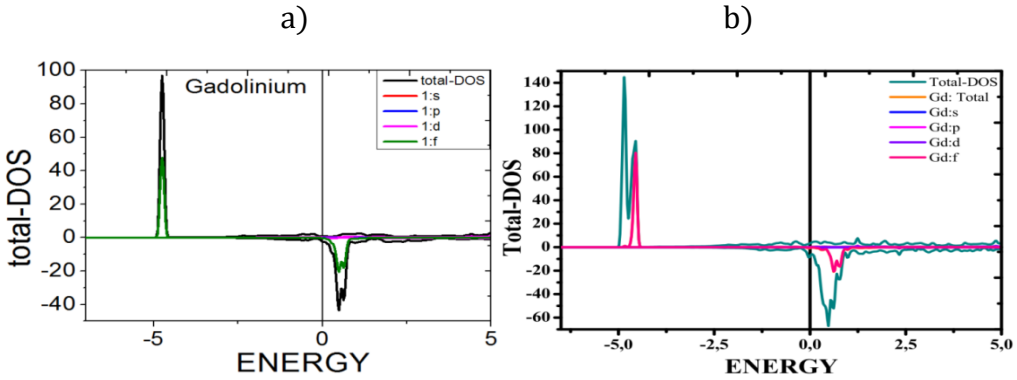

FIGURE V.2: Total and partial density of states for Gadolinium with the GGA approximation, a) Gd Bulk and b) Gd thin film (2nm).

The conduction band is partially occupied, which allows the electrons of this band to pass to higher energy levels, without violating the Pauli Exclusion Principle, and thus participate in the conduction.

V.2.2 Magnetic anisotropy calculation: Easy and difficult axis magnetization

To understand the anisotropy shown by Gadolinium compound, we calculated the energy of the system following each axis using DIPAN package implemented in WIEN2k program. The calculation consists to compute the total energy for different axes to find the minimal one. For Gadolinium Bulk , the lower value corresponds to the z-axis, and

Table V.1: Magnetic anisotropy of Gadolinium using GGA approximation.

	Gd(bulk)	Gd thin film (0.5 nm)	Gd thin film (2nm)
Axes	$E_{an}(J/m^3)$	$E_{an}(J/m^3)$	$E_{an}(J/m^3)$
001	-0,72999	0,16585	$0.8578417.10^5$
100	0,364998	-0,82925	$-0.4289209 .10^5$
010	0,364998	-0,82925	$-0.4289209.10^5$
110	0,364998	-0,82925	$-0.4289209.10^5$
101	-0,63384	0,15502	$0.8475449.10^5$
011	-0,63384	0,15502	$0.8475449.10^5$

We see from the table V.1 that for gadolinium Bulk the easy magnetization axis is the z-axis. On the other hand, the thin layer of Gadolinium the energy is minimal along axes [100], [010] and [110], so the a-axes and b-axes are easy axes magnetization from our thin film Gadolinium. We conclude that the electrons for our thin layer of Gadolinium can be moved easily along the plane (ab). This result served us to choose the orientation of our thin layer of Gd100nm in our experimental study.

V.3 Study of Gadolinium thin film: Experimental results

Gadolinium and some Gd based alloys have been considered as reference materials for applications of the magnetocaloric effect (MCE) mainly because their magnetic phase transition occur near room temperature. The production of an efficient magnetic cooling system is a challenge of all scientific researchers. We find it in very diverse applications such as air conditioning of buildings and vehicles, preserving food, gas liquefaction (hydrogen, nitrogen, helium) and the cooling of electronic devices. The most used technology at the moment is the compression refrigerator. It is based on the phase change (liquid / gas) of a refrigerant fluid. These fluids have been used for almost 60 years until their responsibility for the destruction of the ozone is established. In addition to environmental constraints,

compression refrigeration has reached it's the limit of efficiency, this is why research is moving towards other technologies for the production of cold such as thermoelectric, thermoacoustics and magnetic refrigeration. We are interested in magnetic refrigeration. This technology is based on the magnetocaloric effect, an intrinsic property of some magnetic materials, which results in a temperature change of these materials when subjected to a magnetic field variation. Several prototypes of magnetic refrigeration have been made around the world but there is still progress to be made both fundamentally and practically to make this technology industrially viable and competitive. A study of the literature shows that gadolinium (Gd) metal and its alloys have been considered as reference materials in magnetocaloric refrigeration systems. As indicated, currently gadolinium (Gd), a rare earth with an important EMC in the vicinity of the room temperature, is the material used in most demonstrators and magnetic refrigeration prototypes. However, despite its magnetocaloric power, Gadolinium is not suitable for market applications because of its very high price. To replace gadolinium in refrigeration systems magnetic, new magnetocaloric materials have been developed. The giant magnetocaloric effect in the $Gd_5(Ge_{1-x}\ Si_x)_4$ compounds was discovered. The compound $Gd_5Ge_2Si_2$ has a maximum entropy variation of 18 J/kg.K at 276K under a field of 5T, more than one and a half times greater than the gadolinium. The maximum entropy temperature can be adjusted by changing the proportion of Ge and Si of the compound.

Rare earth elements have recently aroused great interest in applications of magnetic refrigeration. Their magnetocaloric properties have been studied in a way intensive. This interest in rare earth metals is mainly due to their properties structural and the diversity of magnetic transitions presented by these elements, with broad values of the magnetic moment, and finally the localized nature of the magnetic moments 4f. This latest property makes rare earth alloys a practical model for theoretical and experimental investigations. Studied by neutron diffraction [177], the gadolinium reveals a ferromagnetic structure which is ordered in the vicinity of 293 K. The axis of easy magnetization is parallel to the axis c of the hexagonal structure between the temperature of Curie and the spin reorientation temperature T_{sr}, below which the magnetization is deviated from the easy axis giving rise to a conical magnetic structure [177].

Table V.2: Heavy rare earth magnetic structure. These data are taken from reference [178].

Metal	T_N(K)	Magnetic structure	T_C (K)	Magnetic structure at 4.2K
Gd	292.2	Ferromagnetic	293.2	Ferromagnetic
Tb	229	Helical	221	Ferromagnetic
Dy	179	Helical	87	Ferromagnetic
Ho	133	Helical	20	Conical
Tm	56	Amplitude modulated	38	Ferromagnetic

The elements Tb, Dy, and Ho have a helical antiferromagnetic structure (AFH) in the temperature range between the Curie temperature and the temperature Néel T_N. In an AFH structure, the magnetic moments which are in the same plane are ordered in a ferromagnetic structure and rotate by the same angle with respect to the magnetic moments which are in the neighboring plane. This magnetic structure can be transformed into a ferromagnetic structure if the applied field exceeds a certain value critical. Erbium has an even more complex structure, between 53 and $T_N = 80$ K with a longitudinal spin wave along axis c. Below 53 K the magnetic structure becomes cycloidal. Finally for temperatures below 18 K, it is arranged in a structure ferromagnetic. Thulium is antiferromagnetic below 56 K. It has a phase ferromagnetic for temperatures below 32K. Neodymium has a double hexagonal and cubic crystallographic structure. Magnetic moments are ordered in the hexagonal site at 19.2 K and in the cubic site at 7.8 K. For more details, see the reference [178]. The magnetic structure of heavy rare earths is presented in Table V.2.

V.3.1 Magnetic measurements of Gd_{100nm}

Because of its importance in the concept of refrigeration applications magnetic we started by studying the different magnetic properties and magnetocaloric of a gadolinium sample. The Curie temperature of 292 K and the high magnetic moment (7 μ B) of gadolinium makes it a benchmark for refrigerants magnetic. This metal has been the subject of several investigations [179-183]. In this paragraph, we let us report some of the main results relating to its magnetocaloric properties to compare with our results. This will be used in particular to check the quality of the thin layer that will be used subsequently to develop magnetic refrigerators.

There are several ways to calculate the magnetocaloric effect. However the measures direct consist in determining the initial temperature T_I and the final temperature T_F corresponding to the variation of the magnetic field from B_I to B_F under adiabatic conditions. Consequently, ΔT_{ad} (T_I, $B_I \rightarrow B_F$) is given as the difference T_F -T_I. In addition, the EMC can be determined from specific heat measurements at constant pressure. This technique allows a complete characterization of the magnetocaloric effect such that one can determine both the variation of the temperature and the isothermal variation of the entropy.

Both techniques are difficult to apply implemented. Indeed, the accuracy of the measurement depends a lot on the quality of the thermometer, thermal insulation and also the magnetization process. For our part, we will use magnetic measurements to calculate the variation of the magnetic entropy (Figure V.4). This technique is easy to implement and it is faster than calorimetric measurements. The Figure V.4 shows the magnetization isotherms for different temperatures of gadolinium thin film. The variation of the entropy is calculated by Maxwell's relation. For a field varying from 0 to 2T, SΔ is given by:

$$\Delta S\left(T,0\to H\right)=\int_{0}^{H}\left(\frac{\partial M}{\partial T}\right)_{H'}dH \qquad (V.1)$$

However, the magnetization measurements are carried out at discrete temperatures and fields. The Maxwell's relation can be compared by the numerical integration of the equation (V.1), which becomes:

$$\Delta S=\sum_{i}\frac{M_{i+1}-M_{i}}{T_{i+1}-T_{i}}\Delta H_{i} \qquad (V.2)$$

With M_{i+1} and M_i represent the magnetizations at temperatures T_{i+1} and T_i respectively under a field H_i. We notice that the variation of the entropy is equivalent to the area between two isotherms divided by the temperature difference between these curves as illustrated in the figure V.4.

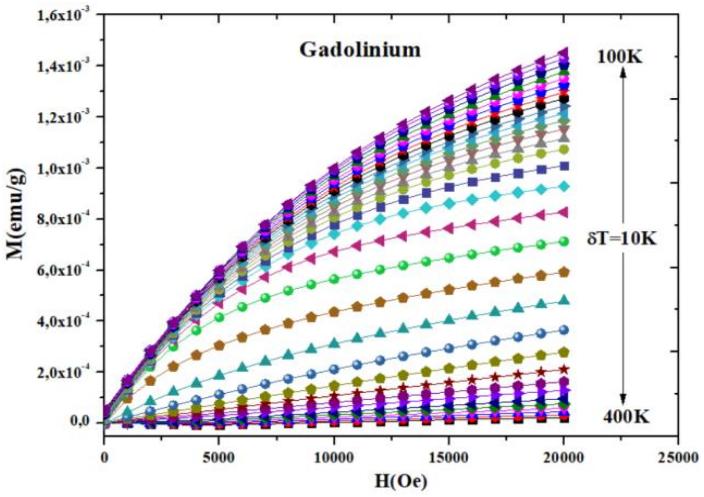

FIGURE V.4: Magnetic isotherms of the studied Gd_{100nm} thin film as a function of the applied magnetic field from 0 to 20 kOe with a sweeping rate of 250 Oe/s.

Figure V.5 shows the evolution of the variation of the entropy as a function of the temperature under different magnetic fields. For a field varying from 0 to 4 T, the change in entropy is equal to 4.5 J / kg.K for a magnetic field equal to 4T.

The width of the peak ΔS(T) as seen in Figure V.5 gives a large value of the refrigerating capacity of Gd_{100nm}. On the other hand, the variation of the entropy evolves almost linearly with the field applied. In addition, its remarkable magnetocaloric performance, the gadolinium is the only magnetocaloric material commercially available. This is how the most prototypes of magnetic refrigeration use it.

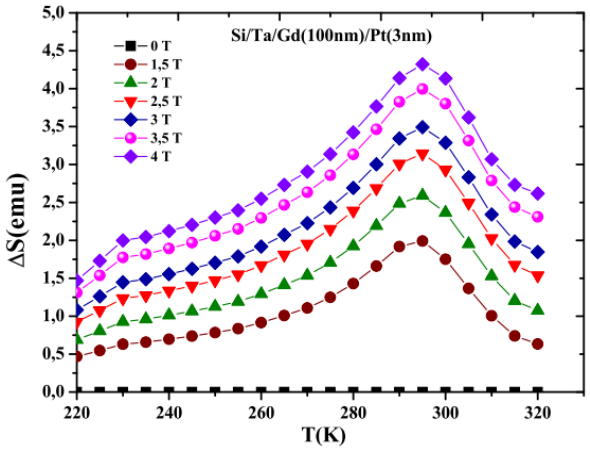

FIGURE V.5: Magnetic isotherms of the studied Gd_{100nm} thin film as a function of the applied magnetic field from 0 to 20 kOe with a sweeping rate of 250 Oe/s.

For the calculation theoretical of the variation of the entropy, we proceed as follows: In the molecular field model where the valence electrons are located, this is the case for example of alloys based on rare earth metals (4f), the magnetization of the material magnetic can be described using the Brillouin function given by [179,185]:

$$\sigma = B_J(y) = \frac{2J+1}{2J}\coth\left(\frac{2J+1}{2J}y\right) - \frac{1}{1J}\coth\left(\frac{1}{2J}y\right) \tag{V.3}$$

with:

$$y = \frac{1}{T}\left[3T_C\left(\frac{J}{(J+1)}\right)\sigma + \frac{g_J\mu_B J}{k}B\right] \tag{V.4}$$

σ: relative magnetization M/M_0 (M_0: magnetization at saturation), B_J: Brillouin function, g_J: Landé factor, Bμ: bohr magneton, J: total angular momentum and k is the Boltzmann constant.

The magnetocaloric effect represented by the variation of the magnetic entropy can be calculated from the values of the function y obtained by solving equation V.3. Over there next, ΔS is evaluated by injecting the values of y into the Smart relation [179] given by:

$$S_m = R.\left[\ln\left(\frac{\sinh\left(\frac{2J+1}{2J}y\right)}{\sinh\left(\frac{y}{2J}\right)}\right) - yB_J(y)\right] \tag{V.5}$$

S_m represents the magnetic entropy and R the universal constant of ideal gases. So at using this relationship we can determine the variation of the magnetic entropy as a function of the temperature and magnetic field.

Indeed, for materials where the valence electrons are located, the Weiss model gives a simple estimate of the magnetic entropy and the variation of the adiabatic temperature. ΔT_{ad} can also be calculated using the Weiss model. ΔT_{ad} is given by:

$$\Delta T_{ad} = -\frac{T}{C_p}\Delta S \qquad \text{(V.6)}$$

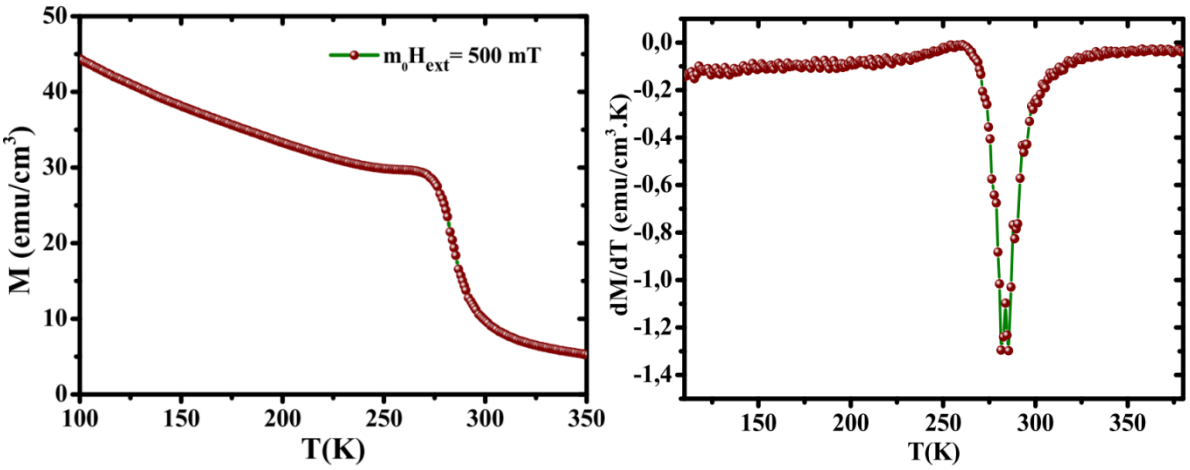

FIGURE V.6: (a)Temperature dependence of the magnetization under a magnetic field of 500Oe for the studied Gd thin film. (b) The evolution of dM/dT as a function of temperature.

The temperature dependent magnetization is measured using a Quantum Design© Squid Vibrating Sample Magnetometer with an external field applied in in-plane direction. Figure V.6 (a) shows the temperature dependence of magnetization M under an applied magnetic field of 500 Oe for the studied Si/Ta/Gd(100nm)/Pt(3nm) sample. A typical paramagnetic to ferromagnetic phase transition can be observed at T_C. In order to estimate the T_C, we have used the inflection point method as described by Moreno-Ramirez et al. [172]. Following this, a value of $T_C = 275$ K can be determined from the minimum of the derivative of the magnetization dM/dT as shown in Figure V.6 (b).

Concerning the M(T) curve of the Gd_{100nm} film (Figure V.6(a)), a transition from ferromagnetism to paramagnetism at 275 K can be noted. Thus, considering that bulk Gd metal has its Curie temperature (T_C^{hcp}) at about 292 K, and that the dimensionality effect may reduce the T_C values of Gd thin films, the observed magnetization behavior 275 K in Fig. V.5 can be attributed to the order-disordered magnetic transition of the hcp fraction in the Gd thin film.

V.3.2 Electrical measurements of Gd_{100nm}

Our Gadolinium film is grown at room temperature on silicon substrate (Si) using sputtering disposition with a base pressure lower than 10^{-7} Torr. A 5 nm of Tantalum (Ta) buffer layer was used as well as 3 nm of platine (Pt) capping layer to avoid

oxidation of the Gadolinium rare-earth. The total magnetic thickness of the samples is kept constant and equal to 100 nm. For electrical transport measurement rectangular Hall cross structure were prepared with optical lithography. A constant DC current of 2 mA is applied along the x direction, and the voltage is measured along the x direction. Furthermore a magnetic field is applied along the plane.

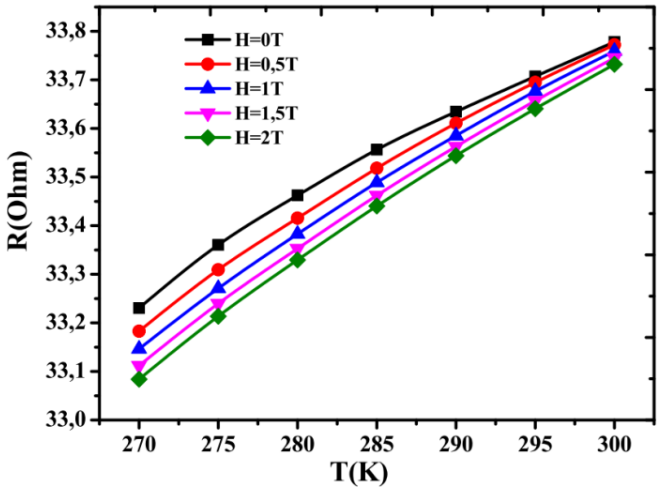

FIGURE V.1 Variation of the electrical resistivity as a function of T for I=2mA.

According to Figure V.1 and for a thin layer of Gadolinium (Si/Ta/Gd(100nm)/Pt(3nm) directed along the plane (ab) with an application of a magnetic field from 0 to 2T, we see very well that the increase in temperature causes a slight increase in electrical resistivity. Therefore for each temperature step, the resistance-field R(H) were measured for increasing and decreasing magnetic field. The resistance dependent magnetic field is shown in figure V.2. The slopes clearly decrease with increasing the magnetic field.

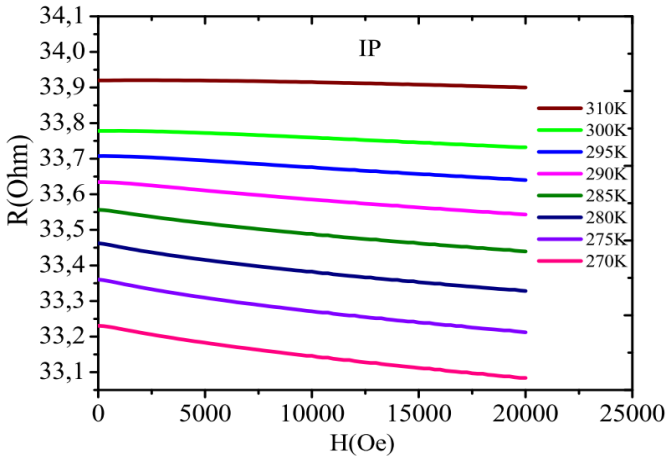

FIGURE V.2: Variation of the electrical resistivity as a function of the magnetic field, for I=2mA.

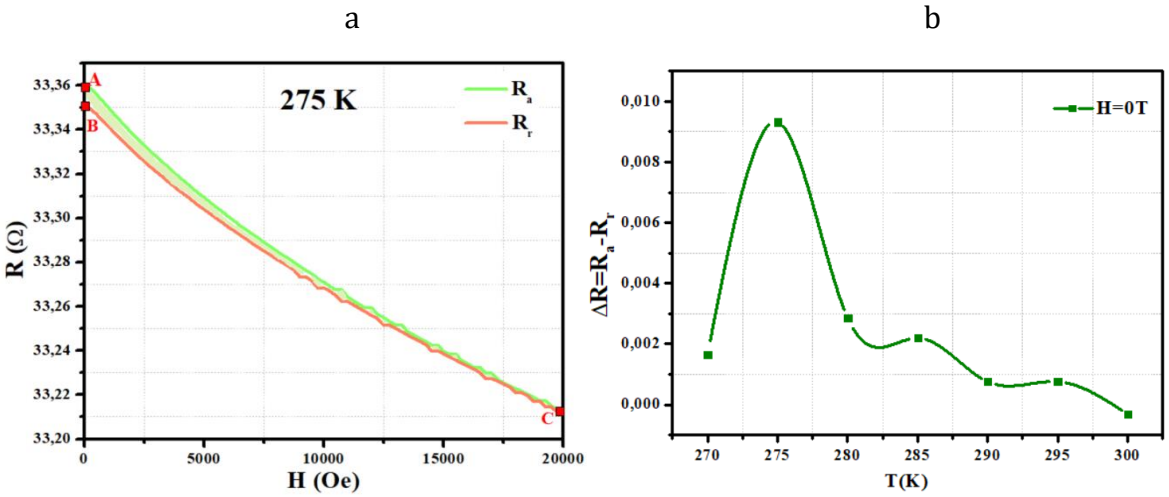

FIGURE V.4: Variation of the electrical resistivity (a) and ΔR (b) as a function of the magnetic field at T=275K.

In order to check the magnetocaloric effect of the present thin film used in this study, the variation of resistance can be obtained in a cooling process. Thus, the reliabily of the thermograms can be examined with an equation:

$$\Delta R = R_{H,T}\ (\text{heating}) - R_{H,T}\ (\text{cooling})$$

Where $R_{H,T}$(heating) and $R_{H,T}$ (cooling) are resistance obtained

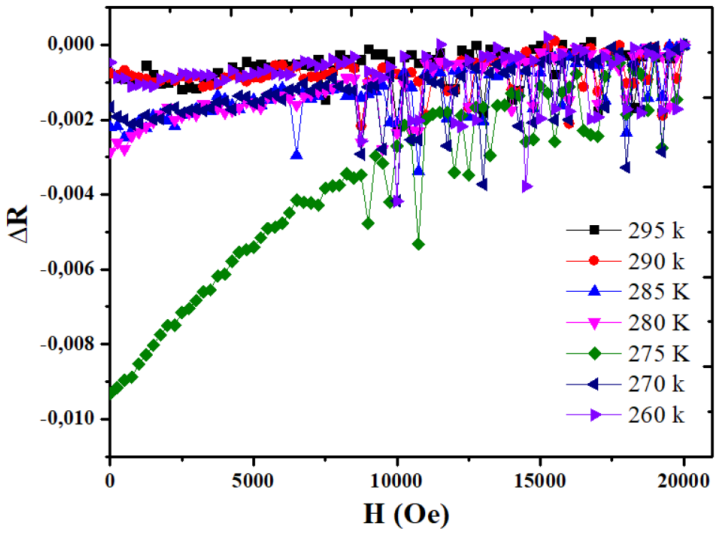

FIGURE V.3: Variation of the ΔR as a function of the magnetic field.

To explain why we have this variation in resistance at 275K, we have studied the behavior of the resistance change ΔR at 275K as a function of the magnetic field and temperature, and by comparing this variation with the magnetic entropy change as a function of temperature we notice that this peak is due to a magnetic transition between 275 and 280K. We can therefore find the amount of heat given or removed to the thin layer of gadolinium from the entropy change. We can conclude from these measurements that the fact of making a change on the resistance value we can cool our system.

Conclusion

In this thesis, we studied the structural, magnetic and magnetocaloric properties of materials based on rare earth elements, $LaCr_2Si_2C$, the multiferoique $TbMn_2O_5$, and the Gadolinium thin layer in order to show the main characteristics sought for magnetic refrigeration. ie a great magnetocaloric effect and a great cooling capacity. The key problem that we have addressed after the characterization and simulation of these different materials is the potential of thin film materials for cooling electronic circuits. Each atom of a material has a net magnetic moment which is the sum of the spin of its electrons. The sum of the net magnetic moment of all the atoms contained in a unit of volume of the magnetic material represents magnetization. Of $TbMn_2O_5$ and the thin layer of Gadolinium, atoms in a similar spin state tend to join together to form distinct zones for which the magnetization is saturated. At low temperature, the magnetic energy necessary to modify the orientation of the atomic spins is less since the thermal excitation is minimum. The application of a weak magnetic field to a paramagnetic material causes a variation in magnetization sufficient to generate a notable increase in temperature. Under the Curie point, the material adopts a ferromagnetic behavior and past the Curie point, it adopts paramagnetic behavior. This type of transition is often classified as second order. The ferromagnetic behavior is explained by the concept of exchange energy which represents the interaction of the electronic charges of neighboring atoms. The exchange energy tends to align the magnetic moments of the neighboring atoms creating the saturated magnetic domains as described in the previous section. The thermal agitation opposes the alignment effect of the exchange energy and the local order which defines the magnetic domains fades at higher temperature. The magnetization therefore undergoes an abrupt variation at the Curie temperature generating a maximum value of the MCE. The MCE associated with a phase transition is high enough only at temperatures near the Curie point where the variation in magnetization occurs. The magnetic behavior $LaCr_2Si_2C$ of this compound is investigated, using first principle methods, Monte Carlo simulation and mean field approximation. The structural, electronic and magnetic properties are described using ab-initio method in the framework of the Generalized Gradient Approximation (GGA), and the Full Potential-Linearized Augmented Plane Wave (FP-LAPW) method implemented in the WIEN2K packages. We have also computed the coupling terms between magnetic atoms which are used in Hamiltonian model. A theoretical study realized by mean field approximation and Monte Carlo Simulation within the Ising model is used to more understand the magnetic properties of this compound. Thereby, our results showed a ferromagnetic ordering of the Cr magnetic moments below the Curie temperature of 30 K in $LaCr_2Si_2C$. Other parameters are also computed as: the magnetization, the energy, the specific heat and the susceptibility. Also, the calculation predicts that the compound $LaCr_2Si_2C$ owns a metal character and the analysis of the difference energy between FM and AFM states confirmed that the FM is more stable with

the Curie temperature below 30K. Future work on this material can be oriented towards the improvement of Tc for spintronic applications.

For $TbMn_2O_5$, The interest of this compound lies in the coupling between orders, magnetic and electrical, with the possibility, from a static point of view, to manipulate the magnetization by applying an electric field. In $TbMn_2O_5$ the hybrid excitations, called electromagnons can be understood as magnons excited by the electrical component of a wave electromagnetic and are the signature in the dynamic regime of magneto-electric coupling. Understanding the mechanisms behind these new excitations was our objective, and the possibility of modulating these excitations via a field electric and / or magnetic is also an avenue explored for future applications to be defined in the field of information transport, magnetic refrigeration and spintronic devices for example, so the magnetism and the ferroelectricity in $TbMn_2O_5$ are coupled. On the other hand, the multiferroic $TbMn_2O_5$ material is characterized also by different exchange interactions involving Mn^{4+}, Mn^{3+} and rare earth R^{3+} ions sublattices, leading to a complex magnetism character. As a result, $TbMn_2O_5$ reveals various magnetic and electric phase transitions. Recently, a reversible and a giant rotating magnetocaloric effect has been pointed out in the multiferroic $TbMn_2O_5$ single crystal, opening the way for new designs of low-temperature magnetic cooling. Our preliminary calculations using the density functional theory study of $TbMn_2O_5$ unveil that it is possible to determine some key parameters such as magnetic moments, magnetic anisotropy and electronic structures that are of great interest for the investigation of its entropic behavior (MCE). Particularly, the obtained magnetic moments as well as the anisotropic energies are in fair agreement with experimental reports. However, the main challenge remains the simulation of some important magnetothermal parameters of $TbMn_2O_5$ such as specific heat, entropy and adiabatic temperature changes.

The refrigeration techniques developed and potentially marketable require efficient refrigeration materials which meet many other criteria such as structural stability, resistance to oxidation or good electrical conductivity. The magnetocaloric effect has been extensively studied in the past forty years, and much experimental data has been reported in the literature. The majority of studies have focused on rare earths and compounds based on rare earths and transition metals. For refrigeration applications around room temperature, the reference element is pure gadolinium. At its Curie temperature of around 292K, its magnetocaloric properties ΔS_m and ΔT_{ad} are approximately -10 $J.kg^{-1}.K^{-1}$ and 12 K, respectively with a field variation magnetic from 0 to 5T. Our Gadolinium film is grown at room temperature on silicon substrate (Si) using sputtering disposition with a base pressure lower than 10^{-7} Torr. A 5nm of Tantalum (Ta) buffer layer was used as well as 3 nm of platine (Pt) capping layer to avoid oxidation of the Gadolinium rare-earth. The total magnetic thickness of the samples is kept constant and equal to 100 nm. The electrical measurements we made on this layer of Gadolinium using a PPMS-7T shows that the increase in temperature causes a slight increase in electrical resistivity. Therefore, for each temperature step, the electrical resistance was measured by varying the magnetic field, and from the maximum entropy variation we found the amount of heat given or removed from our thin layer.

References

[1] V. K. Pecharsky and K. A. Gschneidner, Jr., —Giant Magnetocaloric Effect in $Gd_5(Si_2Ge_2)$,‖ Phys. Rev. Lett., vol. 78, pp. 4494–4497, 1997.

[2] C. Zimm, A. Jastrab, A. Sternberg, V. K. Pecharsky, K. A. Gschneidner Jr, M. Osborne, and I. Anderson, —Description and performance of a near-room temperature magnetic refrigerator,‖ Adv. Cryog. Eng., vol. 43, pp. 1759–1766, 1998.

[3] E. Warburg, —Über Einige Wirkungen der Coercitiv Kraft,‖ Lepzig Magn. Untersuchungen, vol. 13, pp. 141–164, 1881.

[4] P. Weiss, A Piccard, —Sur un nouveau phénomène magnétocalorique,‖ CR Acad. Sci., vol. 166, p. 352, 1918.

[5] P. Debye, —Einige bemerkungen zur magnetisierung bei tiefer temperatur,‖ Ann. Phys., vol. 81, pp. 1154–1160, 1926.

[6] W. F. Giauque, —A thermodynamic treatment of certain magnetic effects. A proposed method of producing temperatures considerably below 1° absolute,‖ J. Am. Chem. Soc., vol. 49, pp. 1864–1870, 1927.

[7] W. F. Giaugue and D. P. MacDougall, —Attainment of Temperatures Below 1° Absolute by Demagnetization of Gd 2 (SO 4) 3 . 8H 2 O,‖ Phys. Rev., vol. 43, p. 768, 1933.

[8] W. F. Giauque and D. P. MacDougall, —The Production of Temperatures below One Degree Absolute by Adiabatic Demagnetization of Gadolinium Sulfate,‖ J. Am. Chem. Soc., vol. 57, pp. 1175–1185, 1935.

[9] W. F. Giauque, —Some consequences of low temperature research in chemical thermodynamics,‖ Nobel Lect., 1949.

[10] M. Balli, D. Fruchart, D. Gignoux, and R. Zach, —The ‗colossal' magnetocaloric effect in Mn1−xFe x As : What are we really measuring?,‖ Appl. Phys. Lett., vol. 95, p. 072509, 2009.

[11] M. Balli, O. Sari, D. Fruchart, and J. Forchelet, —Influence of the materials magnetic state on the accurate determination of the magnetocaloric effect,‖ EPJ W. C, vol. 29, p. 00005–p.10, 2012.

[12] B. Yu, Q. Gao, B. Zhang, X. Z. Meng, and Z. Chen, ―Review on research of room temperature magnetic refrigeration,‖ Int. J. Refrig., vol. 26, pp. 622–636, 2003.

[13] S. LIONTE, ―Caractérisation, étude et modélisation du comportement thermomagnétique d'un dispositif de réfrigération magnétique à matériaux non linéaires et point de Curie proche de la température ambiante,‖ Thèse de doctorat, UNIVERSITÉ DE STRASBOURG ÉCOLE DOCTORALE MSII (ED 269) Laboratoire LGeCo, France, 2015.

[14] A. Kitanovski and P. W. Egolf, ―Thermodynamics of magnetic refrigeration,‖ Int. J. Refrig., vol. 29, pp. 3–21, 2006.

[15] J. A. Barclay, ―The theory of an active magnetic regenerative refrigerator,‖ in Proceedings of the Second Biennial on Refrigeration for Cryogenic Sensors and Electronic Systems, NASA-CP 2287, Goddard Space Flight Center Greenbelt, 1983.

[16] C. MAYER, ―Nouveaux matériaux magnétocaloriques pour la réfrigération magnétique,‖ Thèse de doctorat, UNIVERSITÉ BORDEAUX 1 ÉCOLE DOCTORALE DES SCIENCES CHIMIQUES, France, 2011.

[17] H. R. E. Bouchekara, ―RECHERCHE SUR LES SYSTEMES DE REFRIGERATION MAGNETIQUE. MODELISATION NUMERIQUE, CONCEPTION ET OPTIMISATION, ‖ Thèse de doctorat, Grenoble INP, G2ELab - Laboratoire de Génie Electrique de Grenoble, France, 2008.

[18] J. Tušek, A. Kitanovski, S. Zupan, I. Prebil, and A. Poredoš, ―A comprehensive experimental analysis of gadolinium active magnetic regenerators,‖ Appl. Therm. Eng., vol. 53, pp. 57–66, 2013.

[19] S. Dan'kov, A. Tishin, V. Pecharsky, and K. Gschneidner, ―Magnetic phase transitions and the magnetothermal properties of gadolinium,‖ Phys. Rev. B, vol. 57, pp. 3478–3490, 1998.

[20] F. ALLAB, ―Etude et conception d'un dispositif de réfrigération magnétique basé sur l'effet magnétocalorique géant,‖ Thèse de doctorat, Grenoble INP, G2ELab - Laboratoire de Génie Electrique de Grenoble, France, 2008.

[28] K. A. Gschneider Jr., V. K. Pecharsky, and A. O. Tsokol, ―Recent developments in magnetocaloric materials,‖ Reports Prog. Phys., vol. 68, no. 6, pp. 1479–1539, 2005.

[29] A. M. Tishin and Y. I. Spichkin, The Magnetocaloric Effect And Its Applications, Institute of Physics Publishing, 2003.

[30] « Structure_Catalysis_Fortunelli_supplementary.pdf ».

[31] J. Hafner, « Ab-initio simulations of materials using VASP: Density-functional theory and beyond », J. Comput. Chem., vol. 29, no 13, p. 35.

[32] Kohn, W.; Sham, L. J. Phys Rev A 1964, 140, 1133.

[33] Perdew, J. P. ; Kurth, S. In A Primer in Density Functional Theory; Fiolhais, C.; Nogueira, F.; Marques, M., Eds.; Lecture Notes in Physics, vol. 620; Springer: Berlin, 2003.

[34] Perdew, J. P.; Zunger, A. Phys Rev B 1981, 23, 5048.

[35] Perdew, J. P. Phys Rev B 1986, 33, 8822.

[36] L. de Broglie, Ann. Physik 3, 22 (1925).

[37] E. Schrödinger, Ann. Physik 84, 361 (1926).

[38] M. Born et J. R. Oppenheimer, Ann. Physik 84 (1927).

[39] J. C. Slater, Phys. Rev. 34, 1293 (1929).

[40] W. Pauli, Z. Physik. 31, 765 (1925).

[41] D. R. Hartree, Proc. Cam. Phil. Soc. 24, 89 (1928).

[42] V. Z. Fock, Z. Physik. 61, 126 (1930).

[43] A. Szabo et N. S. Ostlund, "Modern Quantum Chemistry". McGraw-Hill, New York, 1982.

[44] C. C. J. Roothan, Rev. Mod. Phys 23, 69 (1951).

[45] G. G. Hall, Proc. Roy. Soc. (London) A205, 541 (1951).

[46] G. Berthier, J. Chem. Phys. 51, 363 (1954).

[47] J. A. Pople et R. K. Nesbet, J. Chem. Phys. 22, 571 (1954).

[48] J. C. Slater, Phys. Rev. 57, 57 (1930).

[49] S. F. Boys, Proc. Roy. Soc. (London) A200, 542 (1950).

[50] E. Clementi, IBM J. Res et Dev. 9, 2 (1965).

[51] C. Møller et M. S. Plesset, Phys. Rev. 46, 618 (1934).

[52] S. F. Boys, Proc. Roy. Soc. (London) A201, 125 (1950).

[53] J. A. Pople, J. S. Binkley, et R. Seeger, Int. J. Quant. Chem. Symp. 10, 1 (1976).

[54] W. Heisenberg, Z. Physik 43, 172 (1927).

[55] P. Hohenberg et W. Kohn, Phys. Rev. B 136, 864 (1964).

[56] M. Levy, Proc. Natl. Acad. Sci. 76, 6062 (1979).

[57] M. Levy, Phys. Rev. A 26, 1200 (1982).

[58] W. Kohn et L. J. Sham, Phys. Rev. A 137, 1697 (1965).

[59] J. Harris et R. O. Jones, J. Phys. F 4, 1170 (1974).

[60] R. A. Harris, J. Chem. Phys. 81, 2403 (1984).

[61] O. Gunnarson et B. I. Lundqvist, Phys. Rev. B 13, 4274 (1976).

[62] C. O. Almbladh et A. C. Pedroza, Phys. Rev. A 29, 2322 (1984).

[63] A. Savin, H. Stoll, et H. Preuss, Theor. Chim. Acta. 70, 407 (1986).

[64] J. C. Slater, Phys. Rev. 81, 385 (1951).

[65] S. J. Vosko, L. Wilk, et M. Nussair, Can. J. Phys. 58, 1200 (1980).

[66] D. M. Ceperley et B. J. Alder, Phys. Rev. Lett. 45, 566 (1980).

[67] A. D. Becke, Phys. Rev. A 38, 3098 (1988).

[68] J. P. Perdew et Y. Wang, Phys. Rev. B 33, 8800 (1986).

[69] N. C. Handy et A. J. Cohen, Mol. Phys. 99, 403 (2001).

[70] J. P. Perdew et Y. Wang, Phys. Rev. B 45, 244 (1992).

[71] J. P. Perdew, K. Burke, et M. Ernzerhof, Phys. Rev. Lett. 77, 3865 (1996).

[72] A. D. Becke, J. Chem. Phys. 84, 4524 (1986).

[73] C. Lee, W. Yang, et R. G. Parr, Phys. Rev. B 37, 785 (1988).

[74] A. D. Becke, J. Chem. Phys. 98, 5648 (1993).

[75] A. D. Becke, J. Chem. Phys. 98, 1372 (1993).

[76] P. J. Stephens, F. J. Devlin, C. F. Chabalowski, et M. J. Frisch, J. Phys. Chem. 98, 11623 (1994).

[77] V. Barone, Chem. Phys. Lett. 226, 392 (1994).

[78] M. D. Wodrich, C. Corminboeuf, et P. von Ragué Schleyer, Org. Lett. 8, 3631 (2006).

[79] E. M. Sproviero, J. A. Gascon, J. P. McEvoy, G. W. Brudvig, et V. S. Batista, J. Inorg. Biochem. 100, 786 (2006).

[80] J.M. Meichtry, H.J. Lin, L. de la Fuente, I.K. Levy, E.A.Gautier, M.A. Blesa and M.I. Litter. 'Low-Cost TiO_2 Photocatalytic Technology for Water Potabilization in Plastic Bottle for Isolated Regions', Journal of Solar Energy Engineering, Vol. 129, N°1, pp. 119 – 126, 2005.

[81] F.M. Salih, 'Enhancement of solar inactivation of E. Coli by titanium dioxide photocatalytic oxidation', Journal of Applied Microbiology, Vol. 92, N°5, pp. 920 - 926, 2002.

[82] Y. Leprince-Wang, 'Elaboration et Caractérisation des Matériaux à l'Echelle Micro et Nanométrique', Mémoire HDR, Université Marne La Vallée, 2003.

[83] A. Billard, Laboratoire d'Etudes et de Recherches sur les Matériaux, les Procédés et les Surfaces, LERMPS, Belfort-Monbéliard, France.

[84] CITRA, Centre d'Ingénierie en Traitements et Revêtements de surface Avancés, Rue Atlantis, 87068, Limoges, France.

[85] X. Chen and S.S. Mao, 'Titanium Dioxide Materials', Chemistry Review Vol. 107, N°7, pp. 2891 – 2959, 2007.

[86] H. Granier, 'Les Techniques de Dépôts et d'Intégration dans les Centrales de Technologie du Réseau Renatech', Journée des Utilisateurs, 21 mars 2011.

[87] C. Sarantoupolos, 'Photocatalyseurs à base de TiO_2 Préparés par Infiltration Chimique en Phase Vapeur (CVI) sur Support Microfibreux', Science et Génie des Matériaux, INP Toulouse 2007.

[88] A. Atyaoui, 'Elaboration de TiO_2 sous forme de Couche Mince Dopée et Nanotubulaire: Caractérisation Electrochimique et Performance Photocatalytique', Université Pierre et Marie-Curie, Paris VI, 2013.

[89] T. Kodom, 'Etude et Caractérisations de Couches Minces de Semi-Conducteurs Nanostructurés Dopés en Vue de leur Utilisation pour la Dépollution des Eaux', Thèse de Doctorat, Université de Poitiers, avril 2011.

[90] O. van der Straten, Y. Zhu, J. Rullan, K. Topol, K. Dunn and A. Kaloyeros, 'Atomic Layer Deposition of Tantalum Nitride On Organosilicate and Organic Polymer-Based Low Dielectric Constant Materials', Materials Research Society Symposium Proceedings, Vol. 812, pp. 165 - 170, 2004.

[91] V. Géhanno, « Anisotropie magnetique perpendiculaire des couches minces epitaxiees d'alliages ordonnes FePd », p. 160.

[92] A. P. Popa, « Elaboration et caracterisation de nanostructures magnetiques », p. 211.

[93] T. Jiang, L. Xie, Y. Yao, Y. Liu, et X. Li, « Large magnetocaloric effect in CrO_2/TiO_2 epitaxial films above room temperature », Mater. Lett., vol. 76, p. 25-27, juin 2012, doi: 10.1016/j.matlet.2012.02.057.

[94] G. Delaizir et al., « Synthèse et caractérisation de matériaux à base de SnTe pour la conversion d'énergie par effets thermoélectriques », p. 337.

[95] P. Lemoine, « Contribution à l'étude des propriétés structurales et magnétiques de composés intermétalliques isotypes de CeScSi et Th_6Mn_{23} », p. 278.

[96] K. A. Borup et al., « Measuring thermoelectric transport properties of materials », Energy Environ. Sci., vol. 8, no 2, p. 423-435, 2015, doi: 10.1039/C4EE01320D.

[97] F. Issaoui, « Etude des propriétés magnétiques des matériaux à bases des métaux de transition sous forme de poudre et monocristaux (RMX) », p. 181.

[98] B H. Elias, "Theoretical investigation of the structural, electronic, elastic, and optical properties of zinc-blende BeS under high pressure" IJIRSET, 2319-8753, 2013.

[99] H Zaari, M Boujnah, A Benyoussef, A El Kenz, Computational Materials Science 93, 91-96.

[100] H Zaari, AG El Hachimi, A Benyoussef, A El Kenz, Journal of Magnetism and Magnetic Materials 393, 183-187.

[101] C Azahaf, H Zaari, A Abbassi, H Ez-Zahraouy, A Benyoussef, Optical and Quantum Electronics 47 (8), 2889-2897.

[102] K. Mukherjee et al, E. V. (2010). Magnetic behavior of bulk and fine particles of RCr2Si2C (R= La, Ce) compounds: possible magnetic ordering from Cr. Journal of Physics: Condensed Matter, 22(29), 295603.

[103] V. Klosek, A. Vernière, and B. Malaman, "Quenching of the magnetic moment of Cr in RCr2Si2 compounds upon filling with carbon", 30-059 Krakow, Poland, 2008.

[104] Perdew, J.P., Burke, K., Ernzerhof, M.: Phys. Rev. Lett. 77, (1996) 3865–3868.

[105] Blaha, P., Schwarz, K., Madsen, G., Kvasnicka, D., Luitz J.: WIEN2k, augmented plane wave localorbitals program for calculating crystal properties, Vienna, Austria. (2001) .

[106] P.Schmüser, Superconductivity Workshop, Argonne National Laboratory, (2004).

[107] V. Klosek, « Contribution à l'étude des propriétés structurales et électroniques de composés équiatomiques RTX (T = Ti, V, Cr, Mn, Fe; X = Si, Ge) et des quaternaires RTiGeCx et RCr_2Si_2C, où R est un alcalino-terreux,l'yttrium, le lanthane ou un lanthanoïde. », thèse d'état, Université Henri Poincaré, Nancy 1, 2002.

[108] Marcela Janatova, JanaVej pravova, Martin Divis, Vladimir Sechovsky Physica B: Condensed Matter ; Volume 403, Issues 13–16, 1 July 2008, Pages 2338-2343.

[109] G.W.Fernando, A.N.Kocharian, R.E.Watson, M.Weinert Physica B: Condensed Matter, Volumes 230–232, February 1997, Pages 509-512.

[110] R. Masrour, A. Jabar, M. Hamedoun, A. Benyoussef, E. K. Hlil, Journal of Magnetism and Magnetic Materials, 2017.

[111] N.N. Bogoliubov, J. Phys. (USSR) (1947) 11–23.

[112] R.P. Feynmann, Phys. Rev. (1955) 97–660.

[113] S. Naji et al. New Statistical Lattice Model from Double Honeycomb Structure, International Journal of Modern Physics B,28,1450086 (2014).

[114] S. Naji et al. Electronic and magnetic properties of iron adsorption on graphene with double hexagonal geometry, International Journal of Quantum Chemistry, Wiley, 114, 7, 463–467(2014).

[115] S. Naji, A. Benyoussef, A. El Kenz, H. Ez-Zahraouy M. Loulidi , Physica A: Statistical Mechanics and its Applications, Volume 391, Issue 15, 1 August 2012, Pages 3885–3894.

[116] O. El Rhazouan et al., Magnetic properties of double perovskite Sr_2CrReO_6: Mean field approximation and Monte Carlo simulation, Physica A, North-Holland, 397, 31-39(2014).

[117] S. Naji et al., Phases Diagrams and Magnetic Properties of Tri-layer Superlattices: Mean Field Study, Physica A, North-Holland, 399, 106–112 (2014).

[118] F. El Hallani et al, First-principles study of the magnetic stability and the exchange couplings of LaMn2O5, Journal of Applied Physics, AIP, 114 (16), 163909 (2013).

[119] S. Naji, A. Belhaj, H. Labrim, L. Bahmad, A. Benyoussef, A. El Kenz, Monte Carlo study of phase diagrams and magnetic properties of Trilayer superlattices . Acta Physica Polonica B, 45, 4, 947, (2014).

[120] Luther, A, & Peschel, I. (1975). Calculation of critical exponents in two dimensions from quantum field theory in one dimension. Physical Review B, 12(9), 3908.

[121] M. Balli, S. Jandl, P. Fournier, and D. Z. Dimitrov, Appl. Phys. Lett 108, 102401 (2016).

[122] H. Katsura, N. Nagaosa, and A. V. Balatsky, Phys. Rev. Lett. 95, 057205 (2005).

[123] M. Fiebig, J. Phys. D: Appl. Phys. 38, R123 (2005).

[124] Graeme Eoin Johnstone, “Neutron and X-ray Scattering Study of Magnetic Manganites”, University of Oxford, 2012.

[125] S.-W. Cheong and M. Mostovoy, Nature Materials 6, 13 (2007).

[126] A. B. Sushkov, R. V. Aguilar, S. Park, S-W, Cheong and H. D. Drew, Phys Rev Lett. 98, 027202 (2007).

[127] J. Varignon, S. Petit, A. Gellé, and M. B. Lepetit, “J Phys Condens Matter.;25(49):496004”, 2013.

[128] L. C. Chapon, P. G. Radaelli, G. R. Blake, S. Park, and S.-W. Cheong, Phys. Rev. Lett. 96, 097601 (2006).

[129] A. RAMIREZ, Geometrical Frustration, chapter 4, p. 423, Elsevier Science B.V., 2001.

[130] N. Hur, S. Park, P.A. Sharma, J. S. Ahn, S. Guha and S-W.Cheong, Nature 429, 392 (2004).

[131] G. R. Blake, L. C. Chapon, P. G. Radaelli, S. Park, N. Hur, S-W. Cheong, and J. Rodríguez-Carvajal, Phys. Rev. B 71, 214402 (2005).

[132] Tay-Rong Chang, Horng-Tay Jeng, Chung-Yuan Ren, and Chen-Shiung Hsue, Phys. Rev. B 84, 024421 (2011).

[133] N. Hur, S. Park, P. A. Sharma, S. Guha, and S-W. Cheong, Phys. Rev.Lett. 93, 107207 (2004).

[134] D. Tzankov, V. Skumryev, M. Aroyo, R. Puzniak, M.D. Kuz'min, M. Mikhov, Solid.Stat. Comm. 147, 212 (2008).

[135] L. C. Chapon, G. R. Blake, M. J. Gutmann, S. Park, N. Hur, P. G. Radaelli, and S. W. Cheong, Phys. Rev. Lett.93, 177402 (2004).

[136] I. A. Sergienko and E. Dagotto, Phys. Rev. B. 73, 094434 (2006).

[137] A. Muñoz, J. A. Alonso, M. T. Casais, M. J. Martínez-Lope, J. L. Martínez, and M. T. Fernández-Díaz, Phys. Rev. B 65, (2002)144423

[138] P. Blaha, K. Schwarz, G. Madsen, D. Kvasnicka, and J. Luitz, WIEN2k, Augmented Plane Wave Local Orbitals Program for Calculating Crystal Properties, Vienna, Austria, 2001.

[139] J. P. Perdew, K. Burke, and M. Ernzerhof, Phys. Rev. Lett. 77, 3865 (1996)

[140] J. P. Perdew, K. Burke, M. Ernzerhof, Generalized Gradient Approximation Made Simple, Phys. Rev. Lett. , Vol. 77, No. 18, (1996).

[141] L. Hedin, B. I. Lundqvist, Explicit local exchange-correlation potentials, J. Phys. C: Solid St. Phys. , Vol. 4, (1971).

[142] S.Y. Savrasov and G. Kotliar. Phys. Rev. Lett., 84, 3670 (2000).

[143] B.-T. Wang, H. Shi, W. Li, and P. Zhang, Phys. Rev. B 81, 045119 (2010).

[144] H. J. Monkhorst and J. D. Pack, Phys. Rev. B 13, 5188 (1976).

[145] P. Carra, B. T. Thole, M. Altarelli and X. Wang, Phys. Rev. Lett., 70, 694, Feb. 1993.

[146] L. C. Chapon, G. R. Blake, M. J. Gutmann, S. Park, N. Hur, P. G. Radaelli, and S.-W. Cheong, "Structural anomalies and multiferroic behavior in magnetically frustrated $TbMn_2O_5$," Phys. Rev. Lett., vol. 93, p. 177402, Oct 2004.

[147] P. G. Radaelli, C. Vecchini, L. C. Chapon, P. J. Brown, S. Park, and S.-W. Cheong, “Incommensurate magnetic structure of YMn_2O_5 : A stringent test of the multiferroic mechanism,” Physical Review B, vol. 79, p. 020404, jan 2009.

[148] C.Tay-Rong, J.Horng-Tay, R. Chung-Yuan, H. Chen-Shiung, Phys Rev B, 84 .024421 (2011).

[149] B. T. Thole, P. Carra, F. Sette and G. van der Laan, Phys. Rev. Lett., 68, 1943 (1992).

[150] C. Wilkinson, P. J. Brown, and T. Chatterji, Phys. Rev. B. 84, 224422 (2011).

[151] M. Balli, S. Jandl, P. Fournier, D. Z. Dimitrov, Crystals 2017, 7, 44.

[152] J. Jensen and A. R. Mackintosh, Rare Earth Magnetism (Oxford Univ. Press, Oxford, 1991)

[153] H. Bouhani, A. ENDICHI et al, Journal of “Materials Chemistry and Physics”, 10.1016/ 2019.04.044.

[154] Chenjie Wang, Guang-Can Guo, and Lixin He, Materials Science, 2007, arXiv:0711.2539v1.

[155] M. Balli, B. Roberge, P. Fournier, et S. Jandl, « Review of the Magnetocaloric Effect in $RMnO_3$ and RMn_2O_5 Multiferroic Crystals », Crystals, vol. 7, no 2, p. 44, févr. 2017, doi: 10.3390/cryst7020044.

[156] G. S. Burkhanov et al., « Magnetocaloric properties of distilled gadolinium: Effects of structural inhomogeneity and hydrogen impurity », Appl. Phys. Lett., vol. 104, no 24, p. 242402, juin 2014, doi: 10.1063/1.4883744.

[157] C. W. Miller, D. V. Williams, N. S. Bingham, et H. Srikanth, « Magnetocaloric effect in Gd/W thin film heterostructures », J. Appl. Phys., vol. 107, no 9, p. 09A903, mai 2010, doi: 10.1063/1.3335515.

[158] R. Gimaev, D. Kopeliovich, Y. Spichkin, et A. Tishin, « Measurements of the magnetic and magnetothermal properties of heavy rare earths », J. Magn. Magn. Mater., vol. 459, p. 215-220, août 2018, doi: 10.1016/j.jmmm.2017.11.018.

[159] X. Hai, « Magnetocaloric materials for magnetic refrigeration at room temperature », p. 283, 2006.

[160] V. K. Pecharsky and K. A. Gschneidner Jr., J. Magn. Magn. Mater. 200 (1999) 44.

[161] A. Lebouc, F. Allab, J. M. Fournier, and J. P. Yonnet, Techniques de l’ingénieur RE 28 (2005) 1–16.

[162] A. H. Morrish, The physical principles of magnetism, Wiley, New York (1964).

[163] N. A. de Oliveira and P. J. von Rankle, Phys. reports 489 (2010) 89–159.

[164] K. A. Gschneidner Jr., V. K. Pecharsky, and O. Tsokol, Rep. Prog. Phys. 68 (2005) 1479 –1539.

[165] V. K. Pecharsky and K. A. Gschneidner Jr., J. Appl. Phys. 86 (1999) 565–575.

[166] M. Foldeaki, R. Chahine, and T. K. Bose, J. Appl. Phys. 77 (1995) 3528.

[167] S. Yu. Dan'kov, A. M. Tishin, V. K. Pecharsky, and K. A. Gschneidner Jr., Phys. Rev. B 57 (1998) 3478.

[168] D. Petrovič, R. Šturm, I. Naglič, B. Markoli, et T. Pepelnjak, « Microstructural Anisotropy of Magnetocaloric Gadolinium Cylinders: Effect on the Mechanical Properties of the Material », Materials, vol. 9, no 5, p. 382, mai 2016, doi: 10.3390/ma9050382.

[169] V. K. Pecharsky and K. A. Gschneidner Jr., Phys. Rev. Lett. 78(3) (1997) 4494–4497.

[170] V. K. Pecharsky and K. A. Gschneidner Jr., J. Magn. Magn. Mater. 167 (1997) L179-L184.

[171] C. Mayer, « Nouveaux matériaux magnétocaloriques à base de terres rares pour la réfrigération magnétique », p. 186.

[172] O. Gutfleisch, M. A. Willard, E. Brück, C. H. Chen, S. G. Sankar, and J. P. Liu, Adv. Mater. 2 (2011) 821–842.

[173] C. Bauer, « Magnetocaloric Effect in Thin Films and Heterostructures », p. 98.

[174] O. Fruchart, « Couches minces et nanostructures magnétiques », p. 47.

[175] L. Helmich, M. Bartke, N. Teichert, B. Schleicher, S. Fähler, et A. Hütten, « Gadolinium thin films as benchmark for magneto-caloric thin films », AIP Adv., vol. 7, no 5, p. 056429, mai 2017, doi: 10.1063/1.4977880.

[176] Manh-Hng Phan and Seong-Cho Yu. Review of the magnetocaloric effect in manganite materialsuo. "Journal of Magnetism and Magnetic Materials", 308(2) :325 – 340, 2007.

[177] J.W. Cable, E.O. Wollan, Phys. Rev. B, 165 (1968) 733

[178] B. Coqblin, The Electronic Structure of Rare-earth Metals and Alloys : the Magnetic heavy Rare-earths, Academic Press, London, 1977.

[179] A.M. Tishin, Y.I. Spichkin, The Magnetocaloric Effect and its Applications, IOP Publishing, Bristol and Philadelphia, 2003.

[180] Y.L. Wu, A. O. Pecharsky, V.K. Pecharsky and K.A. Gschneidner Jr, Adv. Cryog. Eng, 48 (2002) 3.

[181] A. Lebouc, F. Allab, J.M. Fournier et J.P. Yonnet, réfrigération magnétique, Technique de l'Ingénieur, RE 28, 2005.

[182] V.K. Pecharsky, K.A. Gschneidner Jr, Phys. Rev. Lett., 78 (1997) 4494.

[183] K.A. Gschneidner, V.K. Pecharsky, A.O. Pecharsky and C.B. Zimm, 1999 Rare Earths ’98 vol 315–3, pp 69–76

[184] E. Brück, J. Phys. D: Appl. Phys., 38 (2005) R381–R391.

[185] Magnétisme, fondement, Edt : Etienne du Trémolet de Lacheisserie, EDP Sciences, 2000, ISBN : 2.86883.4